

1 INTRODUCTION

In steel making practice, refining of the metal and alloying processes are carried out in various vessels. Columbus Stainless Steel Company operates a 100t CLU-converter that forms the basis of this work. The refining process in the converter involves the oxidation of excess carbon in the metal whilst increasing or keeping the levels of other elements constant. Conditions have to be provided to keep valuable elements like chromium and nickel in the metal phase or else the elements would be oxidised and lost to the slag.

A top lance and nozzles at the bottom of the vessel are used to deliver the oxygen and other purging gases to the bath. The process continues until the specified metal composition has been achieved. Sometimes final adjustments to the metal composition have to be done outside the converter. For the refining process to proceed in the CLU-converter, it is required that the impurities in the metal be brought into intimate contact with the oxidizing gases and slag. The products of the chemical reactions that take place at the provided conditions have to be moved away from the reaction sites to the slag phase.

Gas injection continues to play an increasingly important role in steelmaking processes. The gases purged into the converter through the nozzles bring about thorough mixing of the bath thus accelerating the chemical reactions taking place in the converter, moving the oxidized impurities to the slag phase and promoting bath homogenisation. Since inefficient stirring leads to a longer blowing period, the result is poor energy, time and vessel utilization. These factors impact negatively on the process economics as they increase the operating costs.

The stirring power is directly affected by the size of the bath load for a given gas blowing rate. Although the slag phase increases the bath load, it is a vital component of the process. Efficient stirring is only possible when the influence of the slag phase on the process has been established. Knowledge of the slag impact on mixing and mass transfer rates in the converter operation helps to accurately

determine the necessary gas blowing rate for efficient stirring of the bath. It is therefore widely accepted that, a thorough understanding of the slag phase influence on mass transport in the bath is vital for efficient operation of the CLU-converter.

The refining processes take place at elevated temperatures and the large sizes of the industrial vessels used make direct experimental measurements and observations difficult. As a result, physical process models embodying water baths have generally been used to represent steel baths in research work^(1,2,3). In many cases the rate of an operation in a manufacturing vessel is determined or limited by how fast material and energy can be transferred⁽⁴⁾. This is called the rate of mass transfer.

By modelling the different processes in metallurgical vessels using water models, detailed relationships for mass transfer can be established. This information helps engineers to eliminate or significantly reduce over design and develop sound control structures thus improving the vessel operating revenues. By combining the model and empirical correlations that have been developed over time, it is possible to accurately predict for example the mixing time in the industrial vessel. This finding is of paramount importance for efficient operation of the converter as it defines the time needed for stirring under industrial conditions and enables the development of improved rules for sampling⁽⁵⁾. The predictions regarding the velocity fields within the system may also be quite helpful in the assessment of optimal stirring arrangements if for example, excessive refractory consumption is to be avoided.

The current study was initiated as an extension of previous work by Nyoka *et al.*⁽³⁾. Valuable mass transfer relationships and parameters were established in the work mentioned above. Although the established facts contributed to the knowledge gathered so far on the subject, the results obtained could not be extrapolated directly to the industrial-scale processing vessel without reflecting noticeable shortcomings. The reason for this was the omission of the slag phase

simulation in the investigations. However, this work formed the foundation of the present study to allow for easy comparison of the results thus facilitating the easy determination of the effects of incorporating the slag phase. The current investigation focused on seeking to establish the effect of a simulated slag phase on the mixing and mass transfer rates in the CLU-converter cold-model operation.

The slag phase was simulated by use of commercial grade kerosene. Mixing time and mass transfer rates were investigated under different operating conditions employed in the real system. Although a rigorous simulation of the actual CLU-converter was pursued, the top oxygen lance was not simulated in the investigation. The omission of the top lance was considered acceptable since it is not used continuously and for a long period of time during the actual blowing process in the commercial CLU-converter. Furthermore, the omission of top blowing has been acknowledged as reasonable due to evidence provided by J. M. Chou *et al.*⁽⁶⁾. Their investigations showed that as the gas flow rate of bottom blowing approaches $6.67 \times 10^{-4} \text{ m}^3/\text{s}$, gas blowing from the top has little effect on the mixing behaviour and mass transfer rates in the liquid bath.

2 LITERATURE REVIEW

2.1 The CLU process

The CLU-converter is basically a secondary refining vessel⁽⁷⁾. The metal is melted in the arc furnace and then transferred to the CLU-converter where it is gas purged using a combination of oxygen, nitrogen, steam and argon mixed in predetermined ratios. The aim of the process is to remove excess carbon and other impurities whilst retaining valuable elements. Addition of more alloying elements to the molten metal can also be conducted.

In the first stage of decarburisation, a top lance for oxygen blowing can be added. Conditions in the converter are tailored to favour the retention of chromium in the metal. High temperatures and levels of carbon favour the retention of chromium. The nickel content of the metal is largely unaffected by decarburization reactions.

An outline of stainless steel production in an arc furnace alone is necessary to understand the CLU process. In the arc furnace, decarburisation is brought about by lancing the bath with pure oxygen. The product of decarburisation is carbon monoxide that is essentially at 1atm. The remaining metal is in equilibrium with this gas at the temperature of the bath. These conditions determine the maximum amount of chromium that can remain in the bath at a given carbon content and temperature. As the carbon content decreases the equilibrium chromium content is lowered thus any chromium in excess is rapidly oxidised out. Most stainless steel production requires carbon content at or below 0.03%. At this carbon content, the equilibrium chromium level, even at 1800°C, is only about 4%. As a result, the conventional arc furnace practice for the manufacture of an 18% Cr, 8% Ni and 0.04% C steel could only use a charge mix with about 4% Cr in it. The equilibrium content of chromium can be increased significantly however, if the partial pressure of carbon monoxide in the vessel can be lowered⁽⁷⁾.

The heart of the CLU process is the control of the partial pressure of carbon monoxide in order to control the rate of the oxidation of carbon and chromium in a way that favours the retention of chromium and selective oxidation of carbon to low levels. Unlike the AOD process which uses almost the same principle, the main diluent of oxygen in the CLU process is steam and/or nitrogen not argon gas. The steam is used to control the partial pressure of carbon monoxide. At low carbon monoxide partial pressure, carbon removal is favoured while maintaining high chromium levels in the steel. The metal to be treated can have carbon content up to 3% and silicon content up to 1.2%. However, carbon and silicon contents of up to 1.2% and 0.5% respectively are generally used to reduce the refractory wear.

The process has a gas blowing period of between 1hr and 1.5hours. During the blowing period expert control of steam, oxygen and nitrogen that constitutes the blowing gas, keeps the temperature at less than 1680°C, reduces carbon content and retains chromium in the metal phase. The use of steam however, increases the hydrogen content of the metal. As a result, between 1.5m³ and 5m³ of argon gas per tonne of metal is needed to purge the hydrogen in the metal to less than 1ppm. The process consumables are given in Table 2.1 below. The exact amounts used depend on the grade of the stainless steel being produced and the charge to the CLU-converter.

Table 2.1: Process consumables in a typical CLU process⁽⁷⁾.

Consumable	Use per ton of metal
Steam	10 – 25 m ³
Nitrogen	10 – 25 m ³
Argon	1.5 – 4 m ³
Lime	50 – 80 kg
Silicon	5 – 20kg
Oxygen	10 – 40 m ³

The CLU-process is used in:

- Stainless steel production seeking short process cycles and high flexibility in raw material selection.
- Medium carbon ferrochrome and medium carbon ferromanganese production.
- Foundries specialising in stainless steel and high-alloyed castings.

2.2 Previous studies on mass transport in the CLU-converter

The process of mixing in a Creusot-Loire Uddeholm converter was studied by Nyoka *et al.*⁽³⁾ using one-fifth scale model experiments. The experiments were conducted in the absence of a simulated slag phase. This study would be referred to herein as, earlier work. The bath was stirred by air injection through five bottom-placed nozzles. Gas flow rates between the model and the real CLU-converter were related through the modified Froude number similitude. This was calculated to be 242.92 in both the real system and the model system.

The influences of gas flow rate between 0.010m³/s and 0.0183m³/s and bath height from 0.50m to 0.70m on mixing time were examined. Mixing times were assessed through pH against time measurements. The mixing time was defined as the length of time taken to distribute about 10ml of sulphuric acid in the gas purged bath up to 95% level of bath homogeneity. The results obtained showed that the mixing time reduced with increasing gas flow rate and decreasing bath height and vice versa. For each bath height investigated in this work, there existed a critical gas flow rate at which the mixing time exhibited a minimum value. This critical gas flow rate was found to decrease with increasing bath height. The mixing time results were evaluated in terms of the specific energy to the bath. A correlation was proposed for estimating mixing time in the model vessel under any given conditions of gas flow rate and bath weight. The relationship in Equation [1] below was established to relate the mixing time (T_{mix}) to the gas flow rate (Q) and the weight of the liquid (W) in the converter.

$$T_{mix} = 1.08Q^{-1.05}W^{0.35} \quad [1]$$

The rate of solid-liquid mass transfer was also investigated in this work. This was done by measuring the dissolution rates of solid benzoic acid specimens suspended in the model vessel. The dissolution of the solid specimens was characterised by calculated mass transfer coefficients and turbulence parameter values. The mass transfer coefficients and turbulence values were highest at the bath surface and decreased with increasing depth. The bath surface and the gas-liquid plume regions in the purged bath were identified as the zones exhibiting the highest mass transfer rates and turbulence effects. The mixing time results and the experimentally determined turbulence effects indicated the existence of a correlation between mixing time and turbulence parameter values.

The current study used all the results of this work by Nyoka *et al.*⁽³⁾ to establish the effect of the simulated slag phase inclusion in the model experiments. A further literature survey of the work done by other researchers on the same subject, allowed a better understanding of mixing and mass transfer rates in the model CLU-converter operation.

2.3 Mass transport in the CLU-converter

In steel making it has been found that the melting rate of scrap is dependent on the difference in the carbon content between the scrap and the melt, the degree of superheat above the liquidus temperature and the surface area of the scrap. The diffusion of the carbon from the melt to the solid-liquid interface lowers the melting temperature of the low carbon iron with melting points in excess of 1500°C. This process allows for the complete melting of low carbon scrap in the converter under the limited time available during a heat. Gas purging significantly improves the availability of carbon from the melt on the scrap metal-melt interface.

J.K. Wright⁽⁸⁾ investigated the effect of gas stirring conditions on the dissolution kinetics of steel in iron-carbon melts under conditions similar to those encountered in converter scrap melting processes. Under bottom injection gas stirring, he established that the kinetic power input had little effect on dissolution rates of the suspended metal rod in a hot metal bath. The rod dissolution rates were found to be controlled by the total gas flow rate. However, he noted that under jetting conditions in shallow baths the kinetic energy factor may be of greater significance. Mass transport conditions, under the gas stirring conditions, were measured in terms of derived mass transfer coefficients (K) that were found to have the following dependence on the gas injection rates (Q),

$$K \propto Q^{0.21} \quad [2]$$

Prior to this finding, J.K. Wright⁽⁸⁾ noted that, earlier work performed using the weight loss technique had indicated that the dissolution pattern was non uniform with the maximum dissolution rates occurring in the vicinity of the melt surface. The mass transport coefficients were largely independent of the bath depth away from the bath surface but showed a small increase towards the bottom of the bath. Results of his investigations showed that the rod diameters decreased linearly with the immersion time. He concluded that the dissolution rates are constant for isothermal conditions. The rod dissolution rates also showed an increase with increasing gas-stirring rates.

Another measure that is used to describe mass transport is the mixing time. Mixing time is defined as the length of the time taken before a given degree of homogeneity is established in a bath where a tracer solution has been added. A lower mixing time value indicates better mixing conditions in the bath and vice versa.

2.4 Physical modelling

To design a scale model, the closest geometrical and mechanical analogies must be maintained. Fixing the values of certain selected dimensionless quantities on

both scales allows the results on the scale model to be extrapolated to the true scale if these quantities are controlling the efficiency of the process. For similarity between a model and the real system operation, it is required that constant ratios between corresponding quantities exist. In order to properly represent an industrial system by a cold model, conditions in the model should be such that both geometric and dynamic similarities with the real system prevail. A geometrically similar 0.2-scale CLU-converter model was used for the current study. For this reason, only mechanical similarity of the model system to the industrial scale CLU-converter operation was considered.

Mechanical similarity is subdivided into requirements of static, kinematic and dynamic similarity between a model and the industrial system operation. Kinematic similarity is satisfied when geometrically similar moving systems have corresponding particles tracing out geometrically similar paths in corresponding intervals of time⁽⁵⁾. Proper selection of materials to simulate different phases in the real system is critical to achieving kinematic similarity of the model to the real system operation. Dynamic similarity is concerned with the forces that accelerate or retard moving masses in dynamic systems. It requires corresponding forces acting at corresponding times and locations in both the model and the actual converter operation to correspond.

The main objective of physical modelling is to achieve a realistic representation of a system by using materials and equipment from which useful measurements may be easily made in a cost effective manner⁽⁹⁾. Water modelling has been used successfully as a method for simulating the flow of molten steel within closed metallurgical processes for many years. Water has been acknowledged as a reasonable representation of molten steel due to evidence published by Sharma *et al.*⁽¹⁰⁾. They showed that motion of the bath is only due to the impact of the jet onto the surface of molten material in the electric arc furnace, i.e. the chemistry involved in the oxidation of the carbon does not affect the fluid mechanics. This observation was assumed to hold in the present study because the CLU-converter operation uses even higher gas flow rates. Under these conditions of gas purging,

the effect of chemistry have to be less pronounced in the highly turbulent environment. The feasibility of water modelling is further promoted by water at 25°C having the same kinematic viscosity as molten steel at 1600°C^(2,22).

The fluid flow in the bath is generated by the gas injection through the nozzles placed at the bottom of the vessel. This means that the flow patterns in CLU-converter bath are mainly governed by gravity, buoyancy and inertial force. Therefore, the most important dimensionless number for determining the dynamic similarity for gas injection into the liquid bath, in this case, is the modified Froude number. The trajectories of gas jets in the bath and the shape of the plume are a function of the modified Froude number. The range of the gas stirring rates used in the model were therefore determined using the modified Froude number below^(2,6,12),

$$N_{Fr} = \frac{\rho_g}{\rho_l} \frac{U_{g,nom}^2}{gd} \quad [3]$$

Where,

N_{Fr} is the dimensionless, modified Froude number

g is the acceleration due to gravity

ρ_g is the gas density

ρ_l is the liquid density

d is the diameter of the nozzle

U is the nominal gas velocity in the nozzles.

Table 2.2 and Table 2.3 below show some of the important physical properties that were considered and those adopted respectively, to achieve a close mechanical similarity of the two systems.

Table 2.2: Summary of physical properties of the real system at 1600°C.

Phase	Density $\rho(\text{Kg/m}^3)$	Viscosity $\mu(\text{cP})$	Surface tension (dyne/cm)
Steel	7200	5.85	$\sigma_{\text{steel}} = 1046$ $\sigma_{\text{steel/slag}} = 806$
Slag	3100	71.02	$\sigma_{\text{slag}} = 360$

Table 2.3: Summary of physical properties of the cold model system.

Phase	Density $\rho(\text{Kg/m}^3)$	Viscosity $\mu(\text{cP})$	Surface tension (dyne/cm)
Water	1000	0.2-8	$\sigma_{\text{water}} = 20-75$
Kerosene	860	$55.9^{\text{at } 37^\circ\text{C}}$	$\sigma_{\text{oil}} = 32$

2.4.1 Method of determining gas flow rate in water model

If N_{Fr} (water model system) = N_{Fr} (actual thermal system) then⁽⁵⁾,

$$\left(\frac{\rho_g U^2}{\rho_l g d} \right)_{\text{Model}} = \left(\frac{\rho_g U^2}{\rho_l g d} \right)_{\text{CLU}} \quad [4]$$

It is also known that the gas flow rate is given by, $Q = UA$. Re-arranging Equation [4] above and substituting for U , the gas flow rate in the model (Q_{Model}) can be related to the gas flow rate in the real system (Q_{CLU}) as follows,

$$Q_{\text{Model}} = Q_{\text{CLU}} \left(\frac{\rho_{l-\text{Model}}}{\rho_{l-\text{CLU}}} \right)^{\frac{1}{2}} \left(\frac{\rho_{g-\text{CLU}}}{\rho_{g-\text{Model}}} \right)^{\frac{1}{2}} \left(\frac{d_{\text{Model}}}{d_{\text{CLU}}} \right)^{\frac{5}{2}} \quad [5]$$

Where,

Q is the gas flow rate

U is the gas velocity in the nozzles

A is the cross sectional area of the nozzles

ρ_g is the gas density

ρ_l is the liquid density

d is the diameter of the nozzle

2.4.2 Effect of temperature and pressure on gas flow rate

For the actual vessel and its model system, the gas densities at the bottom nozzles are the two key parameters and are closely related to the gas flow properties. The most common practice for dealing with both parameters is to take the appropriate values under the bath temperature and static pressure observed at the nozzle outlet⁽²⁾.

To calculate the actual gas blowing rate at the operating conditions of pressure and temperature the following relationship can be adopted after a consideration of the gas law,

$$Q_{CLU-Actual} = Q_{CLU-Normal} * \frac{P_1}{P_2} * \frac{T}{273} \quad [6]$$

Equation [6] relates the actual gas blowing rate at the nozzles ($Q_{CLU-Actual}$) to the normal gas blowing rate ($Q_{CLU-Normal}$) taking into consideration the effects of temperature (T) and pressure (P). Where P_1 is the pressure at the bath surface and P_2 is the pressure at the bottom of the bath.

The pressure at the bottom of the bath can be calculated using Equation [7] below,

$$P_2 = P_1 + \rho_{Fe-slag} \cdot g H_L \quad [7]$$

Where $\rho_{Fe-slag}$ is the average density of the metal-slag bath and H_L is the bath height.

If a real system bath at a temperature of 1600°C with 10% slag by volume and a total bath height of 3.22m is considered, P_1 is essentially equal to the atmospheric pressure. The pressure at the bottom of the bath, P_2 , is calculated as follows,

$$\begin{aligned} P_2 &= 1.013 + \{(7200*0.9 + 3100*0.1)*9.81*3.22\}/100000 \\ &= 3.158 \text{ bars} \end{aligned}$$

The actual gas blowing rate ($Q_{CLU-Actual}$) and the normal gas blowing rate ($Q_{CLU-Normal}$) can be related using Equation [6] as,

$$Q_{CLU-Actual} = Q_{CLU-Normal} * \left(\frac{1.013}{3.158} \right) \left(\frac{1873}{273} \right) \quad [8]$$

Therefore

$$Q_{CLU-Actual} = 2.20 Q_{CLU-Normal} \quad [9]$$

Equation [9] can be used to relate the actual gas flow rate at the nozzles outlet of the real converter with the gas flow rate of the system under normal conditions.

2.4.3 Calculation of the similarity criterion

The Froude number was calculated using Equation [3]. The density of the gas used in the industrial CLU-converter was assumed to have the value of the density of oxygen since it is the heaviest of all the gases used. The density of the oxygen at the converter operating conditions can be calculated by considering the effects of temperature and pressure, i.e.

$$\rho_{g-CLU} = 1.43 \left(\frac{3.158}{1.013} \right) \left(\frac{273}{1873} \right) = 0.650 \text{ kgm}^{-3} \quad [10]$$

The density (ρ_{l-CLU}) of the bath with a slag phase constituting 10% by volume is calculated as follows,

$$\begin{aligned} \rho_{l-CLU} &= 7200 * 0.9 + 3100 * 0.1 \\ &= 6790 \text{ kgm}^{-3} \end{aligned}$$

The gas flow rate of $84.91 \text{ Nm}^3 \text{ min}^{-1}$ (i.e. $1.4152 \text{ m}^3/\text{s}$) considered as the average normal gas blowing rate in the real system in the earlier work⁽²⁾, was also adopted in these investigations. Under the real system conditions, this normal gas flow rate gives an actual gas flow rate ($Q_{CLU-Actual}$) in the nozzles of,

$$Q_{CLU-Actual} = 1.4152 \left(\frac{1.013}{3.158} \right) \left(\frac{1873}{273} \right) = 3.1145 \text{ m}^3 / \text{s} \quad [11]$$

The gas velocity in the nozzles ($u_{nominal}$ or U) can then be calculated using the following equation,

$$u_{nominal} = \frac{4Q}{\pi d^2} = \frac{4 * 3.1145}{5 * \pi * 0.0009} = 881.23 \text{ m / s} \quad [12]$$

The information above was used to calculate the Froude number for the real system by substituting the calculated gas velocity, U , into Equation [3] as follows,

$$N_{Fr} = \left(\frac{0.64978}{6790} \right) \left(\frac{881.23^2}{9.81 * 30 * 10^{-3}} \right) = 252.51 \quad [13]$$

If an average bath height of 0.64m and operating temperature of 20°C are considered for the cold system, the density of air that is used in the model operation can be determined using Equation [7],

$$\begin{aligned} P_2 &= P_1 + \rho_{water-oil} g H_L \\ &= 1.013 + [(1000*0.9+860*0.1)*9.81*0.64]/100000 \\ &= 1.0753bar \end{aligned}$$

Therefore

$$\rho_{air-Model} = 1.29 \left(\frac{1.0753}{1.013} \right) \left(\frac{273}{293} \right) = 1.276 \text{ kgm}^{-3} \quad [14]$$

The actual blowing rate ($Q_{Model-Actual}$) and the normal blowing rate ($Q_{Model-Normal}$) in the model can therefore be related to each other as shown in Equation [15] below,

$$Q_{Model-Actual} = Q_{Model-Normal} \left(\frac{1.013}{1.0753} \right) \left(\frac{293}{273} \right) \quad [15]$$

Thus

$$Q_{Model-Actual} = 1.0114 Q_{Model-Normal} \quad [16]$$

Combining Equations [5], [9] and [16] above the gas flow rate in the model under normal operating conditions can be calculated as,

$$1.01 Q_{Model-Normal} = 2.20 Q_{CLU-Normal} \left(\frac{986}{6790} \right)^{\frac{1}{2}} \left(\frac{0.64978}{1.27585} \right)^{\frac{1}{2}} \left(\frac{1}{5} \right)^{\frac{5}{2}}$$

Therefore

$$Q_{Model - Normal} = 1.06 * 10^{-2} Q_{CLU - Normal} \quad [17]$$

Equation [17] relates the gas flow rate in the real system and the model system under normal conditions of temperature (273K) and pressure (1atm).

2.5 Kinetics of reactions

Kinetic studies can be used to examine the step-by-step progress of a reaction. They help to identify conditions that should be varied in order to achieve an increase in the rate of a particular reaction. At the high temperatures involved in steelmaking, reactions that occur in a homogenous gas or liquid are usually rapid. When heterogeneous reactions occur between two phases in addition to any chemical reactions involved, the mechanism usually involves mass transport. The various species involved in the chemical reaction are moved to or from the interface and transferred across the interface between the phases. Any one of the steps may control the overall reaction rate and the rate-controlling step may change when the imposed conditions are changed⁽¹⁸⁾. Since the mixing and mass transfer processes are an integral part of the chemical reactions taking place, investigations of these parameters in a model can give useful pointers to efficient CLU-converter operation.

By studying the output characteristics of the tracer concentration, it is possible to diagnose the reactors mode of behaviour and likely chemical efficiency. Mixing time measurements have been utilized a lot in the study of mass transport in metallurgical vessels. Measurement of the mixing time has proved to be an indication of the intensity of mixing in the vessel⁽⁵⁾. Several chemical reactions are controlled by liquid phase mass transfer between the gas jet and the liquid, therefore knowledge of variables such as nozzle diameter, flow rate and the depth of the nozzle is important⁽⁴⁾.

2.6 The slag phase

The primary function of a refining slag is to serve as a receiver of impurities from the metal. It may be required also to fulfil other needs such as controlling the supply of oxygen from the atmosphere into the metal or act as a physical barrier to passage into the metal of gaseous species such as hydrogen, nitrogen and sulphur. The formation of slag from solids is endothermic and generally the thermal efficiency of a process is related inversely to the volume of the slag. The most important characteristic of slag to the current study is its effect on the mixing and mass transfer processes taking place in a metallurgical reactor like the CLU-converter.

When considering the mixing and mass transfer processes in a converter operation, density is a vital physical property of the slag phase. The slag density determines the maximum mixing possible for the metal and slag phases in a purged bath. The slag density is dependent on the oxide components constituting it and their ratios in the slag⁽⁹⁾. Different operations require different slag compositions. Therefore, the slag density value depends on the product to be produced, the chemical compositions of the fluxing material and the initial composition of the metal to be purified. Generally the density of the silica is much lower than that of the other oxides in slag, therefore slag densities decrease with increasing silica content at a given temperature.

The average slag density that is employed at Columbus Stainless Steel was taken into consideration during the selection of an appropriate liquid to use for slag simulation in the model. Selection of the material to simulate the slag in the model was based on its satisfaction of the metal/slag density ratio, the viscosity and more importantly the modified Froude number value as in the actual system. The use of water to represent the metal phase posed difficulties on the selection of an appropriate liquid to simulate the slag phase. In the absence of a viscous enough liquid that has a density less than half that of water, a compromise liquid was adopted instead for slag simulation.

Viscosity of liquid slag has a marked effect on the speed and efficiency of the extraction and refining operations especially in the absence of forced convection conditions⁽¹⁾. At constant composition, the rates of mass transfer by diffusion and convection are related inversely to the viscosity of the melt. The viscosity and the metal/slag density ratio have a huge influence on the equilibrium metal-slag separation possible. When the ratio is large and the viscosity of the slag is low, the metal-slag separation possible during cooling of the refined metal from the converter is great. The result is a more efficient process.

Since the density of the slag is one of the most important properties in a gas stirred converter operation, a slag phase of mainly kerosene reflecting the same density value as the real system slag could be tailored with the aid of low density solid particles. The only draw back though, is the fact that the use of solid particles in slag simulation results in the alteration of viscous forces of the simulated slag phase. However for the purposes of the current study, solid particles could have been used to simulate slag. In this instance, the change in the simulated slag phase viscosity could have been overlooked on the grounds that the viscous effects are confined to the smallest eddies in the jet of the purge gases. Such eddies have little effect on the transport of momentum by the larger turbulent eddies associated with moderate and high Reynolds number flows⁽⁵⁾. Therefore, the absence of viscous forces when solids are used could not have significantly affected the validity of the results of the experiments. Although solid particles incorporation in the simulation of the slag phase appeared possible, commercial grade kerosene alone was considered a better option for purposes of the current study.

2.6.1 Effect of slag phase on mixing time

The presence of an oil layer in the model CLU-converter was found to increase the mixing time significantly for all the three nozzle configurations investigated by Akdogan and Eric⁽¹⁵⁾. They reported that the mixing time values recorded in the presence of a simulated slag layer tended to be longer than those for similar

experiments performed without slag simulation. The observation was explained in terms of the simulated slag layer tending to dissipate some of the input energy.

Manabu Iguchi *et al.*⁽¹⁶⁾ studied the effects of surface flow control on fluid flow phenomena and mixing time in a bottom blown bath. They concluded that the mixing rates in bottom blown baths could be changed by controlling the surface flow. This finding is useful for controlling the mixing time in actual refining processes where bottom gas injection can be accompanied by solid scrap addition in the converter.

In an earlier study, Manabu Iguchi *et al.*⁽¹⁷⁾ revealed that when a swirling motion of a bath contained in a cylindrical vessel took place, the mixing time was shortened greatly. This was not observed in a case where the swirl motion was stopped by bringing a circular cylinder into contact with the bath surface. This showed that the mixing time in the bath could be changed drastically by controlling the surface flow. As a consequence of a marked density difference between the metal and slag, the proportion of the slag phase is higher on the bath surface than at the bottom even during bath stirring. In light of this, the presence of the viscous slag phase can be seen as slightly inhibiting the swirling of the bath thus prolonging the bath homogenization.

2.7 Mixing in the gas stirred systems

The results of several studies^(2,12,18) showed that the rate of mixing in metal processing operations depends on the rate of energy input or energy dissipation. In gas-stirred metallurgical vessels the turbulence caused by the gas-liquid plume rising through the bath facilitates the increase in mixing. The result of that is increased surface contact of two immiscible liquids, metal and slag. An increase in liquid mixing promotes the overall rate of chemical reactions in the bath because of prevailing high mass transfer rates.

Optimum control of mixing in current refining processes accompanied by bottom gas injection has become increasingly important because the metallurgical reactions in the bath proceed at different sites simultaneously. The intensity of mixing is commonly represented by the mixing time, T_{mix} . Mass transfer coefficients have generally been used to compare the mass transfer characteristics of given systems, as they are independent of vessel size.

The influence of gas stirring on the rates of dissolution of steel has been receiving particular attention recently. In the early days, Mori and Sakura⁽⁸⁾ studied the influence of gas stirring in an indirect way by dissolving iron rods containing up to 1.14% oxygen in Fe/C melts. During the dissolution, the oxygen in the iron reacted with the carbon in the melt to produce carbon monoxide at the surface. It was found that the gas evolution markedly enhanced the dissolution rates especially under normal convection conditions.

Lehner *et al.*⁽¹⁹⁾ immersed graphite rods into argon stirred melts of known composition for specified times. The changes in dimensions were determined and the mean mass transfer coefficients calculated. It was found that the dissolution pattern was non-uniform, with the maximum dissolution rates occurring in the vicinity of the melt surface. The mass transport coefficients were largely independent of the bath depth away from the bath surface but showed a small increase towards the bath bottom.

After investigation of the steel dissolution rates in quiescent and gas stirred Fe-C melts, J.K. Wright⁽⁸⁾ concluded that the orifice size had negligible effect on the dissolution rates at constant gas flow rates. This indicates that the kinetic power input of the injected gas is relatively unimportant compared to the buoyancy mixing power. The dissolution rates of the rods outside the plume region were found to be lower than the rates in the gas-liquid plume region at the same gas flow rate. The rates were found to increase with increases in the gas injection rates.

Castillejos and Brimacombe⁽²⁰⁾ investigated the physical characteristics of gas jets injected vertically upward into liquid metal. Measurements of profiles of bubble velocity and bubble pierced length revealed that the kinetic energy of the gas is dissipated close to the nozzle, and buoyancy dominates flow over most of the plume. In this region the bubble flow velocity increases with increasing gas flow rate but is independent of the orifice gas velocity. This was in agreement with the work by J.K. Wright⁽⁸⁾ and the earlier work by Castillejos and Brimacombe⁽²¹⁾. They made the summary that, different flow regimes existed in the plume region. In the zone close to the nozzle, bubble motion and size are strongly affected by gas injection velocity and density. The bubbles forming in this region are unstable and break up as quickly as they form. It has been found that the discharge velocity of the gas decreases abruptly in the vicinity of the injector. Further from the nozzle is the developed region where the bubbles rise only under the influence of buoyancy. In this region, the bubble-size distribution remains constant and can be fitted by a log normal function. The orifice gas velocity and the liquid physical properties affect the average size of the bubbles in this region.

The effectiveness of gas injection in promoting gas-metal reactions and/or enhancing bath stirring in these processes is linked to the degree of dispersion of the gas in the bath, the residence time or velocity of the gas in the molten metal and the size of the bubbles. The injected gas disperses in the bath due to entrainment of the surrounding liquid into the plume. During bottom injection, the plume takes on a conical shape with an angle of inclination to the vertical of approximately 20° in both water and steel baths⁽²⁰⁾. The dispersion of the gas in the radial direction of the plume being perpendicular to the main flow direction is well represented by the Gaussian distribution. The spatial variation of the gas fraction can be correlated with the Froude number.

2.8 Established correlations

By equating the energy supplied by rising bubbles to turbulent energy losses within the liquid, Sahai and Guthrie⁽²²⁾ showed that the mean rising plume velocity (u) is given by,

$$u = \frac{Q^{1/3} L^{1/4}}{r^{1/3}} \quad [18]$$

Where, L is the liquid depth, r is the radius of the vessel and Q is the gas flow rate.

In order to explain the effect of gas flow rate (Q) on the mass transfer rate constant (K), several researchers have come up with different mathematical relationships to explain the mixing phenomenon in the reactors. Asai *et al.*⁽²³⁾, presented the results of earlier studies and their own work in terms of the values of exponent n , in the relationship,

$$K \propto Q^n \quad [19]$$

Where n is the stirring factor of the gas flow rate, Q .

As n is increased, the effect of gas flow rate on mass transfer becomes more significant. Numerous values of n have been reported in various plant and pilot plant studies of the desulphurisation of steel as well as in many model experiments. The value of the exponent n , as reported by Asai *et al.*⁽²³⁾, varies approximately from 0.25 to 2.1.

Akdogan and Eric⁽¹⁵⁾ studied the mixing intensity induced by jets during ferroalloy refining using a simulated one-seventh water model of the CLU-converter. Their investigations were aimed at establishing the influence of bath mixing intensity on mass transfer induced by bottom blown jets in high strength vessels. They established that the mixing time decreased with increasing gas flow

rates up to a critical point. After the critical point increasing the gas flow rate had adverse effects on the mixing time as it started to increase with gas flow rate at a constant bath height.

2.8.1 Effect of specific energy input on mixing time.

Energy input to the bath is in the form of gas injection into the reactor through nozzles at the bottom of the vessel. Generally an increase in the gas injection rate results in higher mass transfer rates thus, quick mixing. Akdogan and Eric⁽¹⁵⁾ evaluated the effect of gas injection on the mixing time in terms of specific energy input (stirring power density) to the system. The specific mixing energy (E_t) supplied to the bath by a gas jet comes from two sources i.e. kinetic energy (E_k) of the gas in the jet and buoyancy energy (E_b) supplied by the gas bubbles rising per unit weight of the bath liquid.

$$E_t = E_b + E_k \quad [20]$$

The specific buoyancy energy is given as⁽²³⁾,

$$E_b = \frac{855 QT}{W} \log \left(1 + \frac{H}{10.339} \right) \quad [21]$$

Where, H is the bath depth, W is the weight of the bath, T is the temperature and Q is the gas flow rate.

The rate at which the gas jet transfers kinetic energy to a specific weight of the bath is given by⁽²⁵⁾,

$$E_k = \frac{\rho_g Q^3}{2WA^2} \quad [22]$$

Where A is the cross sectional area of the nozzles, Q is the gas flow rate, ρ_g is the gas density and E_k is the kinetic energy of the gas jet.

Nakanishi *et al.*⁽¹⁸⁾ correlated the mixing time in various systems to the stirring power input per unit weight of the bath. They were the first to plot the mixing time (T_{mix}) data against specific energy dissipation rate (E_t). The functional relationship adopted is expressed as:

$$T_{mix} = aE_t^{-b} \quad [23]$$

Where a is a constant and b is a coefficient. Both quantities are determined experimentally.

Akdogan and Eric⁽¹⁵⁾ showed that increased energy input to the bath would increase the turbulence and the bulk velocity, that in turn decreased the mixing time.

2.9 Water properties

The properties of water that were of much significance to the current study were pH and temperature. The two properties can be related to each other by the Nernst equation. Since the experiments were carried out through different seasons, water properties changed accordingly. The pH values had to be temperature compensated before they could be compared. The output of all pH electrodes varies with temperature in a manner predicted by the Nernst Equation⁽²⁶⁾.

The need for temperature compensation depends on three variables:

1. The changes in temperature.
2. The pH value being measured.
3. The desired measurement accuracy.

As shown in Appendix 1, the pH error due to temperature is a function of both the temperature and the pH value being measured. Temperature effects are only absent if the liquid is at a temperature of 25°C or has a pH of 7. The more the

temperature changes from the ambient calibration temperature and the more the pH departs from 7, the greater is the pH error.

2.10 Two-phase mass transfer

Alloying is usually performed by adding solid material to the molten primary metal in the converter. It is therefore in the best interest of the metallurgist to know the general dissolution characteristics of the additions under varied conditions for easier process control. Mass transfer data has generally been expressed in the form of dimensionless numbers. These numbers are a combination of physical quantities whose values determine for example, bath movement, mass transfer rates, etc in a reactor.

In cold model experiments, benzoic acid specimens in water can be used to simulate solid additions in the metal bath in the converter. The dissolution of benzoic acid in the agitated water bath may be expressed as,

$$\frac{dm}{dI_t} = KA (C_s^* - C_s) \quad [24]$$

Where K is the mass transfer rate constant, A is the total surface area of the benzoic acid, C_s^* saturation concentration of acid, C_s is the bulk concentration of the acid and dm/dI_t is the dissolution rate of benzoic acid.

Many factors influence the mass transfer from benzoic acid specimen immersed in the liquid bath. The dissolution rate is determined by diffusion that is influenced by several factors that include:

- Concentration gradient between the bulk liquid and the inner region of the pores and the specimens' surface.
- Viscosity and density of the liquid medium dissolving the specimens.
- Operating temperature
- Porosity of the benzoic acid specimens.

Temperature variations in the experiments needed to be closely followed since diffusion is affected by these changes. Table 2.4 below shows the variation of dissolving capacity of water for benzoic acid at different temperature levels. The concentration gradient, $C_s^* - C_s$, represents the driving force of the dissolution process. An increase in the value of, K , indicates better mixing in the bath, which results in faster approach to equilibrium conditions. The value of K is independent of temperature, thus mass transfer characteristics of the bath can be compared for experiments carried out at different temperatures.

Table 2.4: Solubilities of benzoic acid in water⁽²⁶⁾.

Temp. (°C)	g/100g water	Temp. (°C)	g/100g water
0	0.17	50	0.85
10	0.21	60	1.20
20	0.29	70	1.77
25	0.34	80	2.75
30	0.42	90	4.55
40	0.60	95	6.80

The mass of a solid benzoic specimen (m) and the surface area of the specimen (A) can be calculated as, $m = \rho_s \pi R^2 L$ and $A = 2\pi RL$ respectively. Where ρ_s is the average density of the benzoic acid specimens, R is the specimen's radius and L is its length. Considering the calculated mass, the benzoic acid surface area and taking the benzoic acid concentration in the bulk liquid (C_s) to be zero, from Equation [24] the mass transfer coefficient may be estimated from,

$$K = \left(\frac{dR}{dI_t} \right) \frac{\rho_s}{C_s^*} \quad [25]$$

The local value of the mass transfer coefficient may also be estimated theoretically. For similar experimental work, J. Szekely *et al.*⁽⁵⁾ used the Sherwood based correlation,

$$Sh = 2 + 0.72(Re_{loc,r})^{0.5}(Re_t)^{0.25}(Sc)^{0.33} \quad [26]$$

Where Sh is the Sherwood number, $Re_{loc,r}$ is the local nominal Reynolds number, Re_t is the turbulent Reynolds number and Sc is the Schmidt number.

Mazumdar *et al.*⁽²⁷⁾ reported results on dissolution of benzoic acid cylinders submerged in water and suggested the following correlation,

$$Sh = 0.73(Re_{loc,r})^{0.25}(Re_t)^{0.32}(Sc)^{0.33} \quad [27]$$

The Sherwood number (Sh) incorporates the mass transfer coefficient and it is a factor of vessel geometry and operating process conditions. It is represented by,

$$Sh = \frac{KD}{D_o} \quad [28]$$

Where K is the mass transfer rate constant, D is the vessel diameter and D_o is the mass diffusion coefficient.

The Reynolds Number is directly proportional to the inertial forces and inversely to the viscous forces. It is divided into two parts, the local nominal Reynolds number ($Re_{loc,r}$) and the turbulent Reynolds number (Re_t). The Schmidt Number can be defined as the ratio of momentum diffusivity to mass diffusivity and represents the relative ease of molecular momentum and mass transfer. It is directly proportional to the kinematic viscosity and inversely to the molecular diffusivity, i.e.

$$Sc = \frac{\nu}{D_o} \quad [29]$$

Where ν is the kinematic viscosity, D_o is the mass diffusion constant and Sc is the Schimdt number.

2.11 Factors affecting dissolution of additives

In the real systems the factors that affect the dissolution rates are,

- the method of introducing the additives
- the particle sizes of the additives
- the temperature of the bath
- the carbon content of the bath
- the gas stirring rates and
- the chemical and the physical properties of the material being added

Dissolution under natural convection carried out by J.K. Wright⁽⁸⁾ indicated that dissolution rates increase with temperature. Experiments carried out under gas stirring in a 1kg apparatus showed that the dissolution rates were higher in melts with a higher carbon content. The gas flow rate was found to increase the dissolution rate of the rods in the 25kg apparatus. He explained the higher rates of dissolution to be a result of an increase in turbulence as the gas flow rate increased.

2.11.1 Turbulence and its effect on mass transfer

Turbulence has been reported to play an important role in the mass transfer processes. J. Szekely *et al.*⁽⁵⁾ investigated mixing, the flow phenomena and mass transfer in argon stirred ladles. The mass transfer measurements obtained for the dissolution of carbon rods in argon stirred melts provided semi-direct confirmation of predictions made regarding the turbulence patterns within the system. The mass transfer rate was observed to increase with an increase in the

stirring gas flow rate. Turbulence was directly related to the stirring gas flow rate in the converter. They also found that the local turbulence exhibited appreciable spatial variations. The vicinity of the plume recorded high levels of turbulence especially in the upper regions. This is the region where the mass transfer and possibly coalescence of the inclusion particles is greatest. This might be the optimal region to introduce additives in the real system.

Results from similar investigations by J.K. Wright⁽⁸⁾ gave an approximately parallel-sided shape of the rods that were submerged in a purged molten bath with some necking at the surface. Plots of rod diameter against immersion time showed that the rod diameter decreased linearly with immersion time thus, showing that the dissolution rates are constant for isothermal conditions.

2.11.2 Determination of mass transfer parameters

Turbulence characteristics can be estimated using Equation [27] if it is re-arranged to,

$$\left(\text{Re}_{loc,r}\right)^{0.25} \left(\text{Re}_t\right)^{0.32} = \frac{Sh}{0.73(Sc)^{0.33}} \quad [30]$$

The values of the Sherwood Number were calculated for the experimental conditions according to Equation [28]. The kinematic viscosity of the kerosene was provided by the manufacturer as being greater than 65cS at 37.8°C. The provided value of kinematic viscosity was adopted and the Schimidt Number was then calculated from Equation [29]. Its value was found to be 1474 for all the experimental conditions investigated at an average temperature of 20°C.

After re-arranging Equation [30] above and substituting for the Sherwood number (Sh) to make the mass transfer coefficient the subject of the formula, the following relationship was obtained;

$$K = 0.73(Sc)^{0.33} (\text{Re}_{loc,r})^{0.25} (\text{Re}_t)^{0.32} \left(\frac{D_o}{D} \right) \quad [31]$$

Using Equation [31], the rate of dissolution of additives in the hot molten bath can be estimated accurately.

3 EXPERIMENTAL MEASUREMENTS

3.1 Introduction

The equipment used and the experimental set-up adopted was similar to that used in the earlier study⁽²⁾. The slag simulation procedure adopted in the current study provided the major difference. The experimental set-up consisted of a clear cylindrical PVC tank that is one-fifth the size of the CLU-converter that was being simulated. Figure 3.1 shows the experimental set up that was adopted for part of the investigation.

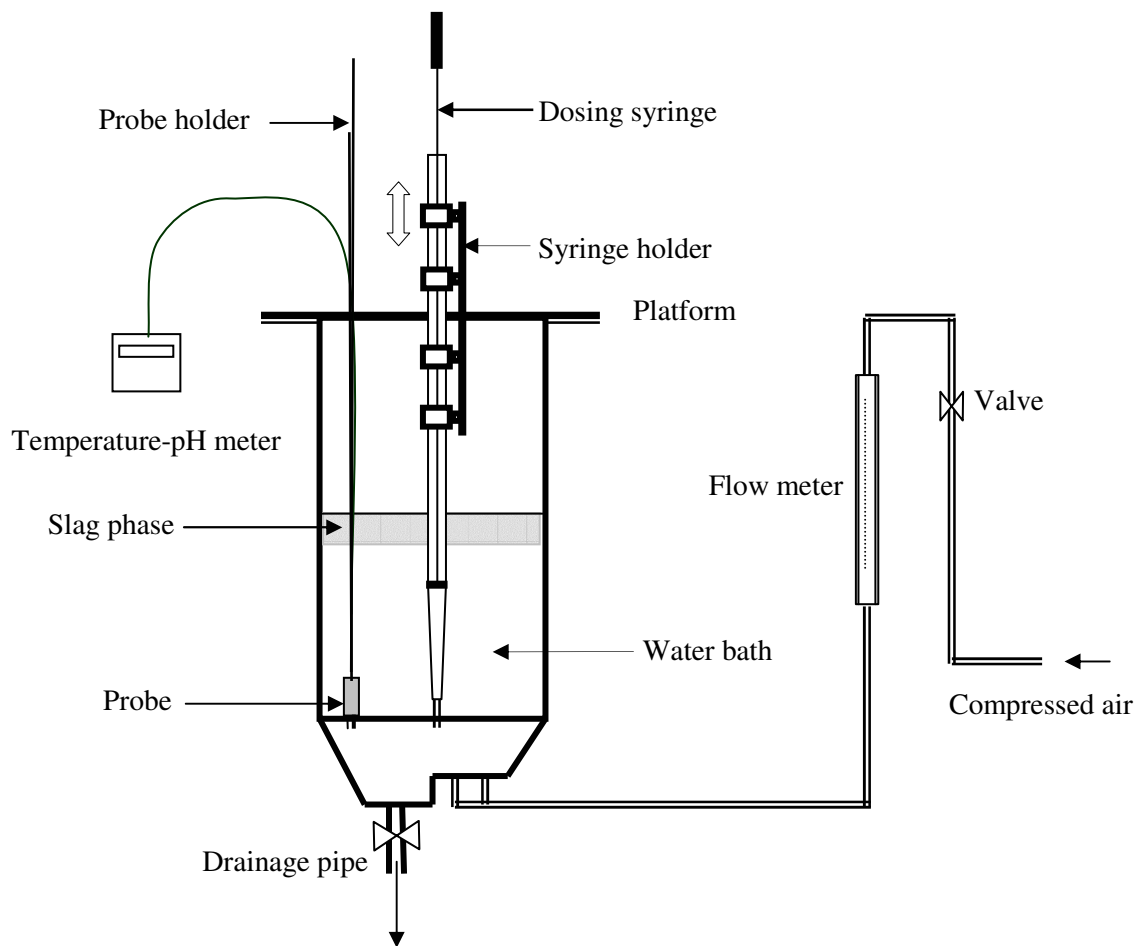


Figure 3.1: The schematic representation of the 0.2-scale CLU-converter model showing the general set-up of the apparatus used in the experiments.

Ideally de-ionised water should have been used for the experiments. However for the majority of the experiments carried out, a measured volume of tap water mixed with about 25l distilled water was adopted to simulate the metal bath. Comparable results were obtained in experiments performed using either distilled water or a mixture. The observation was then used as the basis for justifying the use of the distilled water-tap water mixture to represent the steel phase in the model experiments. Ten percent, by volume, commercial grade kerosene (with density 0.867g/cm^3) was added to simulate the slag phase.

Air was purged into the bath through the five nozzles at the bottom of the model. The experiments were divided into two parts i.e. the mixing time experiments and the solid-liquid mass transfer experiments. The modified Froude number was considered as the similarity criterion to correlate the gas flow rate between the scale model and the full-scale system. During the experiments the gas flow rates varied from $0.0100\text{m}^3/\text{s}$ to $0.0212\text{m}^3/\text{s}$. The bath height in the model was varied from 0.50m to 0.70m excluding the kerosene layer. This bath height that did not include the slag phase was defined as the water bath height.

3.2 Experiments and sample preparation

1. About 25l distilled water was first introduced into the model and then fresh tap water added until the water bath height had reached the required mark. In the case when pure distilled water was used, it was slightly purged to bring its temperature to that of the surroundings before the experiment started. This was found necessary, as results obtained from experiments performed without this preparatory stage were inconsistent. The tap water used had a pH value greater than 8.30 as a result of the dissolved basic species. The distilled water that was added being at a lower pH level reduced the pH of the bath to levels between values 8.10 and 8.30 at an average temperature of about 20°C .
2. Kerosene was used to represent the slag phase in the experiments. The pH value of the kerosene was ± 4 before use. The kerosene representing the

slag phase was re-used in about ten different experimental runs before being discarded. The number of experimental runs that the kerosene could be re-used was limited to reduce the errors that could have arisen from a decrease in its viscosity and/or other changes in its physical properties. A two stage washing process was adopted to clean the kerosene before it was re-used. The first stage of the washing process involved, purging the used kerosene with gas in about 75l fresh tap water that was later drained out after allowing it to settle for 10minutes. The second stage was almost similar to the first one but about 40l distilled water was used to finish the washing process. Sometimes it was necessary to add fresh kerosene to make-up for amounts lost during the experimental runs and cleaning. The volume of the kerosene was maintained at 10% of the total bath volume.

3. Moulding of the benzoic acid specimens that were used for mass transfer experiments was done in steel casting cylinders that had a stainless rod in the middle. Commercial grade benzoic acid was melted in a glass beaker at 250°C and then the molten material poured into the casting cylinders. The molten material was allowed to cool under normal atmospheric conditions. Ordinary white floor polish was used as the mould release agent during the making of the specimens. The hollow specimens produced had an outside diameter of about 44mm and lengths that ranged between 55mm and 69mm.

3.3 Bath mixing intensity measurements

Mixing intensity of the bath was established from measuring the time taken to attain uniform dispersion of commercial grade sulphuric acid in the water-kerosene bath. The experiments were carried out using the pH measurement technique. As a first step, experiments were carried out to establish the best location for the pH-temperature probe in the bath and the point of injecting the tracer solution. The temperature of the fluid system in the CLU-converter model was closely monitored and recorded for every pH reading that was taken.

3.3.1 Establishing location of the probe and the dosing point

For these trial runs, different positions of locating the probe and effecting acid-dosing were investigated. Appendix 2 presents the different set-ups that were investigated. With the probe and dosing syringe firmly fixed on the platform on top of the model, the purge gas valve was opened and the gas flow rate monitored until it stabilized to a required value. The initial pH and temperature of the bath were recorded on a log sheet before a volume of about 10ml concentrated sulphuric acid (98%) was added. The acid was used as a tracer solution during the experiments. The concentration of the tracer in the bath was monitored using an electrode that was linked to a pH meter. A specially made syringe was used for acid dosing at the various positions in the bath. Dosing was simultaneously carried out with the starting of the stopwatch.

Acid dosing involved quickly dipping the syringe into the bath and then injecting the acid. After dosing was completed, the pH and temperature changes with time were followed. On average the process of acid dosing took five seconds thus, all the measurements started after a time interval of at least this period. For every experimental run conducted, measurements continued for at least a period of 15minutes. Time intervals of four seconds were adopted for taking measurements of the pH and temperature during the first 2minutes of purging, thereafter one minute intervals were used for taking readings.

A constant bath height of 0.5m was adopted for these experiments. All the experimental runs carried out to establish the location of the probe and the acid dosing point were performed in the absence of the slag phase. Bath homogeneity was defined at 99.66% acid distribution. The mixing time (T_{mix}) was established by calculating the pH value that gave this level of homogeneity and then checking the corresponding time recorded on the time-pH-temperature log sheets that were used. An average of at least five of these values was then taken as the T_{mix} value for the specified conditions.

To check if the solution had satisfied the 99.66% homogeneity level the following formula was used,

$$\frac{pH_{99.66\%} - pH_i}{pH_{cs} - pH_i} = 0.9966 \quad [32]$$

Where $pH_{99.66\%}$ is the pH value when 99.66% bath homogeneity was established, pH_{cs} is the temperature compensated value of recorded stable pH and pH_i is the initial pH of the bath before acid dosing.

Equation [32] can be reduced to,

$$pH_{99.66\%} = 0.9966 pH_{cs} - 0.0034 pH_i \quad [33]$$

Appendix 1 shows the variation of pH with temperature. The pH versus temperature error chart given shows that, as the temperature drops from 25°C to 15°C a corresponding drop in pH of 0.135units results if the bath pH is between 2 and 3. Thus, a temperature drop of 1°C results in the pH of the bath dropping by 0.0135 pH-units. This adjustment was made on all the ‘stable’ pH values recorded. The pH values that were recorded on the meter were unstable and kept on fluctuating even after 15minutes into the experiments. The stable pH was therefore defined as, the value that recorded most close to the 15minutes mark that was adopted as the duration of the experimental runs. Although the pH was never free of fluctuations, after this period of purging its value displayed on the meter was observed to be relatively stable over longer periods of time.

3.3.2 Mixing time measurements

Trial runs carried out established the position of the probe and the position for effecting acid dosing adopted for this part of the investigations. The bath was stirred by opening the purge gas valve to pre-determined levels as before. Except for one gas flow rate investigated during the earlier study⁽²⁾ all the others were retained for the current mixing time investigations, and so were the other

conditions. This was done to allow for a clear comparison of results obtained in the absence of slag and those in the presence of slag.

The mixing time, T_{mix} , was measured at 99.66% bath homogeneity. Under a given set of conditions a minimum of eight runs were performed. The average of the measured values was taken to represent the T_{mix} , value under the conditions of the experimental runs. Trial runs conducted established that, relatively stable pH conditions in the bath could only be experienced after a stirring period of not less than 15minutes. As a result of this observation, the experimental runs were made at least 20minutes long. The pH value that recorded most after the 18minutes period was taken as the stable pH value of the bath i.e. pH_s . Recording of the pH and temperature values after 18minutes was conducted at 30seconds intervals. To calculate the pH value of the solution at 99.66% homogeneity Equation [33] was used.

3.4 Mass transfer experiments

To establish the mass transfer parameters in a one fifth CLU-converter model the mass loss technique was employed. The experiments involved measuring the mass losses on the specimens and then calculating the mass transfer coefficients values from the experimental data. The prepared benzoic acid specimens were weighed and suspended in the water bath by fastening them onto suspension rods. The rods were mounted on a platform at the top of the CLU-converter model. Both, top and bottom, ends of the benzoic acid cylinders were enclosed between thin PVC plates that were rubber lined on the inside to provide water tightness. The rubber lining was meant to ensure that only radial dissolution of the specimen during the experiments occurred. The suspended specimens were exposed to dissolution/erosion by the agitated water-kerosene bath for periods of 15minutes to ensure that reasonable weight losses were recorded. Appendix 3 shows the pictorial view of the equipment used for the experimental work.

Since benzoic acid is only partially soluble in water, the purge gas valves were opened whilst the specimens were already in the water bath. Dissolution, if any that occurred during this part of the experiment was considered negligible. The stopwatch was started at the same time as the opening of the gas valves. The temperature of the bath was measured before and after bath purging. The average of the two values was taken as the temperature under which the experiment was conducted.

The specimens withdrawn from the bath after the dissolution process were wrapped in an absorbing tissue material for at least 20 hours before their masses were measured. Weight loss was calculated by subtracting the final ('tissue dry') mass of the dried specimen from its initial mass measured before the start of each purging process. At each setup, at least seven independent experimental runs were conducted using the same specimens.

In some cases the final mass of the specimen was found to be more than the initial mass weighed or the dissolution observed was very little during the first two experimental runs. The inconsistencies were attributed to the different levels of absorbed liquid in the specimens before and after the experimental run. The absorbed liquid in the specimens from the first two experimental runs was found to be less than that of a saturated specimen. The specimens were found to be saturated after the second experimental run. When the specimens became saturated the absorbed liquid levels at the beginning of the experimental run equalled that of the tissue dried specimen. Correction of the recorded weight losses was therefore necessary for the first two experimental runs.

The weight losses recorded for the first two experimental runs were corrected by adding the differences in the absorbed liquid mass on the obtained values. This absorbed water-kerosene mass was determined by subtracting the 'oven dry' mass from the 'tissue dry' mass. The 'oven dry' mass was obtained by oven drying and then weighing selected tissue dried specimens. The selected specimens included had been exposed to purging at the different gas flow rates investigated. This kind

of selection was found necessary because the amount of absorbed liquid depended on the gas blowing rate during purging. Oven drying involved washing with soap the weighed tissue dried specimens and then putting them into an oven set at 55°C for 15minutes. The specimens from the oven were allowed to dry for a further 30minutes in open air. After they had dried, the specimens were again wrapped for a further 20hours period before weighing them to determine the ‘oven dry’ mass. This exercise was done for the first two experimental runs of the first set of experiments only. At least three samples that were exposed to purging under specific gas flow rate conditions were investigated for absorbed water-kerosene. The average of the three values was then used to correct the corresponding weight losses at the first two experimental runs of all the experiments carried out under the same conditions of gas purging.

After the first two runs, it was experimentally proven that the specimens had absorbed enough water-kerosene that was retained after drying the specimen in a tissue paper for 20hours. The same procedure explained above was adopted to establish this. Therefore, the weight losses recorded from the third experimental run were attributed entirely to dissolution of the specimens. The radii of the specimens were calculated from weight loss measurements.

The exact spatial positioning of the specimens in the baths was as shown in Appendix 5 for the first part of the experiments and as in Appendix 6 for the second part of the investigations. The first part of the experiments sought to establish the effect of bath height and gas flow rate on mass transfer at selected locations in the bath. These investigations were performed at water bath heights of 0.40m, 0.50m and 0.65m. For each bath height investigated, kerosene was 10% by volume of the bath. Under a given set of conditions, about four different tests were carried out and an average taken to represent the dissolved mass of the specimen under the conditions.

The second part of the investigations sought to map out the variations of the mass transfer coefficient in the cold model at a water bath height of 0.50m. Although

the bath height was kept constant for this part, the gas flow rate was varied to establish its effect on the mapping of the mass transfer coefficient in the bath. Under a given set of conditions two tests (each composed of at least seven experimental runs) were carried out and an average taken to represent the dissolved mass. Gas flow rates of $0.010\text{m}^3/\text{s}$, $0.0150\text{m}^3/\text{s}$ and $0.0212\text{m}^3/\text{s}$ were investigated for the mass transfer experiments.

4 RESULTS AND DISCUSSION

4.1 Establishing location of the probe and the dosing point

The results of the experiments that were carried out to establish the positions to place the pH-meter probe and to perform acid dosing are presented in Table 4.2 below. The variations of the average mixing time (*Ave. T_{mix}*) and the median values (*Med.*) of the obtained mixing times were analyzed at all arrangements investigated. The *Q*-test was used in making decisions on which results to keep or discard. Appendix 4 shows some of the statistical methods that are employed during the analysis of the collected data.

4.1.1 The *Q*-test

This was used when dealing with bad data. The *Q*-test is used to help make the decision of whether to retain or discard an experimental value that is thought to be questionable. To apply the *Q*-test, the data is first arranged in order of increasing value and *Q* is calculated by,

$$Q = \frac{\text{gap}}{\text{range}} \quad [34]$$

The gap is the difference between the questionable point and the nearest value. The range or spread is the difference between the highest and the lowest values in the given data set.

If Q (observed) > Q (tabulated), the questionable point should be discarded.

Table 4.1: Critical values of *Q* at the 90% confidence limit⁽³¹⁾.

<i>Q</i> (90%confidence)	0.94	0.76	0.64	0.56	0.51	0.47	0.44	0.41
No. of observations	3	4	5	6	7	8	9	10

Table 4.2: The mixing time values obtained at various gas flow rates and different arrangements of acid dosing and probe location points.

Arrange- Ment	Flow rate m ³ /s	Mixing Time (s)								Ave. T _{mix} (s)	Med. (s)	Std. Dev.
		1	2	3	4	5	6	7	8			
A	0.010	59	37	58	39	53	38			47	46	10
	0.015	35	35	29	30	27	33	34		32	33	3
	0.018	31	29	26	27	17	26	23	33	27	28	5
B	0.010	44	44	46	42	55	37	31	37	42	43	7
	0.015	27	29	30	29	24	24	47*	33	28	29	3
	0.018	26	22	24	24	23	29			25	24	3
C	0.010	43	30	47	49	30				40	43	9
	0.015	11	13	22	47	37	34			27	28	14
	0.018	19	12	26	19	21				19	19	5
D	0.010	59	45	46	39	37	58	35	21*	46	45	10
	0.015	27	21	47	45	46				37	45	12
	0.018	27	17	35	33	26				28	33	7
E	0.010	43	29	38	23	29	31			32	20	7
	0.015	35	29	22	15	29				26	29	8
	0.018	10	17	22	15	21				17	17	5
F	0.010	31	17	26	31	45				30	31	10
	0.015	19	17	26	19	21	34			23	20	6
	0.018	31	17	31	9	18				21	22	10

* the experimental value given was discarded as invalid with the use of the *Q*-test

The analysis of obtained results considered both the spacing of the average T_{mix} values at different gas flow rates and the standard deviation of the individual mixing time results. Using this criterion, Arrangement B (see Table 4.2) was chosen as the best option for positioning the probe and effecting acid dosing. Arrangement B had the least standard deviation figures and the mixing time values obtained were relatively spaced. As a result, it was considered the most viable option for the experimental work. A similar arrangement was also adopted for earlier work⁽²⁾. Arrangement B results indicated that the mixing time values

obtained for the gas flow rates investigated were generally within 10% of each other thus, showing reproducibility of the measurements.

The results of the preliminary experiments showed that the mixing time recorded was dependent on the positioning of the probe. This indicated the influence of the activity of bath liquid in the vicinity of the probe to the rate of approach to homogenisation. The results obtained therefore indicated the existence of several activity zones of in the bath liquid. Position B was positioned in a generally less active zone of the bath liquid because of the relatively high mixing times recorded there.

As opposed to the case in the earlier work⁽²⁾, the gas flow rate $0.0167\text{m}^3/\text{s}$ was not investigated in this case. It was considered to be too close to the $0.0150\text{m}^3/\text{s}$ gas flow rate thus, making it difficult to separate the two with the apparatus used. The other reason was the closeness of the mixing time values that were given by gas flow rates $0.0150\text{m}^3/\text{s}$ and $0.0183\text{m}^3/\text{s}$. Table 4.2 shows the closeness of the mixing time values obtained at the two flow rates, for Arrangement B. It is apparent from the table that the mixing time values were too close to each other to warrant investigations on the $0.0167\text{m}^3/\text{s}$ gas flow rate. A higher gas flow rate, $0.0212\text{m}^3/\text{s}$, which falls within the actual converter operating range, was adopted as the fifth gas flow rate for investigation.

Since temperature had an influence on pH, temperature compensation of the measured bath pH values obtained was necessary. On average, the drop in bath temperature after purging for 15minutes at the gas flow rates $0.010\text{m}^3/\text{s}$, $0.015\text{m}^3/\text{s}$ and $0.018\text{m}^3/\text{s}$ were 0.5°C , 0.8°C and 1.0°C respectively. At face value, these temperature changes seemed to be too small to consider. However, their impact on the value of the bath pH, that was approaching almost complete homogenisation in less than a minute, resulted in significant deviations of the determined mixing time values. To get the correct pH value (critical pH) where the required level of homogeneity occurred was vital because the corresponding time from the measurements recorded was adopted as the mixing time for the

experiment. The critical pH was defined as the pH value that corresponded to 99.66% homogenisation of the bath. The value was calculated from initial bath pH (pH_i) and the temperature compensated stable pH (pH_{cs}) using Equation [33]. The recorded stable pH at a given final temperature after 15minutes of purging was adjusted to get the corrected or temperature compensated stable pH value, pH_{cs} . This was done by adding to the stable pH the error resulting from the temperature changes. The error was dependent on the pH and temperature of the bath. Appendix 1 shows the error chart that was used for pH correction.

The 99.66% level of homogeneity was adopted because it gave consistent values of mixing time. The results obtained from experiments that were designed to determine the position of the probe and performing acid dosing were exhibiting a peculiar pattern. Figure 4.1 below shows how the pH varied with time after acid injection at a bath height of 0.50m. The level of homogeneity when the curve started to approach a constant value was calculated for all the preliminary experiments and the average was 99.66%.

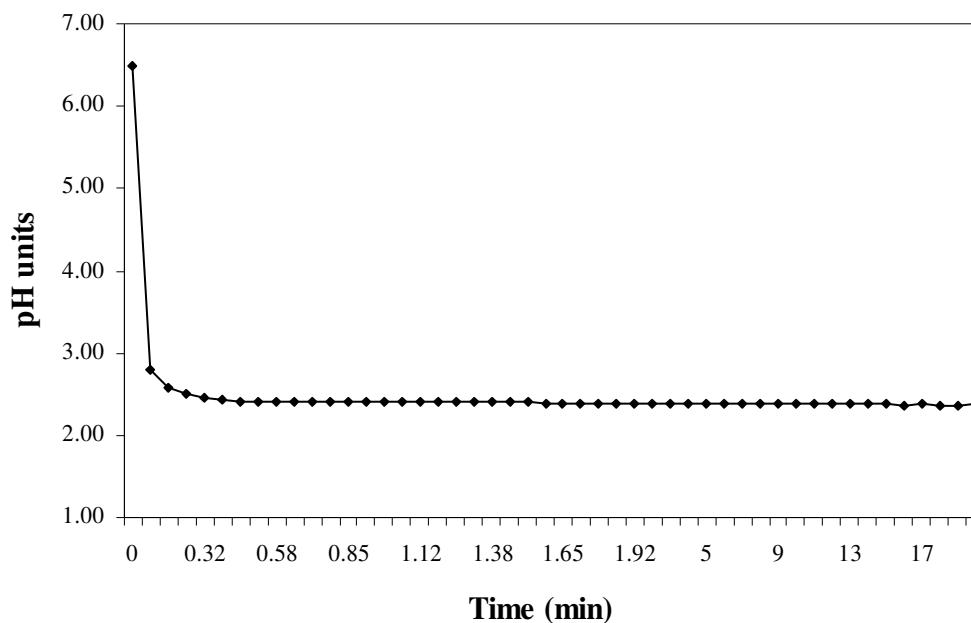


Figure 4.1: The general form of pH variation with time in the experiments as represented by results obtained using pure water at a bath height of 0.50m and a gas flow rate of $0.01\text{m}^3/\text{s}$.

The sampling times adopted were predicted from the preliminary experiments that were conducted. Figure 4.1 above shows that the bath pH was drastically reduced in the early stages of the experiments. Generally after the first 15seconds of purging, the pH dropped by about 0.01units after every four seconds. That necessitated the short sampling times adopted in the early stages of the experiments. During analysis of the experimental data, the recorded pH values obtained in the first 2minutes in which homogenisation occurred were not temperature compensated. The maximum drop in temperature of less than 0.2°C recorded during this period was considered too small to cause a significant error on the observed critical pH and thus the value of the mixing time. Equation [33] reflects the importance that was placed on every measurement taken as it includes almost every variable recorded. The trial runs showed that it was almost impossible to maintain a constant pH of impure water when temperature was varying. For the experiments that followed the initial pH was allowed to vary between 8.10 and 8.30. The experiments were also made to run for at least 20minutes.

4.2 Mixing time measurements

The mixing time measurements were not performed at the 0.0212m³/s gas flow rate in the earlier study⁽²⁾. Additional experiments were therefore carried out at this gas flow rate in the absence of a slag phase. That was done to allow for the determination of the effect of a simulated slag phase on mixing time values obtained under all the conditions adopted in the current study. Table 4.3 below presents the results obtained from the experiments performed under earlier work conditions at 0.0212m³/s gas flow rate. Bath homogeneity was defined at 99.66%.

Table 4.3: Mixing time results obtained at a gas flow rate of $0.0212\text{m}^3/\text{s}$ and in the absence of a simulated slag phase.

Bath Height (m)	Mixing Time (s)										Ave. T_{mix} (s)	Std. Dev
	1	2	3	4	5	6	7	8	9	10		
0.50	39	33	30	35	37	34	35	33	30		34	11.0
0.55	43	37	42	47	41	46	43	37	35		41	14.4
0.60	39	41	38	39	37	42	35	39	33		38	12.2
0.65	43	37	34	45	51	38	39	37	42		41	14.6
0.70	43	49	46	47	41	38	51	31	37		43	14.6

After the measurements summarized in Table 4.3 were taken, the various conditions that affect the mixing time in a converter operation were investigated. Table 4.4 below gives a summary of the experimental results that were obtained in the presence of a simulated slag phase using the established set-up.

Table 4.4: Mixing time results obtained at 99.66% bath homogeneity in the presence of a simulated slag phase.

Bath Height (m)	Flowrate (*10 ⁻³) (m ³ /s)	Mixing Time (s)										Ave. T _{mix} (s)	Std. Dev
		1	2	3	4	5	6	7	8	9	10		
0.50	10.0	47	59	50	51	51	45	52	53	54	53	52	3.8
	12.7	55	47	47	53	45	46	55	47	45	53	49	4.2
	15.0	43	45	35	39	37	43	41	43	41		41	3.2
	18.3	35	35	37	37	41	35	33	31			36	3.0
	21.2	35	37	39	41	37	43	33	33	43		38	3.9
0.55	10.0	59	59	67	65	67	53	55	71	61		62	6.0
	12.7	55	63	42	47	45	63	41	59	53	62	53	8.7
	15.0	39	55	46	47	35	37	47	46	49	38	44	6.3
	18.3	51	51	53	55	39	33	51	59	53	47	49	7.7
	21.2	39	37	41	47	45	35	45	51	45	43	43	4.8
0.60	10.0	77	67	65	67	77	65	67	67	65		69	4.9
	12.7	55	67	61	59	55	53	66	65	70	57	61	5.9
	15.0	39	51	49	47	41	63	59	62	53		52	8.6
	18.3	39		45	43	45	39	43	49	44	45	44	3.1
	21.2	47	37	38	35	37	45	35	45	38		40	4.7
0.65	10.0	83	74	71	73	66	73	71	75	65	74	73	5.0
	12.7	63	61	62	79	53	71	58	66	70	57	64	7.7
	15.0	55	65	47	58	53	57	66	47	59	65	57	6.9
	18.3	58	53	51	45	63	55	41	46	43	49	50	7.0
	21.2	47	51	58	47	51	46	45	50	49		49	3.9
0.70	10.0	89	83	91	65	78	81	90	87			83	8.6
	12.7	70	71	69	77	63	62	77	73			70	5.6
	15.0	59	62	57	74	59	73	58	65			63	6.7
	18.3	53	54	59	47	41	54	57	73			55	9.3
	21.2	43	45	53	63	45	58	53	47			51	7.1

Longer mixing time values were recorded in this stage of the study. Higher mixing time results were recorded because of the increased load coming from the incorporated slag phase. The influence of reduced mass transfer rates of the tracer

between the two liquids constituting the bath also prolonged the mixing time further. Since the incorporated slag phase constituted only 10% of the bath, it was argued that the reduced mass transfer rates of the tracer in the bath liquid had a huge influence.

Investigations by Akdogan and Eric⁽¹⁵⁾ centred on measuring the rate of transfer of a tracer from the water phase to the kerosene phase. They reported that the time taken for the tracer to distribute into equilibrium partitioning ratios was a variable of gas flow rate, bath height and nozzles configuration. As a result of the density differences of the kerosene and water, the purged liquid at the bottom of the bath where dosing was effected had a higher proportion of water than kerosene. The consequence of that was the prolonging of the mixing time. More time was required for equilibrium partitioning of the tracer between water and the viscous kerosene to be attained through out the bath liquid.

The link between mass transfer and mixing time has been raised by many investigators. In their study of the BOF scale-model, using various tuyere arrangements Matway *et al.*⁽²⁸⁾ discussed that the mass transfer rate was found to increase as the mixing time decreased. The data that was collected was analysed in terms of the effects of both the bath height and the gas flow rate on the mixing time. Similar observations were made in the earlier work⁽²⁾.

4.2.1 Effects of gas flow rate

Figure 4.2 below shows the effect that gas flow rate had on the mixing time. Generally the mixing time was observed to decrease with increasing gas flow rate. This trend was explained in terms of the plume velocity changes that resulted from increasing the gas flow rate. At a constant bath height, as the gas flow rate increases, the centre line plume velocity also increases resulting in rapid recirculation of the bath that enhances mixing.

In earlier investigations^(15,29) it was noted that as the gas flow rate increased the plume cone angle increased thus increasing the plume radius at the surface and effectively increasing the plume volume in the bath. The effect of the enlarged high turbulence region was the enhancing of circulation and mixing in the bath.

The largest change in mixing time was observed at the highest bath height. At a water bath height of 0.70m, the mixing time was 83seconds at a gas flow rate of 0.0100m³/s and 51seconds at a gas flow rate of 0.0212m³/s. This was an overall decrease of about 40% on the mixing time as the gas flow rate was increased from 0.0100m³/s to 0.0212m³/s. At the water bath height of 0.50m, the mixing time dropped from 52seconds at a gas flow rate of 0.0100m³/s and only reached a minimum value of 36seconds before it started to increase. This was only a drop of about 31% on the mixing time. The changes in mixing time showed the depreciating influence of gas flow rate at high levels of specific energy input.

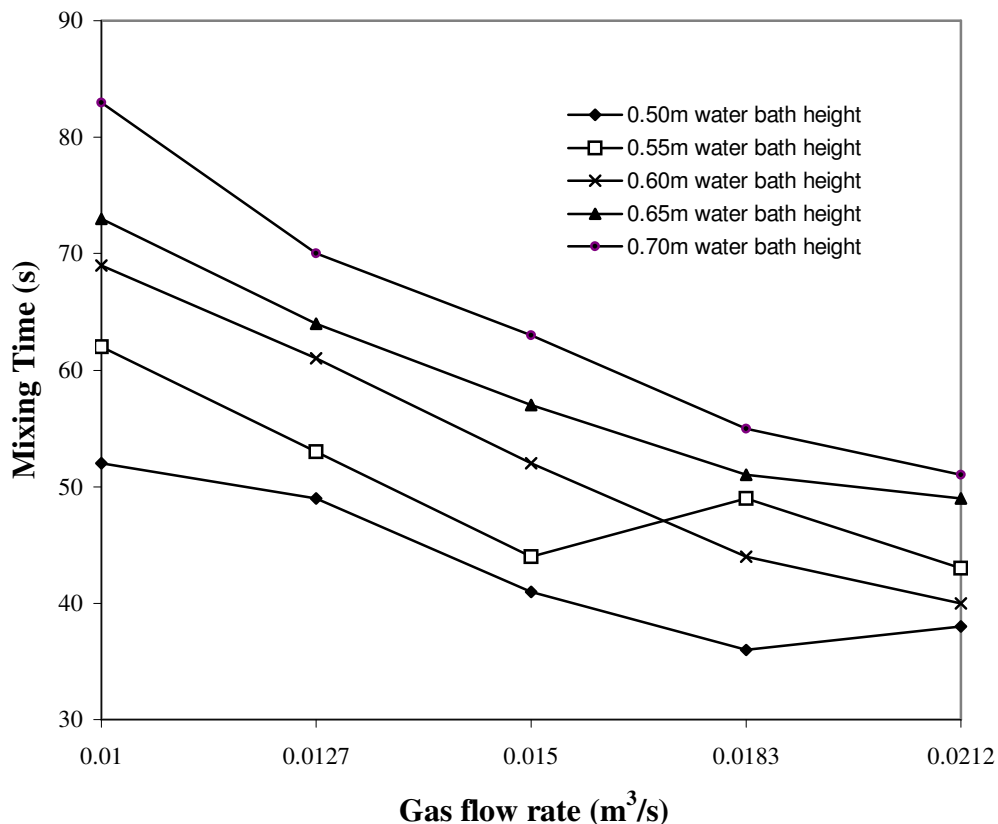


Figure 4.2: Effect of gas flow rate on the mixing time.

At the water bath heights of 0.50m and 0.55m the mixing time was observed to exhibit a minimum value after which its value increased against an increase in the gas flow rate. Minimum mixing time values were exhibited at the gas flow rates of $0.0150\text{m}^3/\text{s}$ and $0.0183\text{m}^3/\text{s}$ at water bath heights of 0.55m and 0.50m respectively. At the 0.55m water bath height the increase in the mixing time after the minimum value exceeded that recorded at the same gas flow rate but at a higher water bath height. This was maintained to the largest gas flow rate investigated. As a result of this inconsistent behaviour of the mixing time values obtained, fifteen experimental runs were conducted but the graph maintained its shape that is shown in Figure 4.2. The abnormal mixing time patterns could be attributed to various factors.

The existence of minimum mixing time values could have resulted from swirling of the bath. Observations by Murthy *et al.*⁽²⁹⁾, of the two-phase plume and flow conditions in the bath revealed that the plume swirled above a certain gas flow rate resulting in enhanced mixing rates in the bath. The minimum mixing times recorded in this study were therefore attributed to probable swirling of the plume that increased the rates of mixing in the bath.

Figure 4.2 show that the all the inconsistencies were observed at low bath heights and high stirring rates only. It was therefore argued that, the increases in mixing time values after a minimum was recorded were linked to the high specific energy input to the bath. Above a certain value of specific energy input, the level of tracer dispersion considered for the mixing time value to be determined could be altered.

Under conditions of very high stirring employed it was possible that, the partially affected zones in the bath were reached by the mixing power of the purging gases. The result was an increase in the volume of the bath liquid where a uniform concentration of the acid was necessary for homogeneity to be established. Consequently, the mixing time increased against an increase in gas flow rate. The mixing time values recorded tended to be longer than normal, thus the

abnormalities observed. However at higher bath heights, it is apparent from the general form of the graphs in Figure 4.2 that the increased energy input to the bath reduced the mixing time. The mostly positive gradients of the graphs support the observation. Better mixing in the bath was attributed to increased turbulence and bulk velocity of the agitated bath as the gas flow rate was increased.

4.2.2 Effects of bath height

For the gas flow rates investigated, the mixing time increased with an increase in the bath height as shown in Figure 4.3. This trend can be explained to be a result of a decrease in the bubble formation as the bath height increased⁽²⁾. The bath height effect on the mixing time value became more apparent especially at lower gas flow rates.

Asai *et al.*⁽²³⁾ reported the opposite to the trend shown in Figure 4.3 under certain conditions. They explained their observations in terms of the increased re-circulatory loop length in the vessel as the bath height increased. They reported that, longer re-circulatory loops resulted in higher liquid velocity in the bath that in turn, decreased mixing time. The decrease in mixing time values at gas flow rates $0.0183\text{m}^3/\text{s}$ and $0.0212\text{m}^3/\text{s}$ when the bath height increased from 0.55m to 0.60m was explained in terms of the increased re-circulatory loop length. However, this effect became less pronounced as the bath height increased further and the specific energy input reduced.

As reported in literature^(2,23), many researchers have observed the abnormal behaviour of the mixing time in gas stirred baths under different conditions. The seemingly consistent occurrence, shown as peaks in Figure 4.3, has been attributed to various reasons. The most convincing explanation for abnormalities was given by Mazumdar *et al.*⁽³⁰⁾. They attributed the anomalies to shifting of the slow moving zones in the bath. In the current study, the probe was positioned in a 'slow moving zone' that was determined under specific conditions adopted in the preliminary experiments. Due to zone shifting it is highly probable that the probe

was situated in a turbulent environment when a minimum value was observed or in a less active zone when the mixing time increased against decreasing bath height. Assuming this was the case then, the mixing times recorded were bound to be the opposite of what was expected since mixing rates in the various regions of the bath vary according to activity or turbulence.

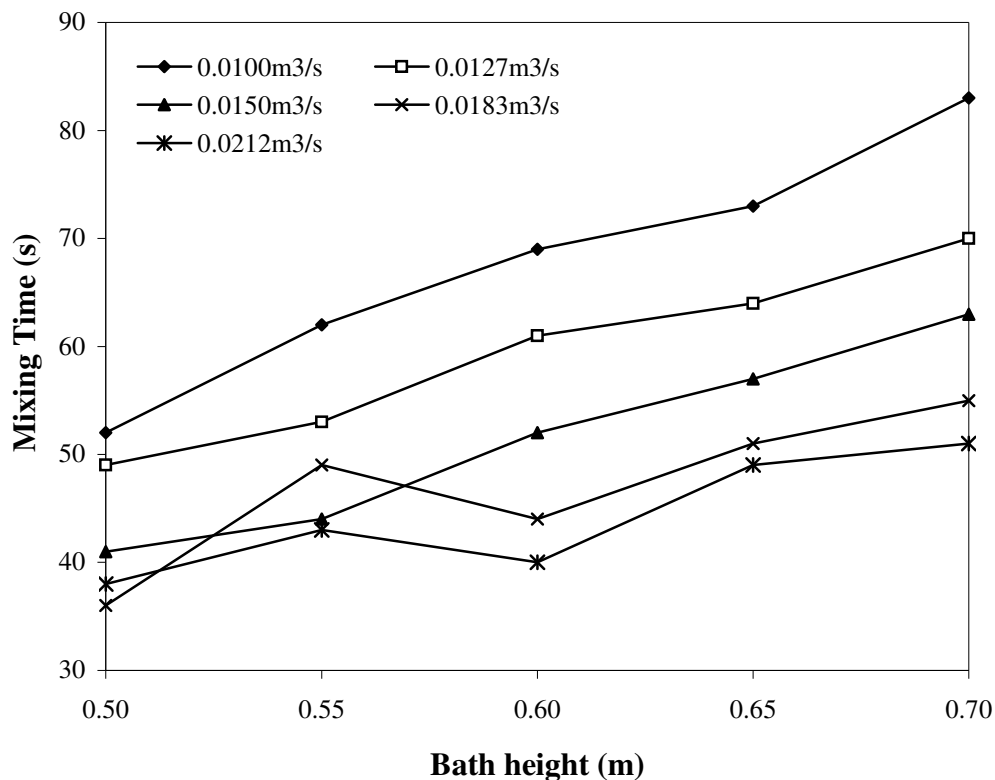


Figure 4.3: Effect of bath height on the mixing time

The mixing pattern at bath heights above 0.55m could be explained in terms of the columnar effect becoming pronounced with an increase in bath height. Castillejos and Brimacombe⁽²⁰⁾ and Asai *et al.*⁽²⁹⁾ discussed that at high ratios of bath height to diameter of the vessel, dead volumes that formed near the bottom of the vessel had the effect of increasing mixing time. Murthy *et al.*⁽²⁹⁾ explained this phenomenon by means of a multiple circulation model, in which the bath consists of several circulation cells in the axial direction that make mixing by bulk flow ineffective. The formation of the circulation cells in the bath inhibits the thorough mixing of the bath solution. Thus, longer periods of mixing are observed under conditions of increased bath load as more circulation cells are formed. When the

formation of circulation cells in the bath occurs at lower bath heights, the mixing time that is recorded tends to be longer than the expected value.

The multiple circulation cells model could be used to explain the large mixing time values recorded at the 0.55m water bath height and gas flow rates of $0.0183\text{m}^3/\text{s}$ and $0.0212\text{m}^3/\text{s}$. The deviation from the 'normal' depends on the extent of circulation cells formation. Using this model, the formation of circulation cells in the bath was therefore more pronounced at the gas flow rate of $0.0183\text{m}^3/\text{s}$ than at $0.0212\text{m}^3/\text{s}$.

4.2.3 Establishing the mixing time correlation

To establish the mixing time correlation as expressed in Equation [23] it was necessary to calculate the specific energies supplied to the bath. The input energy was then related to the experimentally determined mixing time values. Table 4.5 presents the obtained mixing time values, the input energy to the bath and the experimentally determined constant a and coefficient b for the conditions investigated.

Table 4.5: Energy considerations for the different conditions investigated

Water Bath Height (m)	Total Bath Height (m)	Bath Wt. (ton)	Gas Flow Rate (m ³ /s)	T _{mix} (s)	Ave. Temp. (K)	E _b (w/ton)	E _k (w/ton)	E _t (w/ton)	E _b /E _k	a & b Values
0.50	0.542	0.111	0.0100	52	293	500	1422	1922	0.35	a=213 b= -0.187
			0.0127	49	293	634	2915	3549	0.22	
			0.0150	41	293	750	4797	5547	0.16	
			0.0183	36	293	916	8706	9622	0.11	
			0.0212	38	293	1060	13542	14602	0.08	
0.55	0.597	0.124	0.0100	62	291	488	1285	1773	0.38	a=205 b= -0.165
			0.0127	54	292	621	2626	3248	0.24	
			0.0150	45	291	731	4347	5078	0.17	
			0.0183	49	291	893	7876	8769	0.11	
			0.0212	43	291	1035	12241	13276	0.08	
0.60	0.652	0.138	0.0100	69	292	482	1164	1646	0.41	a=600 b= -0.290
			0.0127	61	292	612	2386	2999	0.26	
			0.0150	52	292	723	3934	4656	0.18	
			0.0183	43	291	881	7151	8032	0.12	
			0.0212	40	292	1021	11111	12132	0.09	
0.65	0.707	0.151	0.0100	73	290	472	1063	1535	0.44	a=324 b= -0.205
			0.0127	64	289	599	2179	2778	0.27	
			0.0150	57	290	709	3582	4291	0.20	
			0.0183	50	290	8646	6510	7375	0.13	
			0.0212	49	290	1001	10123	11125	0.10	
0.70	0.762	0.164	0.0100	83	289	466	996	1462	0.47	a=511 b= -0.251
			0.0127	70	289	591	2046	2636	0.29	
			0.0150	63	289	698	3369	4067	0.21	
			0.0183	55	289	851	6120	6972	0.14	
			0.0212	51	289	986	9519	10504	0.10	

Average value of $E_b/E_k = 0.213$ and standard deviation $(E_b/E_k) = 0.119$

The buoyancy energy density (E_b), the kinetic energy component (E_k) and the total energy density of the stirring gases (E_t) were calculated using Equations [21], [22] and [20] respectively. The coefficients for the mixing time, Equation [23], for each bath height were determined using linear regression analysis. Table 4.6 below presents the five different mixing time correlations that were obtained at the five bath heights investigated.

Table 4.6: Mixing time correlations for the investigated water bath heights.

Water Bath Height (m)	Mixing time correlation obtained (s)
0.50	$T_{\text{mix}} = 213E_t^{-0.19}$
0.55	$T_{\text{mix}} = 205E_t^{-0.17}$
0.60	$T_{\text{mix}} = 600E_t^{-0.29}$
0.65	$T_{\text{mix}} = 324E_t^{-0.21}$
0.70	$T_{\text{mix}} = 511E_t^{-0.25}$

The obtained mixing time correlations were combined to establish a mathematical expression that represented the mixing behaviour at all the bath heights investigated. The correlation obtained for the 0.55m water bath height was first modified to exclude the mixing time values obtained at gas flow rates $0.0183\text{m}^3/\text{s}$ and $0.0212\text{m}^3/\text{s}$. The exclusion of these values was considered necessary as the trend displayed was not common for all the other bath heights investigated. The abnormal mixing time values were attributed to flaws in the experimental method used, and thus they were not a true reflection of mixing in the bath. The mixing time and total energy density values obtained for the five bath heights investigated were combined and plotted into a single graph that represents mixing in the model. Figure 4.4 shows the plot of the overall correlation that was obtained.

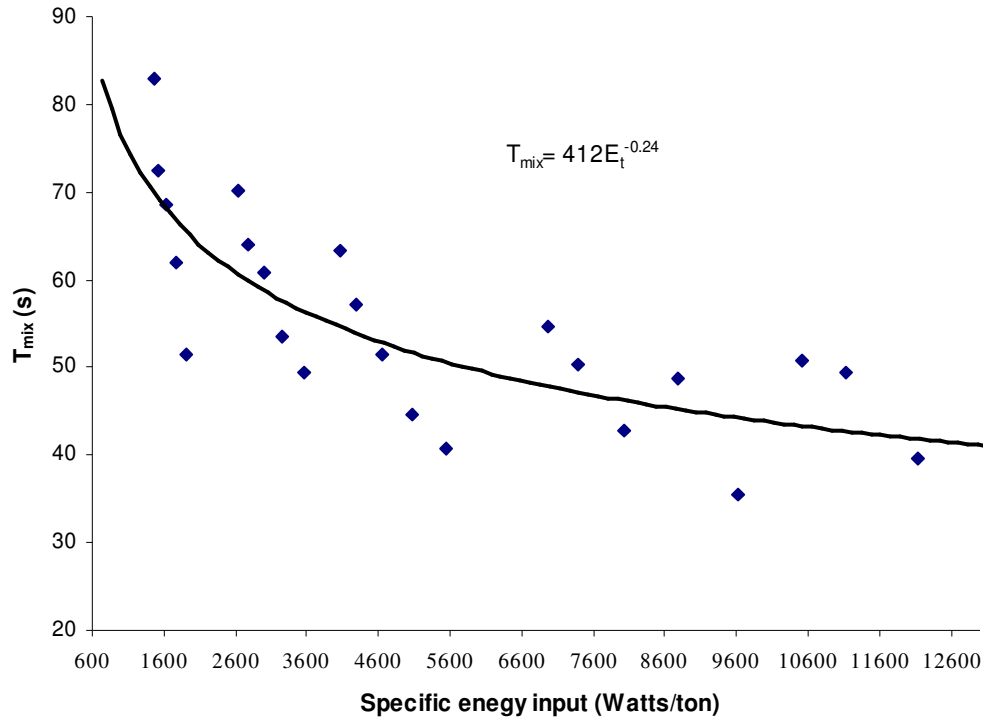


Figure 4.4: Effect of specific stirring energy on mixing time in the model.

From the above analysis the relationship for estimating the mixing time in the model vessel was given as,

$$T_{mix} = 412E_t^{-0.24} \quad [35]$$

The low standard deviation value of E_b/E_k means that the value of E_b in the energy expression for calculating the total stirring energy density can be substituted to modify Equation [20] to,

$$\begin{aligned} E_t &= E_k + 0.213E_k \\ &= 1.213 E_k \end{aligned} \quad [36]$$

Since from Equation [22],

$$E_k = \frac{\rho_s Q^3}{2WA^2}$$

and the average value of $\rho_g = 1.2843 \text{Kg/m}^3$ and $A = 2.829 \times 10^{-5} \text{m}^2$. The established mixing time correlation, Equation [35], can then be expressed as,

$$T_{mix} = 411.62 \left(1.213 \frac{\rho_g Q^3}{2WA^2} \right)^{-0.243}$$

Thus

$$T_{mix} \approx 2.87Q^{-0.73}W^{0.24} \quad [37]$$

The expression above was adequate for comparison purposes of the current study with the earlier work⁽²⁾. A more accurate relationship for estimating the mixing time in the model vessel was obtained by including the bath height (H) component in the equation. The spreading out of the sample points in Figure 4.4 necessitated the inclusion of the bath height contribution. The seemingly haphazard plot of the points could not be attributed entirely on the expected experimental error in T_{mix} measurements. It was therefore attributed to the effect of the bath height on mixing time. The correlation in Equation [37] was obtained from an average of five different relationships that is why some sample points were far off the solid line. Thus, the correlation in Equation [37] above was found to predict mixing time values that were far off the experimentally determined ones in most instances.

To include the bath height component the following expression was adopted,

$$T_{mix,2} = 412E_t^{-0.24} \cdot yH^z \quad [38]$$

The values of the coefficients y and z were obtained using linear regression analysis again. Taking logarithms on both sides of Equation [38] modified it to,

$$\text{Log}_{10} T_{mix,2} = [\text{Log}_{10} T_{mix,1} + \text{Log}_{10} y] + z \text{Log}_{10} H \quad [39]$$

Where $T_{mix,1}$ in the above equation was used to represent the mixing time value obtained using the first mixing time correlation, Equation [35]. $T_{mix,2}$ was

proposed as the new mixing time expression when the bath height influence was considered. During the determination of coefficients y and z , the experimentally determined mixing time values, $T_{mix,exp}$, substituted for $T_{mix,2}$ in Equation [39] above.

An almost similar treatment of the results obtained, as in the previous case, was used to get the refined mixing time correlation. Table 4.7 below shows the calculated values of y and z obtained. The average of the y values, 1.629, and the z values, 1.118, were adopted in the overall equation. Using these values of y and z the final correlation was obtained as,

$$T_{mix,2} = 671E_t^{-0.243}H^{1.118} \quad [40]$$

Adopting the correlation above, the mixing time in the model converter was then represented as,

$$T_{mix} = 671E_t^{-0.24}H^{1.12} \quad [41]$$

Substituting for E_t in Equation [41] modified the mixing time correlation to,

$$T_{mix} = 4.39Q^{-0.73}W^{0.24}H^{1.12} \quad [42]$$

The mixing time values estimated from this correlation had an average deviation of $\pm 3\%$ from the experimentally determined values. The deviation was $\pm 11\%$ when the estimation was done using the correlation that does not include the bath height effect.

Table 4.7: Calculated values of the coefficients y and z required for including bath height effect on mixing time.

Gas Flow Rate (m ³ /s)	Total Bath Height H, (m)	Log H	T _{mix,exp.} (s)	Log T _{mix,exp}	T _{mix,l} (s)	Log T _{mix,l}	Log y	y	z
0.010	0.542	-0.266	52	1.712	65	1.816	0.26	1.739	1.313
	0.597	-0.224	62	1.792	67	1.824	0.25		
	0.652	-0.186	69	1.836	68	1.832	0.24		
	0.707	-0.151	73	1.860	69	1.840	0.23		
	0.762	-0.118	83	1.919	70	1.845	0.23		
0.0127	0.542	-0.266	49	1.693	56	1.751	0.22	1.587	1.041
	0.597	-0.224	54	1.729	58	1.760	0.21		
	0.652	-0.186	61	1.784	59	1.769	0.20		
	0.707	-0.151	64	1.806	60	1.777	0.19		
	0.762	-0.118	70	1.847	61	1.783	0.19		
0.0150	0.542	-0.266	41	1.610	51	1.704	0.25	1.718	1.324
	0.597	-0.224	45	1.650	52	1.713	0.24		
	0.652	-0.186	52	1.712	53	1.722	0.23		
	0.707	-0.151	57	1.757	54	1.731	0.23		
	0.762	-0.118	63	1.802	55	1.737	0.22		
0.0183	0.542	-0.266	36	1.550	44	1.646	0.22	1.581	1.064
	0.597	-0.224	49	1.688	45	1.656	0.21		
	0.652	-0.186	43	1.630	46	1.665	0.20		
	0.707	-0.151	50	1.702	47	1.674	0.19		
	0.762	-0.118	55	1.738	48	1.680	0.18		
0.0212	0.542	-0.266	38	1.579	40	1.602	0.20	1.521	0.850
	0.597	-0.224	43	1.631	41	1.612	0.19		
	0.652	-0.186	40	1.598	42	1.621	0.18		
	0.707	-0.151	49	1.693	43	1.630	0.17		
	0.762	-0.118	51	1.707	43	1.637	0.17		

Figure 4.5 below presents a comparison of the mixing time estimates obtained using the two correlations established.

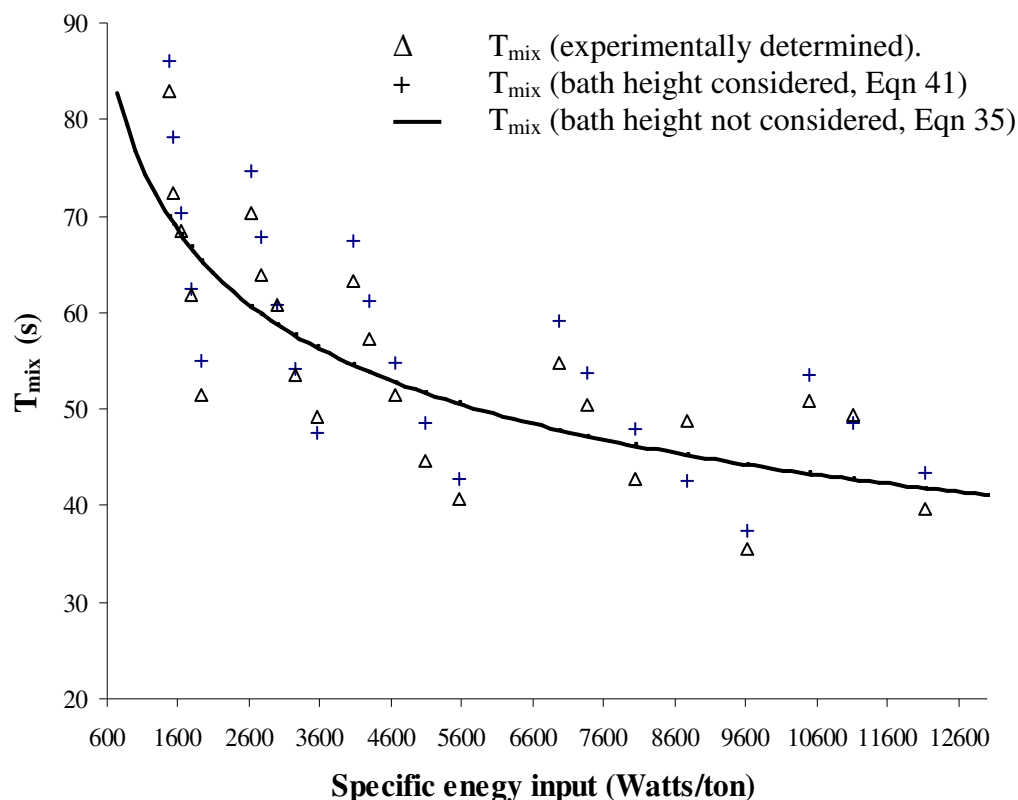


Figure 4.5: A comparison of the deviations of the estimates from the experimentally determined mixing time values.

The crosses in Figure 4.5 above represents the sample points estimated by Equation [41] and the solid line by Equation [35]. The sample points that were determined taking the bath height into consideration, i.e. $+$, are closer to the experimentally determined values represented by the triangles, Δ . These two corresponding values can be identified in Figure 4.5 by checking points falling on the same specific energy input line. The solid line in Figure 4.5 was plotted from the points calculated from the relationship that did not take the contribution of the bath height into account.

4.3 Mass transfer experiments

Solid-liquid mass transfer measurements were performed in a water-kerosene bath. Mass transfer parameters under the investigated conditions were calculated from the changes in specimen radii of benzoic acid cylinders after seven, separate, 15minutes long experimental runs. It was difficult to measure the radii of the specimens that had undergone uneven dissolution during bath purging. Average radii were therefore calculated from the weight losses recorded on the specimens. The results of experiments conducted to establish the effect of bath height and gas flow rate on the mass transfer properties in the bath are presented below.

4.3.1 Effect of gas flow rate on mass transfer rates

Table 4.8: The gas flow rate effect on different mass transfer properties at a water bath height of 0.4m.

Flow rate (m ³ /s)	Sample location	dR/I _t (*10 ⁻⁵ m/s)	Mass transfer coefficient, <i>K</i> (*10 ⁻⁵ m/s)	Sherwood number <i>Sh</i>	Turbulence Parameters (Re _{loc,r}) ^{0.25} (Re _t) ^{0.32}
0.010	S2	2.01	0.82	5776	46832
	S3	1.87	0.76	5374	43570
	S4	4.41	1.80	12672	102750
	S7	1.57	0.64	4511	36580
0.015	S2	2.50	1.02	7184	58248
	S3	2.02	0.83	5805	47065
	S4	5.11	2.09	14684	119060
	S7	1.81	0.74	5201	42172
0.023	S2	3.13	1.28	8994	72927
	S3	2.82	1.15	8103	65704
	S4	6.99	2.86	20086	162862
	S7	2.45	1.00	7040	57083

Table 4.8 above presents the mass transfer coefficients and turbulence parameters in the bath under different gas blowing conditions. The highest values of both quantities were recorded at S4 location for all the gas flow rates investigated. To clearly display the variation of the mass transfer coefficient in the bath at 0.4m water bath height, Figure 4.6 below was plotted.

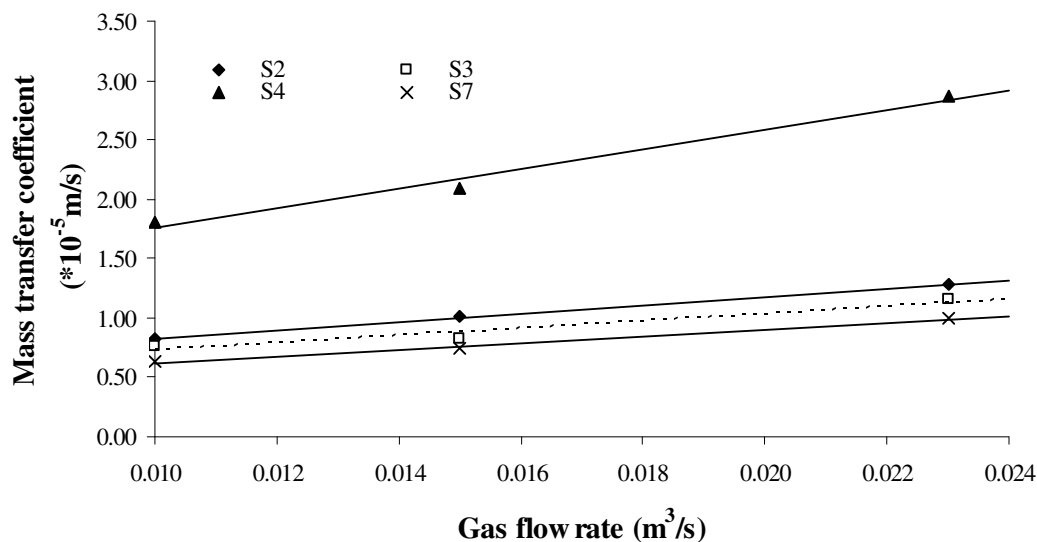


Figure 4.6: Effect of gas flow rate on mass transfer coefficient at 0.4m water bath height.

The graphs in Figure 4.6 show that an increase in gas flow rate had the effect of increasing the mass transfer coefficients in the bath. The increased stirring power imparted by the purging gases was responsible for increasing the energy needed to erode and aide in the dissolution of the benzoic acid specimens. Significant mass transfer rates were observed near the bath surface. The weight of the much reduced overlying liquid near the bath surface had a less negative effect on the multiplication of the rising air bubbles in the buoyancy energy dominated region. Under these conditions more stable gas bubbles were formed, thereby promoting turbulence and mass transfer. Studies by Mori and Sakura⁽³²⁾ on the influence of gas stirring showed that gas evolution markedly enhanced the dissolution rates especially under normal convection conditions.

Sample S7 that was located outside the highly turbulent gas-liquid plume was considered to have been in a dead zone. In that zone, the kinetic energy of the bath liquid and bubble formation were minimal. Having been situated close to the bottom of the model converter, the sample was at the end of the re-circulating bath liquid. Thus, the sample was only exposed to the liquid that had lost most of its energy on its way up and back to the bottom of the vessel where the circulating loop started. The same argument was used to explain the low mass transfer rates recorded at Location S2. Although Sample S3 was situated right in the middle of the bath, the possible existence of a dead volume at the centre of a circulating bath was reflected by the low mass transfer rates recorded.

Mass transfer rates in all the low turbulent regions were dependent on the energy levels of the bath liquid and the dissolved acid levels in those localities. The low mass transfer rates observed at Locations S2, S3 and S7 agreed well with the results of investigations by J.K. Wright⁽⁸⁾. He observed almost constant mass transfer rates inside the bath and high rates at the bath surface. He also observed relatively high mass transfer rates at the bottom of the bath just like the results of the current study suggested.

Figure 4.6 clearly shows that there was almost uniform change in the mean mass transfer rates as the gas flow rate increased. The near constant gradient of the graphs is an indication that the increased stirring power of the purging gases had an almost constant effect at all the locations investigated. The gradient of the graph at S4 is slightly steeper indicating greater turbulence brought to this region as the gas flow rate was increased.

Table 4.9: The gas flow rate effect on different mass transfer properties at a water bath height of 0.5m

Flow rate (m ³ /s)	Sample location	dR/dI _t (*10 ⁻⁵ m/s)	Mass transfer coefficient, <i>K</i> (*10 ⁻⁵ m/s)	Sherwood number <i>Sh</i>	Turbulence Parameters (Re _{loc,r}) ^{0.25} (Re _t) ^{0.32}
0.010	S2	1.89	0.77	5431	44036
	S3	1.71	0.70	4914	39842
	S4	4.38	1.79	12586	102051
	S7	1.11	0.45	3190	25862
0.015	S2	2.04	0.83	5862	47531
	S3	1.97	0.81	5661	45900
	S4	4.50	1.84	12931	104847
	S7	1.13	0.46	3247	26328
0.023	S2	2.36	0.97	6782	54986
	S3	2.78	1.14	7988	64772
	S4	6.05	2.47	17385	140961
	S7	1.25	0.51	3592	29124

Table 4.9 presents an almost similar trend in the variations of the mass transfer rates in the bath, although the investigations were carried out at a higher water bath height. Both the turbulence parameters and the mass transfer coefficients were lower than in the previous case. The overall turbulence levels in the bath were reduced as a result of increased dissipation of the stirring power by the increased bath size.

Figure 4.7 below gives a graphical presentation of the results that were obtained. The cross over of the mass transfer coefficients at Locations S3 and S2 could be due to the possibility of the two regions exhibiting similar activity. As was observed and explained in mixing time experiments, the dynamic nature of the

bath liquid resulted in shifting of the different zones present in the bath. It was argued that, this phenomenon was responsible for the observed increase in rates at Location S3 as the gas flow rate exceeded $0.015\text{m}^3/\text{s}$. As the gas flow rate increased above this level, there was greater mass transfer activity at S3 than at S2.

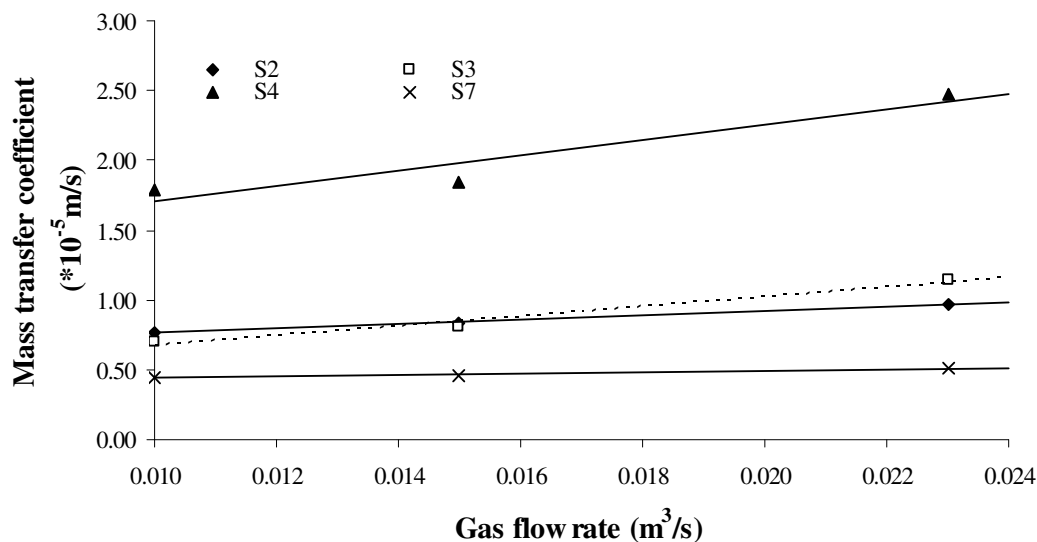


Figure 4.7: Effect of gas flow rate on mass transfer coefficient at 0.5m water bath height.2

An increase in gas flow rate resulted in greater mass transfer rates increases at Locations S3 and S4. This is shown in Figure 4.7 by steeper gradients for mass transfer coefficient variations at Locations S3 and S4 than at Locations S2 and S7. At the latter locations, the change in the gas stirring power did not give rise to appreciable mass transfer rates. This was taken as an indication of low dependence of the turbulence characteristics in the localities of Samples S2 and S7 on gas flow rate changes. The fact that these locations were not in the plume region and existed at the bottom of the bath reduced the effect of gas flow rate. Consequently, the mass transfer rates at Location S3 that was placed in the plume region rose above those recorded at Location S2 as the gas flow rate reached approximately $0.015\text{m}^3/\text{s}$.

Investigations at a higher water bath height of 0.65m gave results in Table 4.10 below. The mass transfer rates displayed significant reductions from the values observed at the 0.40m water bath height. The information in the table was summarized and presented graphically.

Table 4.10: The gas flow rate effect on different mass transfer properties at a water bath height of 0.65m

Flow rate (m ³ /s)	Sample location	dR/dI _t (*10 ⁻⁵ m/s)	Mass transfer coefficient, <i>K</i> (*10 ⁻⁵ m/s)	Sherwood number <i>Sh</i>	Turbulence Parameters (Re _{loc,r}) ^{0.25} (Re _t) ^{0.32}
0.010	S2	1.77	0.72	5086	41240
	S3	1.66	0.68	4770	38677
	S4	4.23	1.73	12155	98556
	S7	0.80	0.33	2299	18639
0.015	S2	1.83	0.75	5259	42638
	S3	1.95	0.80	5603	45434
	S4	4.38	1.79	12586	102051
	S7	0.86	0.35	2471	20037
0.023	S2	2.45	1.00	7040	57083
	S3	2.71	1.11	7787	63141
	S4	4.90	2.00	14080	114167
	S7	1.29	0.53	3707	30056

Figure 4.8 below shows gently sloping, mass transfer coefficient against gas flow rate graphs. This new trend showed a depreciating influence of gas flow rate as the bath height increased. The reduced sensitivity of mass transfer coefficients to increases in gas flow rate at higher water bath heights was explained in terms of the reduced specific stirring energy input to the bath. As the bath height increased, the specific energy input was no longer increasing at the same high rate as was the

case at lower bath heights. However, the increase in mass transfer rates was relatively higher at Location S3 than at all the other locations. Emergence of a turbulent environment in the middle of the bath resulted in the mass transfer rates increasing above those at the bottom of the bath. At approximately $0.012\text{m}^3/\text{s}$ gas flow rate, the mass transfer rates in the middle of the bath were greater than those at the bottom as a more active region moved to the middle of the bath when the gas flow rate was increased. The increase in the mean rising plume velocity favoured greater activity at Location S3 than at the other positions investigated. The relationship of the mean rising plume velocity with gas flow rate is represented in Equation [18].

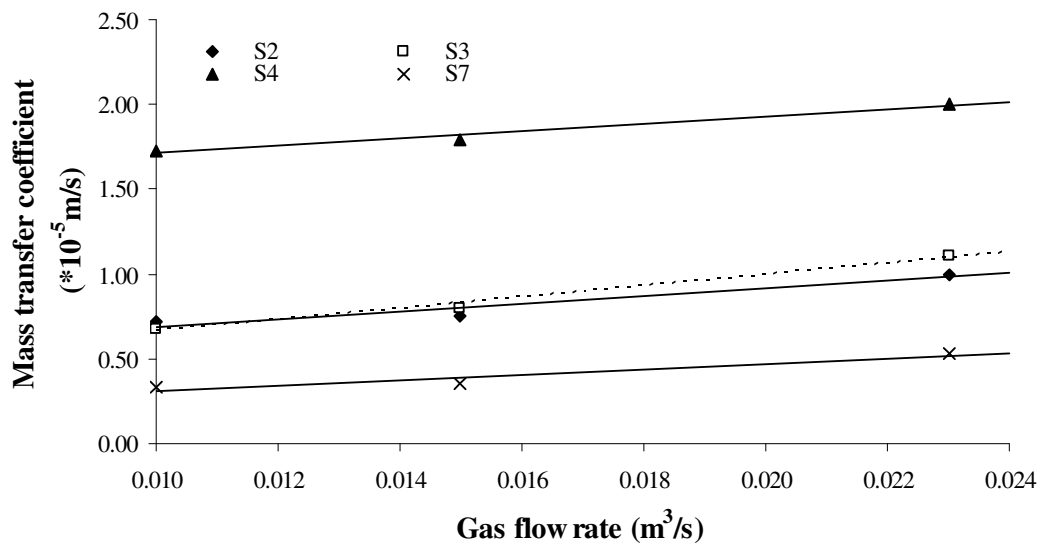


Figure 4.8: Effect of gas flow rate on mass transfer coefficient at 0.65m water bath height.

4.3.2 Effect of bath height on mass transfer rates

Generally, the effect of increasing the bath height was a reduction in the mass transfer properties in the model converter. The presentations below show the effect of bath height changes on the mass transfer coefficient when the gas flow rate was maintained constant.

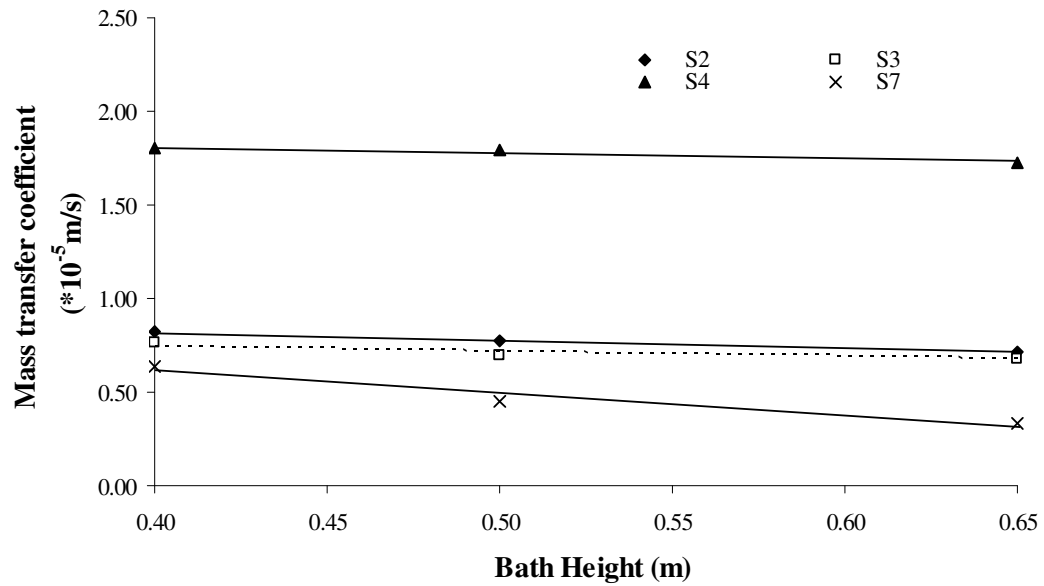


Figure 4.9: Effect of bath height on mass transfer coefficient at a constant gas flow rate of $0.010\text{m}^3/\text{s}$.

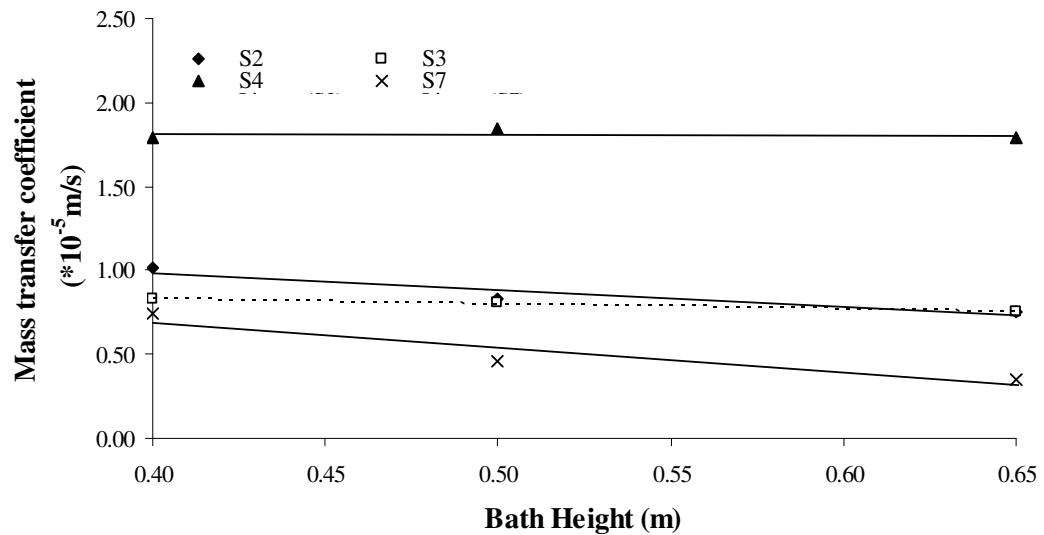


Figure 4.10: Effect of bath height on mass transfer coefficient at a constant gas flow rate of $0.0150\text{m}^3/\text{s}$.

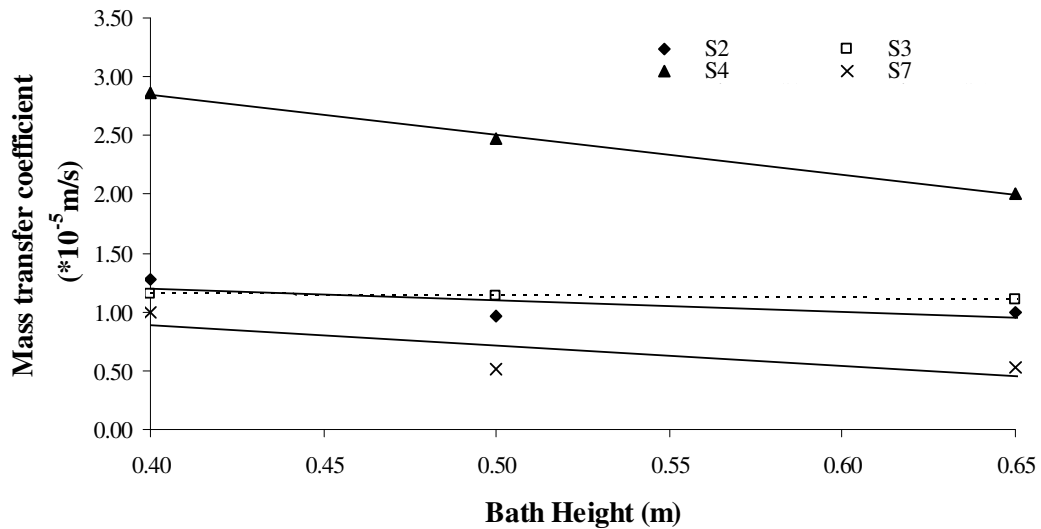


Figure 4.11: Effect of bath height on mass transfer coefficient at a constant gas flow rate of $0.023\text{m}^3/\text{s}$.

The negative gradients of the graphs presented above resulted from a decrease in specific bath energy as the bath load was increased whilst a constant gas flow rate was maintained. The change in mass transfer coefficients was gradual for most locations at $0.010\text{m}^3/\text{s}$ gas flow rate. The gradients of the graphs became steeper as the gas flow rate increased. This was more pronounced at the $0.023\text{m}^3/\text{s}$ gas flow rate. The sensitivity of mass transfer coefficients at higher gas flow rates was attributed to a much large specific energy input drop as the bath height was increased. As the load increased, input energy dissipation also increased hence the reduction in the specific input energy in the bath.

The exponential relationship that exists between mass transfer and the gas injection rate was also responsible for greater sensitivity of the mass transfer coefficients at higher gas flow rates. Equation [2] is an example of the established relationships found in literature. A reduction in gas injection rate therefore reflected as significantly reduced mass transfer rates at high gas flow rates.

Location S3 was the only position that did not display a noticeable change in the mass transfer coefficient as the bath height increased at all gas flow rates. This reflected the stability of the flow regime in the middle of the bath. Mass transfer

rates were observed to be almost constant in the middle of the bath for all the gas flow rates investigated. The mass transfer coefficients at Location S3, for all the investigated bath heights, were almost constant at stirring gas flow rates $0.010\text{m}^3/\text{s}$ and $0.015\text{m}^3/\text{s}$. A relatively small increase in the mean mass transfer coefficient was observed when the gas flow rate increased to $0.023\text{m}^3/\text{s}$. This showed the emergence of a more active but still stable flow regime in the middle of the bath.

4.3.3 Mass transfer coefficient variation with gas injection rates

Mass transfer rates in the bath as pointed out earlier, are best represented by mass transfer coefficients. The variation of the mass transfer coefficient was related to the gas flow rate. Linear regression analysis was used to establish the coefficients in Equation [43] that was adopted,

$$K = mQ^n \quad [43]$$

The value of the coefficient m , is not constant as it is a variable of many quantities. Its value depends on bath height, sample location and the gas stirring rate among other things. For this reason the relationship expressing the variation of the mass transfer coefficient in various positions of the bath and operational conditions took the form of Equation [2] i.e. $K \propto Q^{0.21}$. This equation was established by J.K. Wright⁽⁸⁾ in similar investigations. Table 4.11 below presents the values of the coefficient m and factor n that were calculated from the experimentally determined mass loss measurements.

Table 4.11: Mass transfer coefficients in the model converter vessel under conditions of varying bath height.

Water Bath Height (m)	Sample location	Gas Flow Rate (m ³ /s)	Mass transfer coefficient, K (*10 ⁻⁵ m/s)	Log Q	Log K	m (*10 ⁻⁶)	n
0.40	S2	0.010	0.82	-2.00	-5.086	6.55	0.0967
		0.015	1.02	-1.82	-4.991		
		0.023	1.28	-1.64	-4.893		
	S3	0.010	0.76	-2.00	-5.119	5.94	0.0899
		0.015	0.83	-1.82	-5.081		
		0.023	1.15	-1.64	-4.939		
	S4	0.010	1.80	-2.00	-4.745	13.89	0.1005
		0.015	2.09	-1.82	-4.680		
		0.023	2.86	-1.64	-4.544		
	S7	0.010	0.64	-2.00	-5.194	4.99	0.0969
		0.015	0.74	-1.82	-5.131		
		0.023	1.00	-1.64	-5.000		
0.50	S2	0.010	0.77	-2.00	-5.114	6.77	0.0501
		0.015	0.83	-1.82	-5.081		
		0.023	0.97	-1.64	-5.013		
	S3	0.010	0.70	-2.00	-5.155	5.31	0.1059
		0.015	0.81	-1.82	-5.092		
		0.023	1.14	-1.64	-4.943		
	S4	0.010	1.79	-2.00	-4.747	14.57	0.0699
		0.015	1.84	-1.82	-4.735		
		0.023	2.47	-1.64	-4.607		
	S7	0.010	0.45	-2.00	-5.347	4.17	0.0272
		0.015	0.46	-1.82	-5.337		
		0.023	0.51	-1.64	-5.292		
0.65	S2	0.010	0.72	-2.00	-5.143	5.86	0.0713
		0.015	0.75	-1.82	-5.125		
		0.023	1.00	-1.64	-5.000		
	S3	0.010	0.68	-2.00	-5.167	5.18	0.1064
		0.015	0.80	-1.82	-5.097		
		0.023	1.11	-1.64	-4.955		
	S4	0.010	1.73	-2.00	-4.762	15.89	0.0315
		0.015	1.79	-1.82	-4.747		
		0.023	2.00	-1.64	-4.699		
	S7	0.010	0.33	-2.00	-5.481	2.45	0.1029
		0.015	0.35	-1.82	-5.456		
		0.023	0.53	-1.64	-5.276		

The standard deviation of the values of n and m were 0.03 and 4.48 respectively. Since the standard deviation of the values of n was low, an average of all the calculated values, $n=0.08$, was adopted to give the relationship below,

$$K \propto Q^{0.08} \quad [44]$$

The relationship describes the variation of mass transfer coefficient in the bath with the gas injection rate. The value of the factor n has been reported to vary between approximately 0.25 and 2.10⁽²³⁾. However, the value established in this study was considered valid since it was established under more intense stirring conditions. At very high gas blowing conditions used in the CLU-converter, the effect of gas flow rate on mass transport becomes less pronounced. Thus, the low value of the stirring factor of the gas flow rate obtained.

J.M. Chou *et al.*⁽⁶⁾ in their studies of mass transfer between two phases, established that the mass transfer rate increased with gas flow rate. They attributed this to better mixing of oil and water in the cold model. As the gas flow rate approached 0.000 67m³/s the improvement in the mass transfer rate with gas flow rate became less obvious. In the same studies, the value of n was established as 0.39 regardless of sampling location when the gas flow rate was less than the critical gas flow rate, 0.000 67m³/s. However, this value was 0.032 when the gas flow rates were increased above the critical level. Since only gas flow rates above 0.01m³/s were investigated in the current study, it was assumed that the critical gas flow rate for the investigated conditions had been surpassed already.

Steel dissolution in quiescent and gas stirred Fe/C melts studies by J.K. Wright⁽⁸⁾ also indicated the same trend of results. The mass transfer coefficients initially increased strongly with the gas flow rate, but this effect diminished with further increases. The dissolution rates were observed to be significantly higher in the plume region than in the other parts of the bath. Under the conditions of a maximum gas flow rate of 0.000 1m³/s employed, the value of n obtained was

0.21 only. Figure 4.12 below shows the variation of mass transfer coefficient with gas flow rate as established by J.K. Wright⁽⁸⁾.

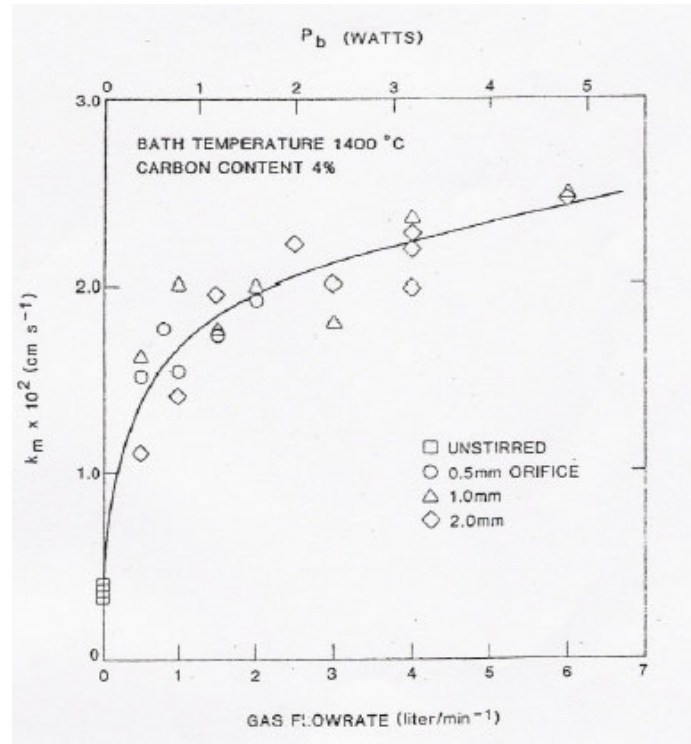


Figure 4.12: Derived mass transfer coefficients vs gas flow rate in the J.K. Wright⁽⁸⁾ 1kg apparatus.

Another important aspect of the results in Figure 4.12 is that, the mass transfer coefficients appeared to be virtually independent of orifice size. He suggested that this was an indication that kinetic power contribution was not important in mass transfer. The high values of the proportionality constant m observed at Location S4 were manifested in this work as the necking behaviour of the immersed graphite rods. The necking of the graphite rods was described as being a result of strong outward surface flow, slopping and wave action at the bath surface. The high mass transfer rates at the bath surface observed in the current study were also described in the same way.

4.4 Mapping experiments

The mapping of the mass transfer coefficients, in three regions, at a constant water bath height of 0.5m was established using the geographical mapping software, Surfer 6. The behaviour of mass transfer rates at a constant bath weight was established for varying purging gas flow rates. Table 4.12 below presents the variation of the turbulence parameters in the three regions investigated as the gas flow rate was varied. These values were calculated using Equation [30]. The results of individual experiments that were carried out to determine mass transfer coefficients for mapping purposes are presented in Appendix 8.

Table 4.12: Turbulence parameters calculated from the mapping experiments

Flow rate (m ³ /s)	Sample location	Bottom region $(Re_{loc,r})^{0.25}(Re_t)^{0.32}$	Near cone region $(Re_{loc,r})^{0.25}(Re_t)^{0.32}$	Near water bath surface region $(Re_{loc,r})^{0.25}(Re_t)^{0.32}$
0.010	S1	71762	63141	82713
	S2	78519	64073	108808
	S3	107410	82014	126748
	S4	92265	168221	187560
	S5	74558	111604	149349
	S6	95993	47764	152611
	S7	71529	53588	126282
0.015	S1	91333	75257	75257
	S2	91566	73626	114400
	S3	133738	95527	123253
	S4	106711	168920	188492
	S5	82247	134204	161697
	S6	103682	54520	131175
	S7	83878	65704	131641
0.023	S1	103449	94595	80849
	S2	108342	94129	101352
	S3	161697	109973	108342
	S4	142825	219014	228333
	S5	103449	167522	181735
	S6	95993	69199	145388
	S7	78519	75956	150281

A close relationship was established to exist between turbulence and mass transfer coefficients in the previous experiments. Therefore, the discussion provided earlier on mass transfer coefficients also apply for turbulence characteristics of the bath and vice versa. The mass transfer coefficient variation in the bath with gas flow rate was presented in the form of contour maps and the corresponding surface plots. The contour maps presented cover the area shown in Figure 4.13 below.

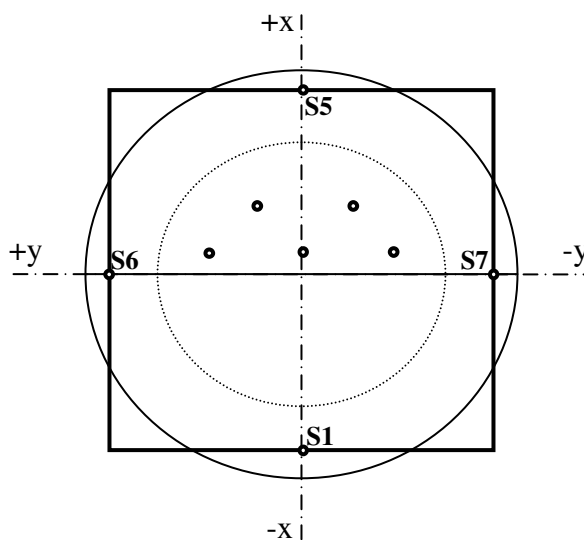


Figure 4.13: The area represented by contour maps.

Figure 4.13 above shows the square that is super imposed on the cross sectional area of the CLU-model vessel. The square represents the area covered on the contour map presentations. The area covered by the contour maps did not take the form of the cross sectional area of the vessel. Therefore, the contour lines presented should show some minor distortions when applied to the actual system. The distortions arise from the contour lines following the geometry of the circular shape of the CLU-converter. The distortions were not expected to significantly affect the mass transfer coefficients mapping in the bath as they would be confined to the peripherals of the tank. Correction of the maps is not necessary for the mappings obtained at the bottom of the bath as they are all radial in nature. Figure 4.14 below presents the mapping of mass transfer coefficients near the cone region of the bath at $0.010\text{m}^3/\text{s}$ gas flow rate. The mapping of all the other conditions investigated can be found in Appendix 10.

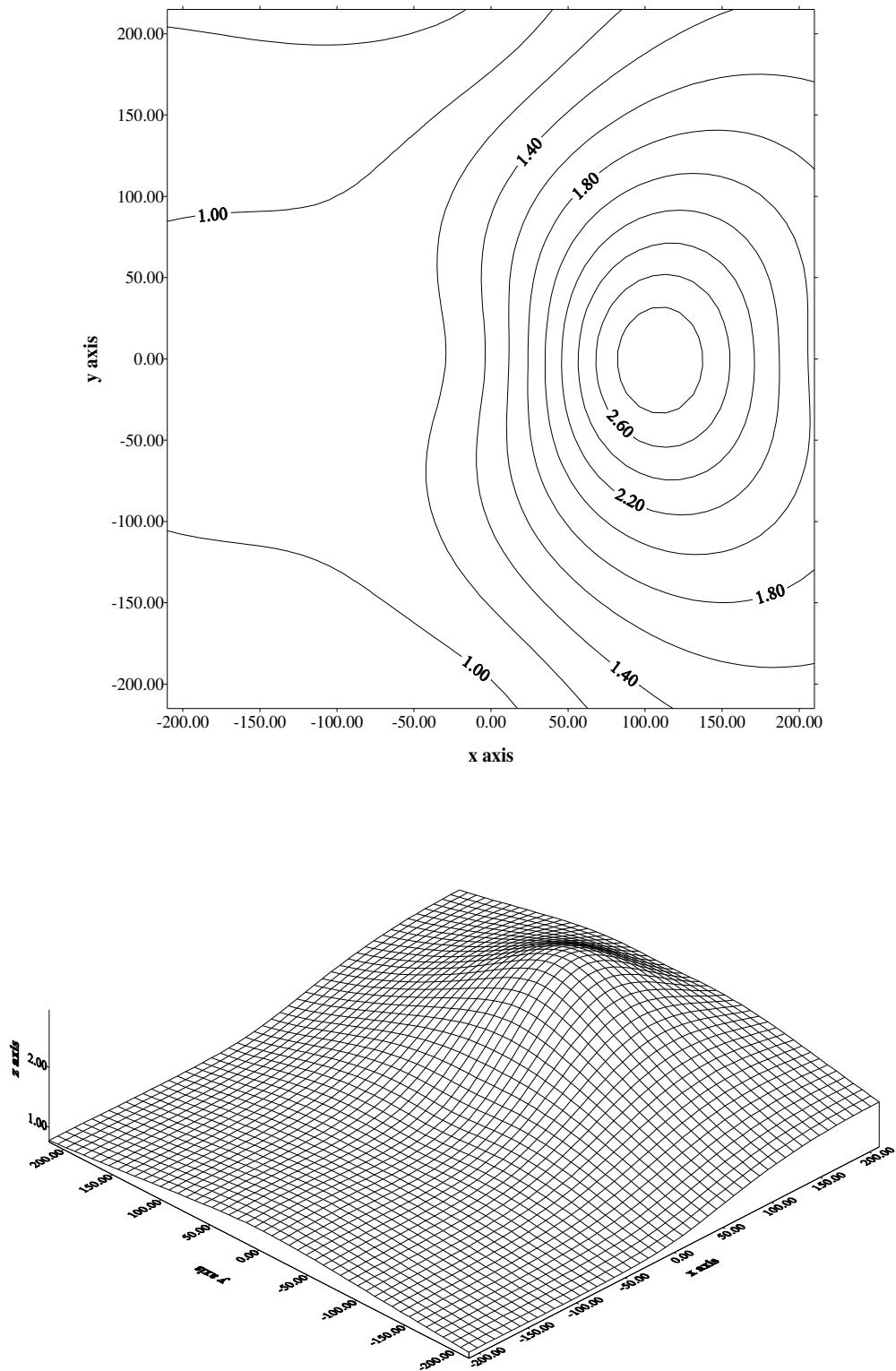


Figure 4.14: Contour and surface plots of mass transfer coefficients near the cone region of the bath at $0.010\text{m}^3/\text{s}$ gas flow rate.

The mass transfer coefficients were highest in the plume region for all the conditions investigated. Figure 4.14 presents contour lines that are denser in the plume region. The mass transfer coefficients reached their maximum values at the crest of the liquid-gas plume in the bath. The surface plot in Figure 4.14 gives a clearer presentation.

Studies by J.K. Wright⁽⁸⁾, showed that the dissolution of a rod that was placed in a purged bath was uniformly eroded along its length with slightly more erosion at the bottom of the bath and greater erosion at the bath surface. In the current study the samples placed in three regions can be viewed to be representative of imaginary long benzoic acid rods with a length similar to the height of the bath. The results obtained can therefore be discussed as representing the whole volume of the bath in the vicinity of a given sample location. For every location investigated in the three regions, the activity of the bath liquid in a column around the imaginary benzoic acid rod was discussed instead.

Figure 4.15 below presents the variation of mass transfer coefficients, at $0.010\text{m}^3/\text{s}$ gas flow rate, in the different bath regions. Locations S1 and S2 were considered to be in quiet regions. Turbulence was relatively minimal in the columnar region that contained these two locations, although it increased close to the bath surface. The turbulence levels were lowest near the cone region for most columnar regions investigated except for the region containing Locations S4 and S5. In the column that contained Locations S4 and S5 turbulence increased all the way to the water bath surface. This was explained in terms of the influence of the gas-liquid plume that dominated mass transfer in the column. Close to the bath surface where turbulence was at its maximum the mass transfer coefficients recorded highest for all locations investigated.

For all the gas flow rates investigated Location S6 recorded the least mass transfer coefficients in the near cone region followed by S7. These two locations were on opposite sides in the model and directly located above the edge of the step at the bottom of the converter. Except near the water bath surface region, the specimens

in these locations were outside the gas-liquid plume region. Thus, the low turbulence and mass transfer rates observed.

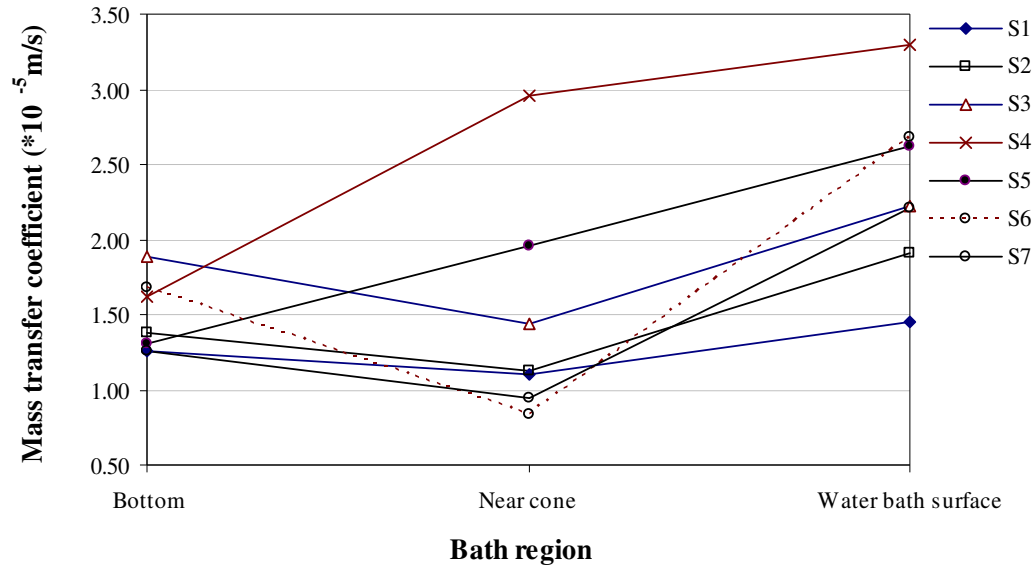


Figure 4.15: Mass transfer coefficient variations in three regions at a gas flow rate of $0.010 \text{ m}^3/\text{s}$.

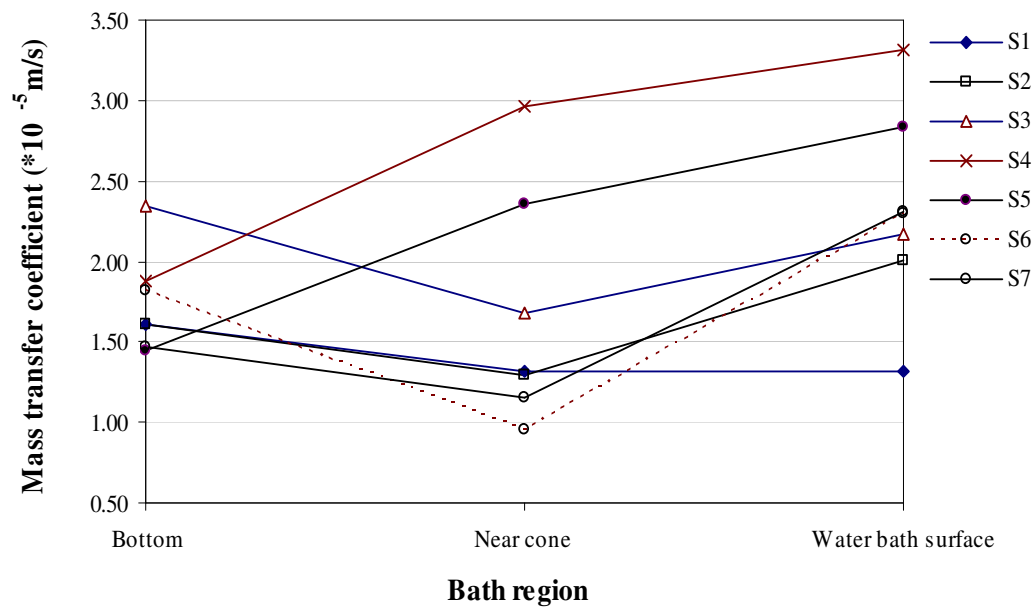


Figure 4.16: Mass transfer coefficient variations in three regions at a gas flow rate of $0.015 \text{ m}^3/\text{s}$.

Figure 4.16 shows that, although the actual mass transfer coefficients values increased from those obtained at $0.010\text{m}^3/\text{s}$ gas flow rate the general shapes of the graphs were almost the same. The only change was observed at S1 near the water bath surface region where the mass transfer coefficient remained the same as that recorded near the cone. The observation was explained to be a result of the fact that, the column was on the opposite side of the plume region crest. Therefore, it was located in the part of the vessel where the bath load from the crest of the plume joined the return path to the bottom of the vessel. At this point, the bath liquid had its minimum energy level at the bath surface under the conditions of operation. As a result, the sample located in this quieter region experienced minimum dissolution/erosion.

It was also discussed that, at this gas flow rate the generally high turbulence exhibited near the bath surface region was not observed at S1 as a result of formation of circulation cells that inhibited effective mass transfer. Presence of circulation cells could have impacted negatively on the mass transfer at this location. The bath liquid in the circulation cells probably had saturated and slow moving liquid around the specimens. A pregnant liquid around a specimen can reduce the driving force for dissolution. This is a result of a small acid concentration gradient existing between the bulk liquid and the liquid film on the surface of the specimen.

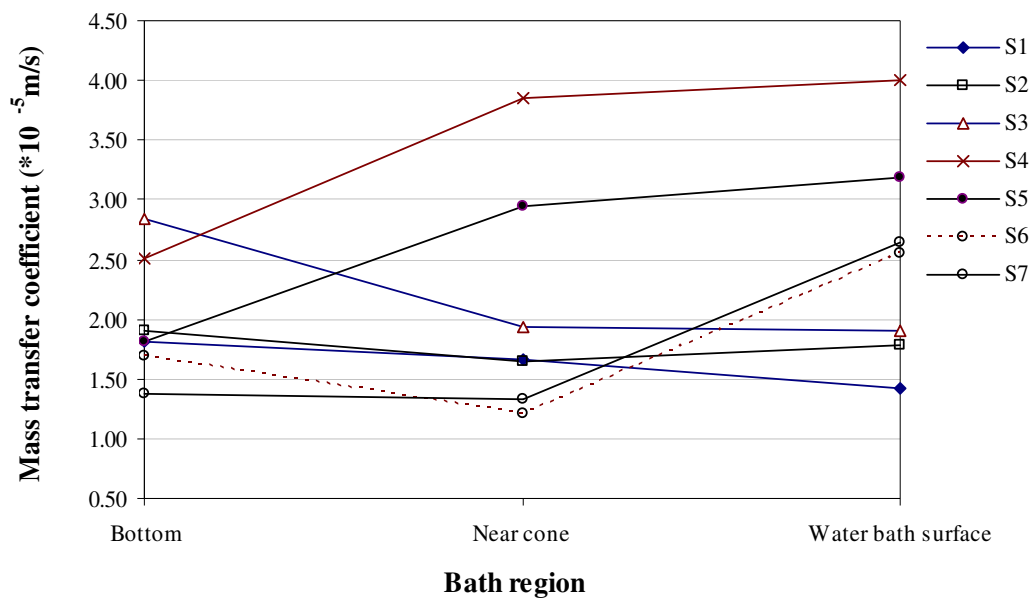


Figure 4.17: Mass transfer coefficient variations in three regions at a gas flow rate of $0.023\text{m}^3/\text{s}$.

As the gas flow rate was increased to $0.023\text{m}^3/\text{s}$, more locations had lower or similar mass transfer coefficients near the water bath surface region as near the cone region. Figure 4.17 above shows that Locations S1, S2 and S3 exhibited this new trend. Zone shifting was used to explain the development of a less active region at the water bath surface at these locations. Mass transfer was highest at this gas flow rate. The mass transfer coefficient values recorded near the cone region and those recorded near the water bath surface were almost similar at most locations. Samples S6 and S7, that were located in areas generally regarded as quiet zones, recorded relatively high mass transfer rates near the water bath surface. The new trend of mass transfer coefficients variation demonstrated that the plume had increased its volume. The high turbulence experienced at the bath surface extended deep into the bath at this gas flow rate. It was therefore concluded that, the growth of the turbulent liquid-gas plume was reaching a mature stage. Thus, the gas-liquid plume extended on to most parts of the vessel above the near cone region.

4.4.1 Effect of the slag phase and gas flow rate on mass transfer

A comparison of mapping results obtained in the absence and presence of the simulated slag phase was done to establish the effect of the simulated slag phase. Comparisons of the respective mass transfer coefficients obtained in the model experiments are shown in bar graphs in Figure 4.18 up to Figure 4.26. The results of the experiments showed that the mass transfer values were lowered by the inclusion of the slag phase. This was attributed to an increased bath load reducing the specific stirring energy under the given conditions. Although to a lesser extent, the change in the dissolving capacity of the bath solution as a result of increased viscosity reduced samples' dissolution when the slag phase was included. The decrease in the mass transfer coefficients with slag inclusion were not constant but averaged 19.3% for all the gas flow rates investigated in the bottom region. The decreases were about 26%, 14% and 18% for the gas flow rates $0.010\text{m}^3/\text{s}$, $0.015\text{m}^3/\text{s}$ and $0.023\text{m}^3/\text{s}$ respectively.

The changes in mass transfer coefficients were highest at low gas flow rates. This was explained by the fact that, when stirring energy is low any opposing energies or factors result in a large change in mass transfer coefficients. The effect was minimised as the gas flow rate increased, resulting in increased stirring energies, whereas the retarding factors remained almost unchanged.

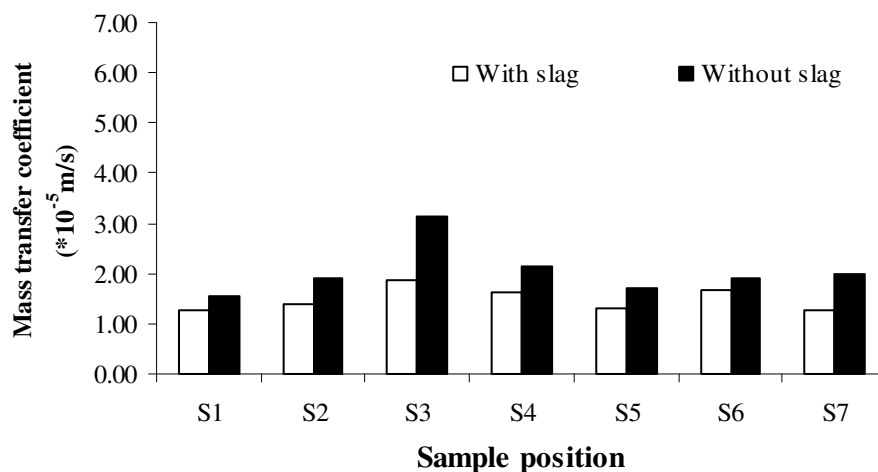


Figure 4.18: Comparison of mass transfer coefficient values at a gas flow rate of $0.010\text{m}^3/\text{s}$ in the bottom region.

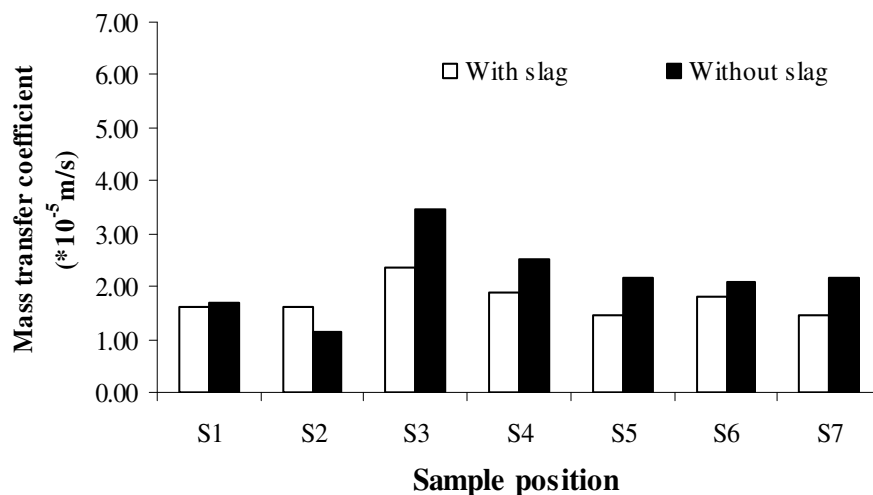


Figure 4.19: Comparison of mass transfer coefficient values at a gas flow rate of $0.015\text{m}^3/\text{s}$ in the bottom region.

The inconsistent behaviour of the mass transfer coefficients comparison at location S2 was attributed to a possible experimental error in the earlier work (without slag). The deduction is supported by the fact that for all the other experiments in both investigations, activity at locations S1 and S2 were similar. In the above case the mass transfer coefficient at S2 was uncharacteristically lower than that at S1 thus, the abnormality observed during the comparison of results.

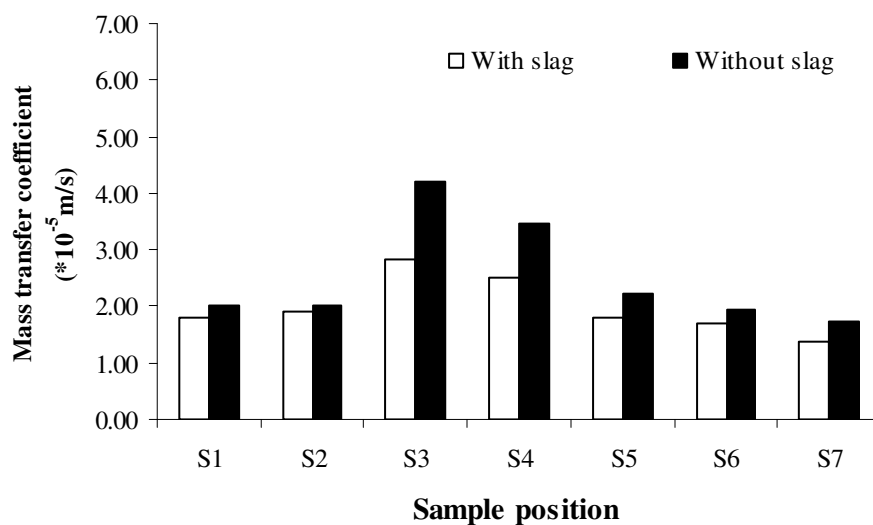


Figure 4.20: Comparison of mass transfer coefficient values at a gas flow rate of $0.023\text{m}^3/\text{s}$ in the bottom region.

As presented in Figures 4.18, 4.19 and 4.20 above, the mass transfer coefficient in the bottom region were higher in experiments performed in the absence of the slag phase. For both investigations considered, mass transfer coefficients were generally higher in the regions close to the nozzles where Samples S3, S4 and S5 were located. The step at the bottom of the model converter was responsible for increased turbulence in its vicinity thus, the higher mass transfer rates observed on Sample S4.

Mass transfer rates in the bottom region increased with purging gas flow rate. An increase in gas flow rate resulted in increased stirring power in the bath hence, more erosion and/or dissolution of the suspended samples. The mass transfer rates in this region were generally low because the samples were placed at the end of the bath liquid re-circulating loop. The liquid in this region had lost much of its kinetic energy thus, the eroding power. Turbulence was limited as gas bubbles were only confined to regions in the vicinity of the nozzles.

Figures 4.21, 4.22 and 4.23 below, show comparisons of the mass transfer coefficients near the cone region. The samples were located slightly above the nozzles, where the cylindrical section of the vessel started. As a result of the close vicinity of the nozzles to the region, Samples S4 and S5 that were inside the high turbulent gas-liquid plume experienced much increased mass transfer rates. Compared to the values in the bottom region, lower mass transfer coefficients were recorded at Location S3 for all gas flow rates. The lowering of mass transfer coefficients showed the decreasing influence of the step as the samples moved away. A greater influence of the gas-liquid plume in this region became apparent.

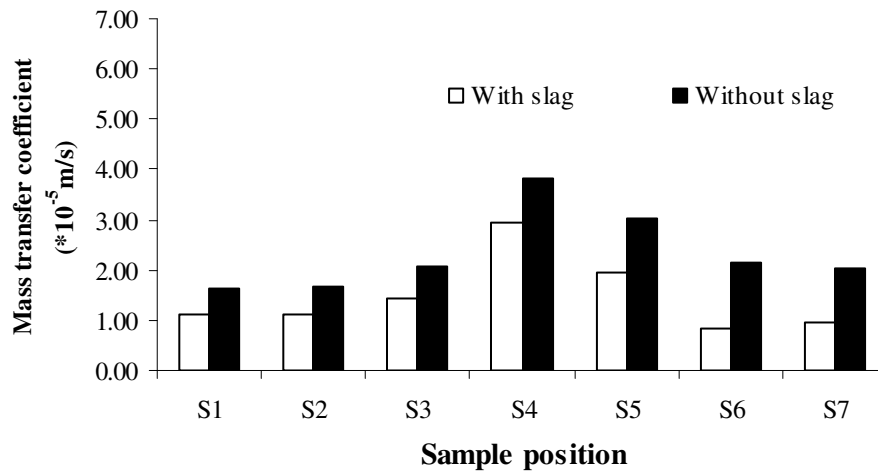


Figure 4.21: Comparison of mass transfer coefficient values at a gas flow rate of $0.010\text{m}^3/\text{s}$ near the cone region.

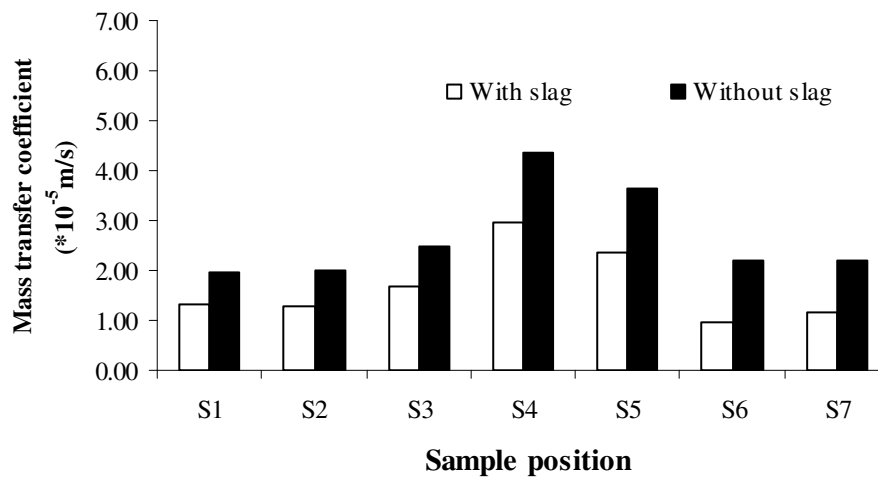


Figure 4.22: Comparison of mass transfer coefficient values at a gas flow rate of $0.015\text{m}^3/\text{s}$ near the cone region.

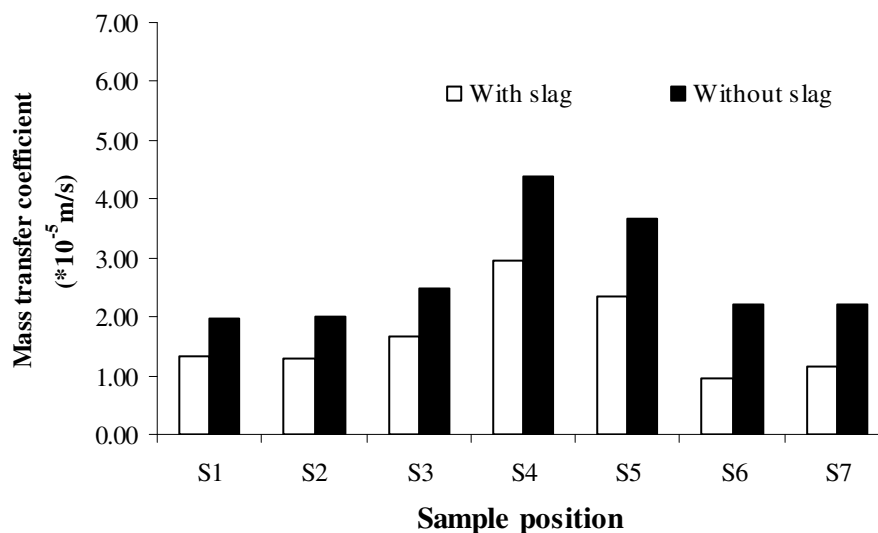


Figure 4.23: Comparison of mass transfer coefficient values at a gas flow rate of $0.023\text{m}^3/\text{s}$ near the cone region.

The mass transfer coefficients decreased at all the other locations except for Locations S4 and S5. This was attributed to the fact that these samples were not located inside the plume region thus, the marginal mass transfer rates observed. The mass transfer rates followed the turbulence patterns that were exhibited in the bath. Generally the mass transfer rates were higher in the bottom region than near the cone region for positions that did not fall inside the plume.

Two distinct regions were observed in the near cone region. There was a region that fell inside the plume and another one that was extending from the vessel walls to the interface between the re-circulating liquid and the plume region. Existence of dead volumes in the latter region was quite probable. Under conditions of low gas purging, slow moving kerosene droplets were observed in this region for quite long periods of time at the beginning of experimental runs before they became invisible. It was therefore assumed that, the slow motion of kerosene droplets was an indication of the existence of dead volumes in the region. This condition resulted in low turbulence levels hence, the lower mass transfer rates that were observed.

J. Szekely *et al.*⁽⁵⁾ investigations in argon stirred ladles indicated that the mass transfer rate was observed to increase with an increase in the stirring gas flow rate. They attributed this to increased turbulence. J.K. Wright⁽⁸⁾ investigations reflected greater mass transfer rates on the bath surface and slightly higher rates at the bottom than in the middle of the bath. The same observation was made in the current study for most locations investigated except for Locations S4 and S5.

The average change in mass transfer coefficients was 37.7% in the cone region. The reductions in mass transfer coefficients with the inclusion of the slag phase were about 38%, 39% and 36% for the gas flow rates 0.010m³/s, 0.015m³/s and 0.023m³/s respectively. A greater reduction in the mass transfer coefficient values near the cone region, than in the bottom region, was observed when the slag phase was included. This probably resulted from a combination of two factors. Firstly, the less exposure of the samples in the bottom region to the aggressive gas-liquid plume turbulent currents encountered near the cone region meant that the samples experienced marginal changes when the slag was included. The major driving forces for samples' dissolution rates in the bottom region were most likely less affected by the reduction in specific stirring energy of the bath. Secondly the reduction in turbulent currents near the cone region as a result of the increased load impacted more on the mass transfer rates in this region. In the near cone region, mass transfer processes were mainly driven by purging gas stirring power related turbulence. The reduced influence of the step at the bottom of the vessel compounded to effects of a reduced gas stirring power. Consequently, the effect of a reduced specific energy input was extensive as only less effective forces were available to promote mass transfer.

Samples near the water bath surface region recorded highest mass transfer rates. As explained earlier, the increased turbulence resulting from a much wider plume region was responsible for the high mass transfer rates. A sudden pressure drop at the bath surface also added to the turbulence in this region. Eddies produced in the liquid by the gas leaving the bath at high velocity were responsible for the increase in the eroding power of the bath liquid in the vicinity of the bath surface.

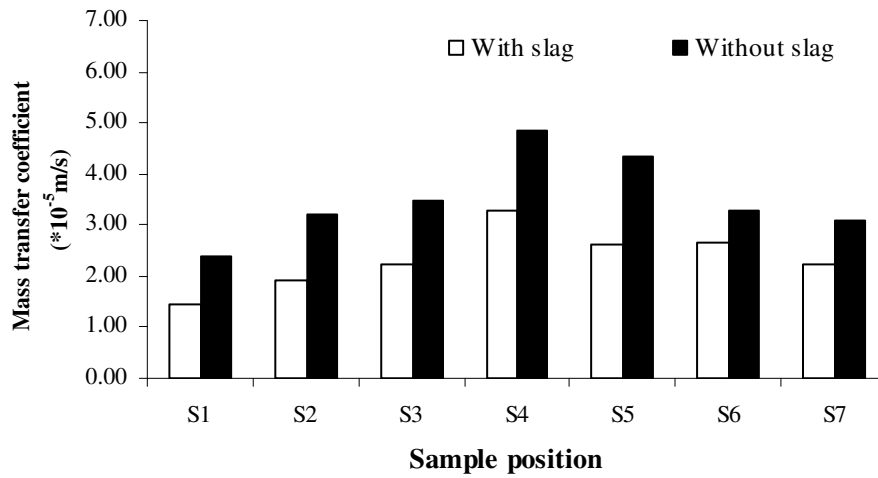


Figure 4.24: Comparison of mass transfer coefficient values at a gas flow rate of $0.010\text{m}^3/\text{s}$ near the water bath surface region.

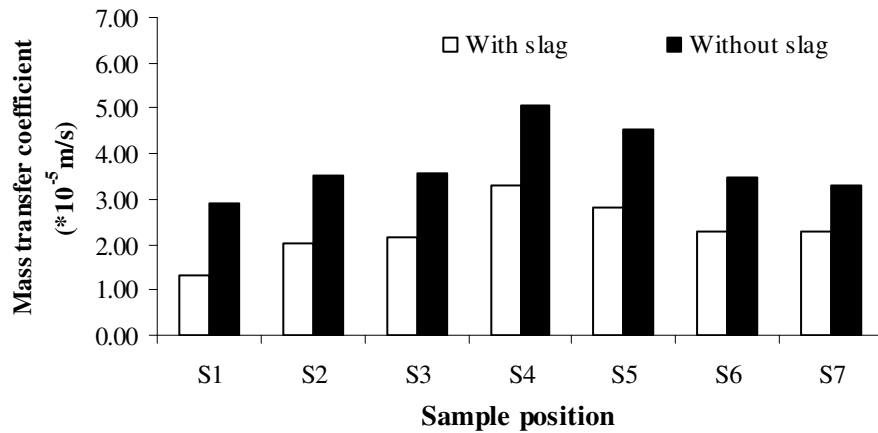


Figure 4.25: Comparison of mass transfer coefficient values at a gas flow rate of $0.015\text{m}^3/\text{s}$ near the water bath surface region.

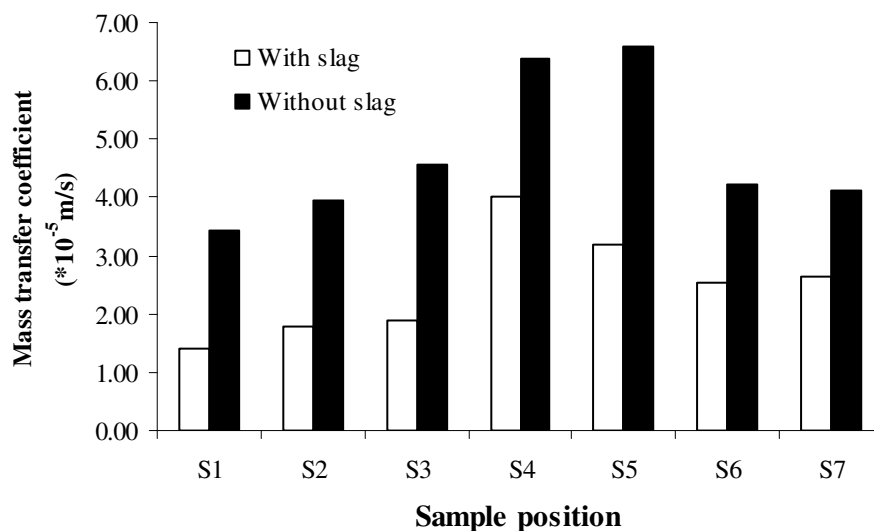


Figure 4.26: Comparison of mass transfer coefficient values at a gas flow rate of $0.023\text{m}^3/\text{s}$ near the water bath surface region.

Figures 4.24, 4.25 and 4.26 above present the effect of slag inclusion to mass transfer coefficients near the water bath surface region. For all measurements taken, samples at Location S4 recorded maximum mass transfer coefficients. The plume effect at this location was marginal only in the bottom region, where the sample was not positioned inside the plume volume. The average change in mass transfer coefficients was 40% near the water bath surface region. The reductions in the mass transfer coefficients with slag inclusion were about 33%, 39% and 48% for the gas flow rates $0.010\text{m}^3/\text{s}$, $0.015\text{m}^3/\text{s}$ and $0.023\text{m}^3/\text{s}$ respectively. Comparable average changes in mass transfer coefficient values in the near cone region and water bath surface region show that the inclusion of the slag phase had the same effect in the two regions. This was to be expected as mass transfer processes in both regions were mostly influenced by turbulence in the bath liquid.

4.5 Effect of the simulated slag phase on mixing time

By considering the correlations obtained in the two cases it was possible to get a clear picture of the effect of including a second phase. The specific energy input was identified as the only variable in the mixing time correlations that could be used to compare the two cases at the same level. The mixing time values predicted

using the established correlations were compared on the basis of their variations with specific energy input to the bath. Figure 4.27 below was plotted from the predicted values.

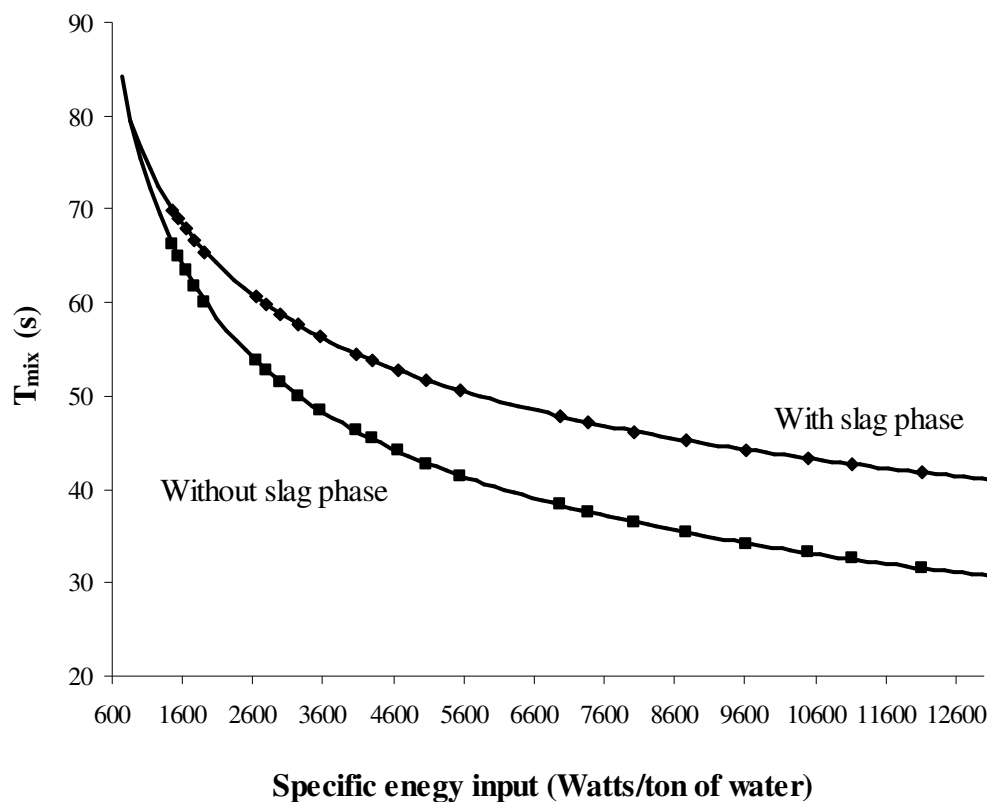


Figure 4.27: Effect of the slag phase inclusion on the mixing time values predicted for model converter operations.

Figure 4.27 compared the mixing time values when the baths were at the same water bath height but had different weights because of the slag included in the other case. It is apparent from the plots in Figure 4.27 that the mixing time increased with the inclusion of the slag phase. It took a longer period for the same energy input rate to produce the same level of acid distribution in an increased bath volume. Thus, the higher mixing time values recorded. The main reason for the rise in mixing time with the inclusion of the slag phase, as pointed out earlier, is the fact that the slag phase dissipated some of the input energy to the bath.

Working on the assumption that, both predictions were accurate a number of deductions were made from the graphs presented in Figure 4.27. The effect of the slag phase, at constant proportion by volume, was observed to increase with the specific stirring energy density. Specific energy density in the bath increased with gas flow rate and decreased with bath height.

J.K. Wright⁽⁸⁾ made an observation that the mass transfer was mainly controlled by buoyancy energy at large bath heights. He also pointed out that at shallow baths the kinetic energy factor might become more significant. Equation [22] shows an exponential relationship between the stirring power and the gas flow rate. Consequently a marginal decrease in gas flow rate in the bath reflects as a huge reduction in the stirring power in the converter. Slag inclusion had the effect of reducing the liquid velocity in the bath. Thus, an increased change in mixing time value was observed when the specific energy input increased.

Low specific energy input conditions in the bath are observed at high bath heights and low gas blowing rates. Under conditions of high bath weight, the kinetic energy factor of input energy has little effect on mass transfer rates that are mainly controlled by buoyancy energy. Other factors therefore become more significant in influencing the mixing behaviour of the bath.

At lower stirring rates, the bath took long periods to homogenize. The extended period observed during bath homogenization allowed the tracer enough time to partition itself, in equilibrium amounts, between the two phases making up the bath liquid. This occurred in almost the same time as it would have in a single phase. This was the reason why the mixing time change with the inclusion of the slag phase was small at lower specific energy input than at high specific energy input. Under the latter conditions, bath homogeneity was quickly achieved in a single phase bath. Thus, the inclusion of a second phase tended to prolong the mixing time more as the tracer distributed itself in a bath that was not homogenous. The different kerosene-water proportions at the bottom and surface was responsible for the inhomogeneity of the bath liquid.

In the absence of stirring or at very low stirring rates, mixing of the tracer is mainly controlled by convection forces that are less affected by a second phase inclusion. Therefore, the mixing time values were predicted to converge or to be very close at some point as the specific energy input was lowered.

The above comparison showed that the simulated slag phase had the effect of increasing the T_{mix} value under the model converter operating conditions. This change in mixing time was not constant as it was affected by the size of the specific energy input to the bath. However, an average change in mixing time of 16.3% was observed for the conditions investigated.

4.5.1 Differences in the way the collected data was analysed

In the current study homogeneity of the bath was defined at 99.66% whilst the earlier work⁽²⁾ defined it at 95%. The seemingly pronounced difference in the levels of homogeneity adopted in the two situations emanated from the difference in the definitions of homogeneity of the bath solution that were used. Whilst in the earlier work the effect of temperature changes on the pH of the bath was not taken into consideration, the values of mixing time obtained in the current study took into account the effect of these changes.

Observations from the performed experiments do not agree with the assertion made in the earlier work⁽²⁾ that there exist stable pH values. The pH values recording on the meter were never stable for long periods of time during the 20minutes long experiments conducted. This has been explained to be a result of a drop in bath temperature caused by the cold compressed air that was used for purging the bath. The relationship between temperature and pH is well represented by the Nernst's equation.

For a meaningful comparison of the mixing time values obtained in the two cases to be made, the degree of mixing considered had to be the same or almost so. The two sets of work were successfully compared by carefully taking into

consideration the difference in the way the collected data was analyzed. Whilst there seem to be a big difference in the homogeneity levels considered, the matter-of-fact is that, these two cases considered mixing time at almost the same level of tracer distribution.

Temperature compensation of the bath pH performed in the current study had the effect of raising the pH level of the solution when a defined homogeneity was supposedly reached. As a result, approximately the same pH value that was defined to describe homogeneity at 95% was used to check for the mixing time at 99.66% homogeneity after temperature compensation. On the basis of this argument, it was reasonably assumed that the level of homogeneity considered in both cases was almost the same. In other words, the bath homogeneity level defined as 95% in the earlier work was approximately defined as 99.66% in the current study. Table 4.13 and Table 4.14 below present a summary of the results obtained in the two cases.

Table 4.13: Mixing time values obtained in the presence of a slag phase.

Water Bath height (m)	Gas flowrate /m³/s				
	0.010 0	0.012 7	0.015 0	0.018 3	0.021 2
0.50	52	49	41	36	38
0.55	62	53	44	49	43
0.60	69	61	52	44	40
0.65	73	64	57	51	49
0.70	83	70	63	55	51

Table 4.14: Mixing time values obtained in the absence of a slag phase^(2,3).

Bath height (m)	Gas flowrate /m³/s				
	0.010 0	0.012 7	0.015 0	0.018 3	0.021 2*
0.50	54	49	39	36	34
0.55	58	48	39	33	41
0.60	65	55	39	33	38
0.65	69	47	39	42	41
0.70	75	39	59	43	43

*The flow rate was investigated in the current study but under earlier work⁽²⁾ conditions.

The effect of slag inclusion was clearly shown by graphical comparisons of the results in Tables 4.13 and 4.14 above. Figures from 4.28 to 4.37 below present the effect of the simulated slag phase under different conditions investigated. The effect of slag under conditions of varying gas flow rate at a constant bath height was presented in Figures from 4.28 to 4.32. The remainder of the figures presents the effect of slag when the bath height was varied whilst the gas flow rate was kept constant.

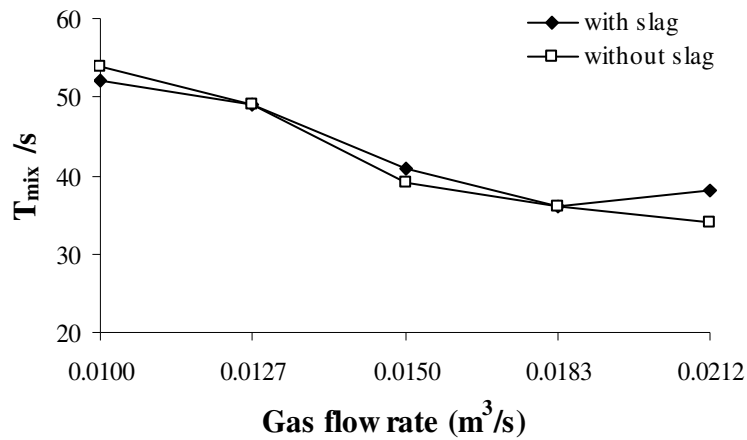


Figure 4.28: Mixing time variation with gas flow rate at a water bath height of 0.50m.

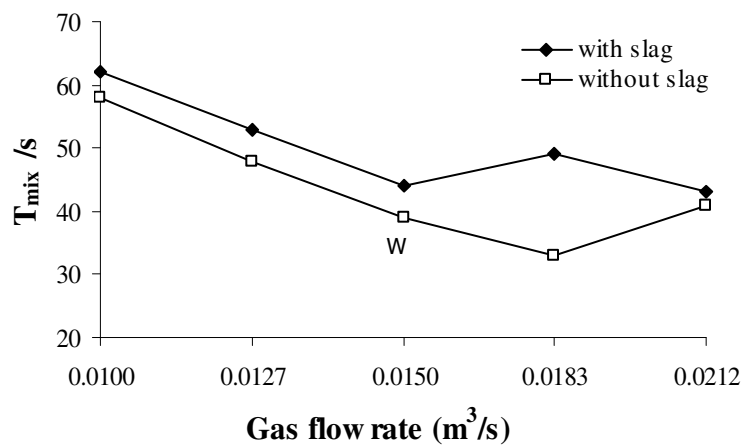


Figure 4.29: Mixing time variation with gas flow rate at a water bath height of 0.55m.

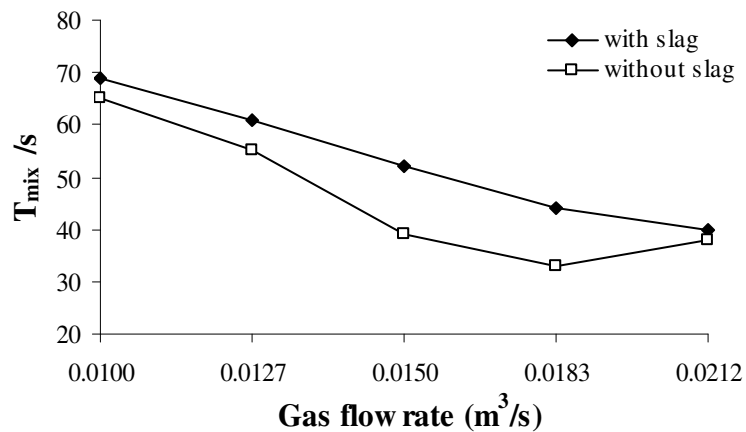


Figure 4.30: Mixing time variation with gas flow rate at a water bath height of 0.60m.

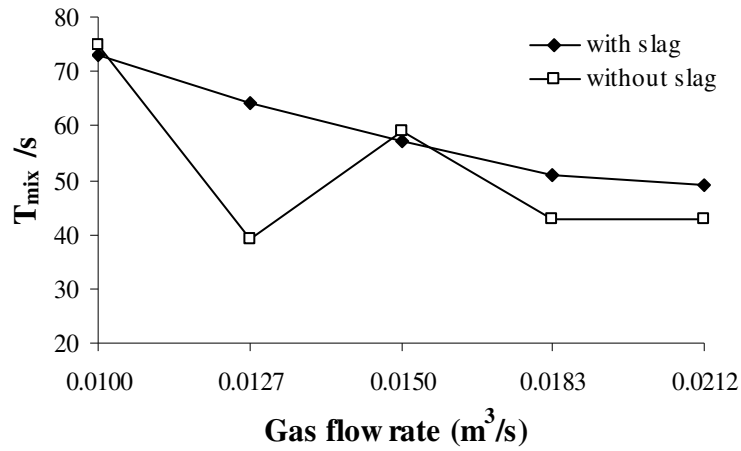


Figure 4.31: Mixing time variation with gas flow rate at a water bath height of 0.65m.

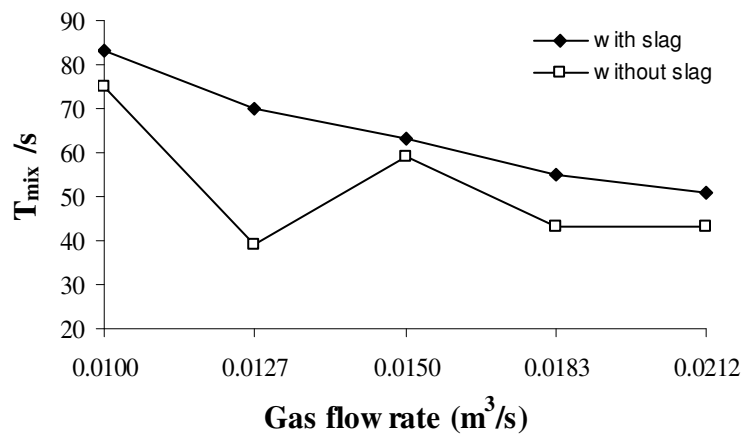


Figure 4.32: Mixing time variation with gas flow rate at a water bath height of 0.70m.

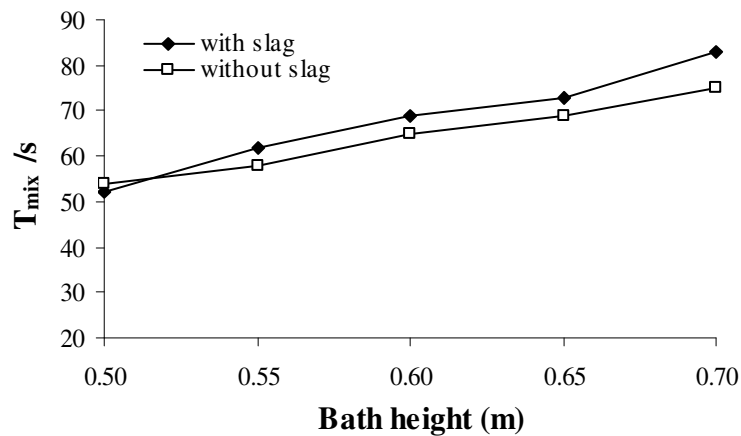


Figure 4.33: Mixing time variation with bath height at a gas flow rate of 0.010 m^3/s .

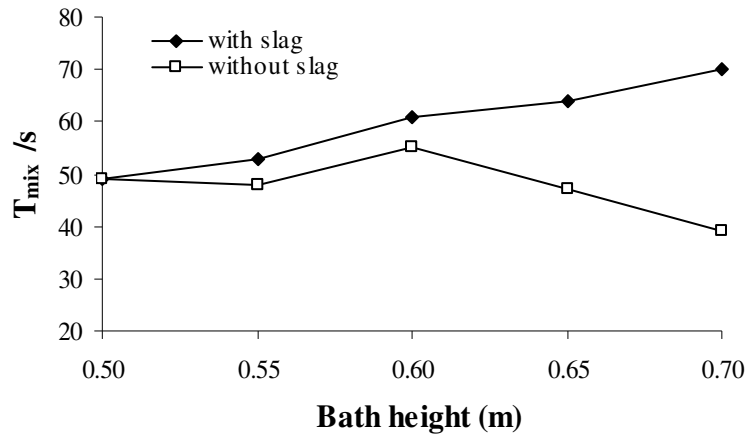


Figure 4.34: Mixing time variation with bath height at a gas flow rate of $0.0127 \text{ m}^3/\text{s}$.

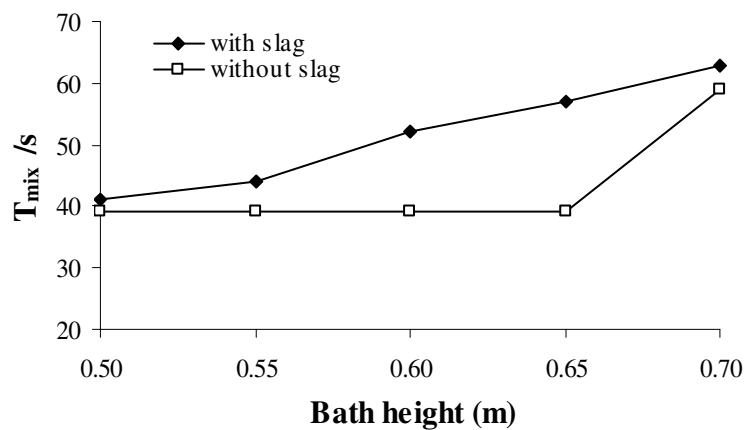


Figure 4.35: Mixing time variation with bath height at a gas flow rate of $0.0150 \text{ m}^3/\text{s}$.

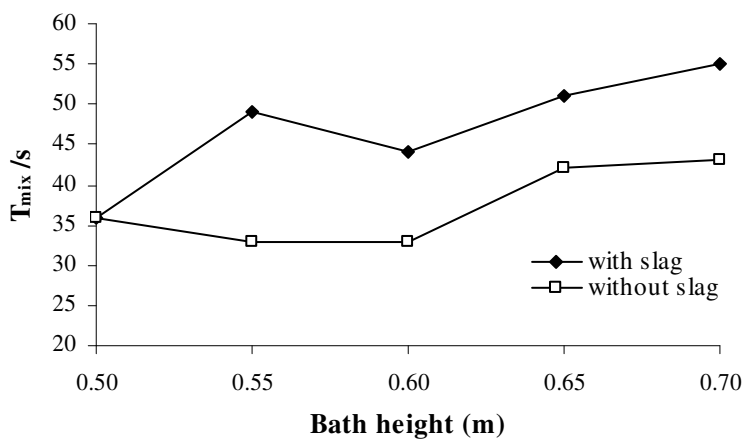


Figure 4.36: Mixing time variation with bath height at a gas flow rate of $0.0183 \text{ m}^3/\text{s}$.

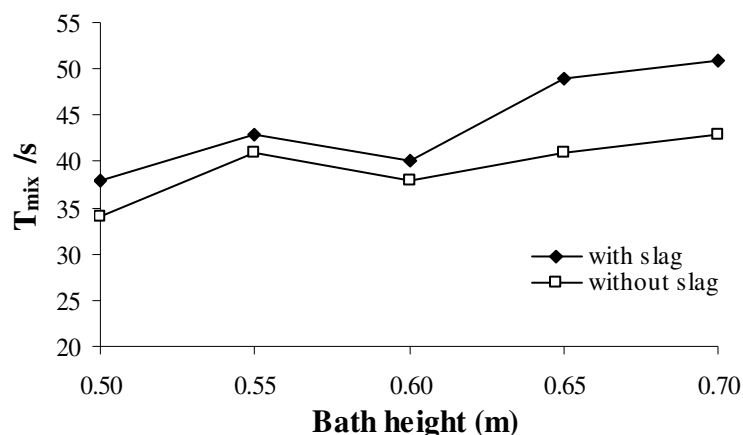


Figure 4.37: Mixing time variation with bath height at a gas flow rate of $0.0212\text{m}^3/\text{s}$.

The graphical presentations above give substance to the observations that were based on the presentation given in Figure 4.27. It is apparent that the inclusion of a second phase had the effect of increasing the mixing time. The effect of the simulated slag phase was further emphasized by comparing the mixing time values that were obtained in this study both in the presence and absence of the simulated slag phase. Table 4.15 below presents the results of mixing time experiments carried out and analyzed at 99.66% bath homogeneity.

Table 4.15: A comparison of the T_{mix} values obtained with and without a second phase.

Flow rate (m^3/s)	Bath height (m)	T_{mix} without Slag phase (s)	T_{mix} with Slag phase (s)	T_{mix} Difference (s)	% T_{mix} Change
0.0100	0.50	42	52	10	23.8
0.0150	0.50	28	41	12	42.9
0.0212	0.50	34	38	4	10.5
0.0212	0.55	41	43	2	4.7
0.0212	0.60	38	40	2	5.0
0.0212	0.65	41	49	8	16.3
0.0212	0.70	43	51	8	15.7

The results in the Table 4.15 show that the change in mixing time that resulted from the inclusion of a second phase was not exactly constant. An average value of the percentage change in mixing time was calculated from these results to be, 17%. The value compares quite well with the 16.3% value obtained from Figure 4.27 presentation. The close similarity of these percentage changes in T_{mix} values as presented is important. It gives substance to the comparisons of the mathematical relationships, Figure 4.37, and the assumption made on the similarities of levels of homogeneity considered in the two cases. It was therefore concluded that the analysis presented gave a true picture of the influence of the slag phase on mixing in the model bath. The comparison of the two investigations was therefore considered successful.

4.6 Comparison of mixing time and mass transfer rates

An effective comparison can be made if measurements obtained under the same operating conditions and at the same location in the bath are compared. The turbulence parameters obtained at Location S6 were used for this purpose as this was also the position of the pH-temperature probe in the mixing time experiments. Figure 4.38 below shows the relationship that existed between the turbulence parameters and the mixing time in the bath. High stirring rates favoured an increase in the turbulence parameters in the bath and a reduction in the mixing time.

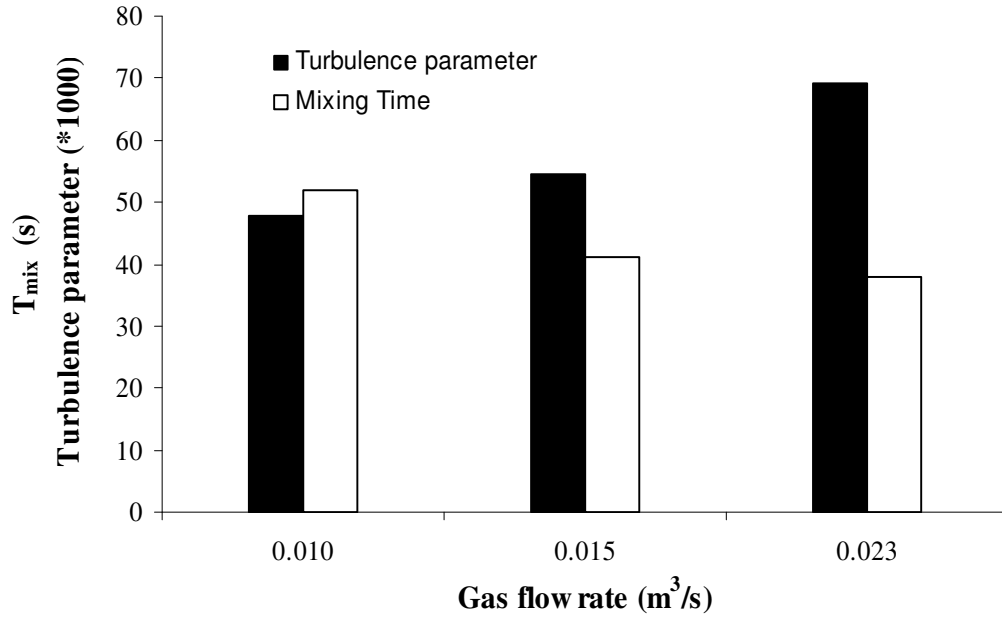


Figure 4.38: Comparison of the mixing time and turbulence parameter variations with an increase in the gas flow rate at a water bath height of 0.5m.

4.7 Scale up of model results to the industrial size vessel

Mazumdar *et al.*⁽³⁰⁾ showed that, in the Froude dominated flow regime the ratio of mixing time in geometrically and dynamically similar gas stirred systems could be represented in terms of the geometrical scale factor (λ). The geometrical scale factor is defined as the ratio of the depth of the liquid in the reduced scale model (L_{mod}) to that in the full-scale model (L_{fs}) or the actual industrial scale vessel, i.e.

$$\lambda = \frac{L_{mod}}{L_{fs}} \quad [45]$$

To relate the mixing time relationship obtained in a reduced scale model to a full scale vessel the equation below was suggested⁽³⁰⁾.

$$\lambda^{\frac{1}{2}} = \frac{T_{mix, mod}}{T_{mix, fs}} \quad [46]$$

Equation [46] above was reported to hold quite well regardless of the definition of mixing, mode of gas injection *etc.* The equation holds well as long as the inertial and gravitational forces in the metallurgical vessel dominate the flow phenomena.

The scaling equations reported in literature are of the form

$$\lambda^n = \frac{Q_{\text{mod}}}{Q_{fs}} \quad [47]$$

Where values of n that have been reported are 1.5, 2.5 and 2.75. The Fruehan⁽²⁴⁾ work represented by Equation [48] below, gave 2.5 as the value of n . He argued that as the full size model was translated to a reduced size model, the similarity requirements needed to be taken into account to calculate the gas flowrate of the reduced size model. This could be obtained by using the following equation,

$$Q_m = 0.963 \lambda^{5/2} Q_{fs} \quad [48]$$

To assess the adequacy and appropriateness of these equations, Mazumdar *et al.*⁽³⁰⁾ made comparisons of experimental ratios of mixing times with the corresponding theoretical ratio ($\lambda^{1/2}$). They confirmed that in the Froude dominated flow regime the most appropriate criterion for dynamic similarity between model and full scale ladles is,

$$\lambda^{2.5} = \frac{Q_{\text{mod}}}{Q_{fs}} \quad [49]$$

The correlation in Equation [49] can be used to calculate the gas flow rates to be used for water models of full size. However, for the purposes of relating the gas flow rates of water model operations to the actual industrial system operation a consideration of the modified Froude number is necessary. To allow the results from cold model experiments to be extrapolated to the industrial scale the Froude number should be maintained the same in the two cases.

Using the scale up method suggested in Equation [46] above, the established mixing time correlation for estimating the mixing time in the one-fifth model was modified to represent the full scale and the actual system as follows,

$$T_{mix} = 9.82 Q^{-0.73} W^{0.24} H^{1.12} \quad [50]$$

Where W (tons) and Q (m³/s) are values from the one-fifth scale model set-up.

Table 4.16: Gas flow rates adopted in the model systems and those used in the actual operation.

0.2-SCALE MODEL FLOW RATE (Nm ³ /s)	FULL SCALE MODEL SYSTEM (Nm ³ /s)	INDUSTRIAL VESSEL BLOWING RATE (Nm ³ /s)
0.0100	0.559	0.945
0.0127	0.710	1.200
0.0150	0.839	1.418
0.0167	0.934	1.578
0.0183	1.023	1.730
0.0212	1.185	2.004

Table 4.16 presents the gas flow rates adopted in the cold model investigations (the one-fifth scale vessel and the full scale vessel) and the normal gas blowing rates in the actual operation. The mixing time in the industrial vessel at a given gas blowing rate can be estimated by first taking the equivalent value in the one-fifth scale model and then using Equation [50].

4.8 Relating the full scale model to the actual vessel

The Froude number similitude adopted should allow for direct extrapolation of observations made in the full scale vessel to the industrial vessel operation. Mixing and mass transfer processes are expected to take place at the same rate and to the same extent in both the full scale vessel and the actual vessel. The

difference in the blowing rates in the two vessels, as presented in Table 4.16, only arises as a result of the density and viscosity differences of the fluids making up the load in the two cases.

By considering the values and ratios of corresponding variables between the one-fifth model system and the actual industrial vessel, the mixing time can be obtained from values of the latter. Equation [51] can be used to determine the mixing time in the industrial CLU-converter operation.

$$T_{mix} = 171 Q^{-0.73} W^{0.24} H^{1.12} \quad [51]$$

Where W (tons) and Q (m³/s) are values from the actual CLU-converter operation.

5 CONCLUSIONS AND FUTURE WORK

Under conditions of a constant slag proportion in the bath, mixing conditions in the CLU-converter improved with an increase in purging gas flow rate but deteriorated with an increase in bath height. The mixing time was found to increase with bath height and decrease with gas flow rate. The mixing time data obtained was related to the specific energy dissipation rate. A functional relationship expressing the effect of the gas flow rate (Q), the bath weight (W) and bath height (H) on the mixing time (T_{mix}) in the model vessel was established as,

$$T_{mix} = 4.39 Q^{-0.73} W^{0.24} H^{1.12}$$

The established correlation above was found to estimate the mixing time to within $\pm 3\%$ of the actual value. Inclusion of the simulated slag phase resulted in the mixing time increasing by an average of about 16%. The mixing time was significantly prolonged at high levels of specific energy input to the bath and only marginally at very low specific energy levels that corresponds to large bath heights and low gas flow rates. The mixing time correlation obtained for the model set-up was extrapolated to represent the actual system using the established scale up methods. A reasonable estimate of the mixing time in the actual vessel can be obtained using the correlation,

$$T_{mix} = 9.82 Q^{-0.73} W^{0.24} H^{1.12}$$

The established mixing time correlation for extrapolating experimental results to the actual vessel may serve as a tool to correctly determine the lengths of blowing during metal refining. Using this relationship the mixing time in the real CLU-converter can be closely estimated provided the slag phase constitutes 10% by volume.

It was established that the mass transfer rates were affected by the inclusion of a second phase in the model investigations. Under experimental conditions the mass transfer coefficients decreased by an average of 32% with the incorporation of the

slag phase. The inclusion of the slag phase did not bring about changes on the patterns of mass transfer parameters in the bath but the rates of mass transfer were reduced. The relationship showing derived mass transport coefficients (K) dependence on the gas injection rates (Q) was established as,

$$K \propto Q^{0.08}$$

The obtained relationship showed the little effect the increase in gas flow rate has under the high gas stirring rates used in the CLU-converter operation. Contour type presentation of mass transfer coefficients (K) variation established maybe useful in the operation of a CLU-converter. The behaviour of melting and dissolution of additives in various regions of the metal bath can now be predicted with improved accuracy.

The results of the investigations can be used as the basis for effecting better control measures. The predictions made from the model investigations should be useful in evaluating any possible operational changes in the process. Using the established mass transfer coefficients and the knowledge of the dissolving capacities of a given molten metal for an additive, the time required for its complete dissolution and mixing can be estimated with greater accuracy. Location S4 at the bath surface was established as the best position for adding alloying elements. The established knowledge of the dead zones may be used in formulating an effective sampling procedure. These regions seem to be the best points to take samples from the bath.

Future work should aim to validate or check the usefulness of the obtained results to the actual converter operation. Since the effect of a simulated slag inclusion was only investigated at a constant proportion with the water phase it would be interesting to see how the relationships and observations made would respond to a varying slag proportion. The incorporation of top blowing to the investigations would also give a clearer picture of the CLU-converter operation.

7 REFERENCES

1. W. Birk I. Arvanitidis A. Medvedev and P. Jonsson: PHYSICAL MODELLING AND CONTROL OF DYNAMIC FORMING IN LD-CONVERTER PROCESS, Royal Institute of Technology, SE-100 44, Stockholm, Sweden, 2002, pp. 2.
2. M. Nyoka: MIXING AND MASS TRANSFER IN A CREUSOT LOIRE UDDEHOLM CONVERTER, MSc Dissertation, Witwatersrand University, Johannesburg, S. Africa, 2001.
3. M. Nyoka, G. Akdogan, R.H. Eric and N. Sutcliffe: *Metallurgical Transactions*, 2003, vol. 34B, pp. 833-842.
4. R.J. Fruehan and L.J. Martonik: 3rd International Iron and Steel congress Proceedings, Chicago, IL, USA, April, 1978, pp. 229-238.
5. J. Szekely, T. Lehner and C.W. Chang: *Ironmaking and Steelmaking*, no. 6, 1979, pp. 285-293
6. J.M. Chou, M.C. Chuang, M.H. Yeh, W.S. Hwang, S.H. Liu, S.T. Tsai and H.S. Wang: *Iron and steelmaking*, 2003, Vol. 30, No. 3, pp. 195-202.
7. C. Moore and R.I. Marshall: *Steelmaking*, The institute of metals, The Bourne Press Ltd, Bournemouth, Great Britain, 1991, pp.108-121.
8. J.K. Wright: *Metallurgical Transactions*, vol. 20B, 1989, pp 363-374
9. V. Whitney: *Iron and steelmaking*, Vol. 30, No. 3, 2003, pp. 209-214.
10. S. K. Sharma, J.W. Nhlinka and D.W. Kern: *Iron Steelmaker*, 1977, pp. 7-18.
11. R.I.L Guthrie: *Engineering in Process Metallurgy*, Clarendon Press, Oxford, UK, 1992, pp.158-9, 165-167 and 187.
12. T. Fabritius, P. Mure and J. Harkki: MODELLING OF BATH OSCILLATION IN THE AOD, University of Oulu, Finland, 2004.
13. C. Bodsworth and H.B. Bell: *Physical chemistry of Iron and Steel manufacture*, Longman, London, UK, 1972, pp100.
14. Richard J. Fruehan Editor: *The making, Shaping and Treating of Steel*, 11th Ed., The AISE Steel Foundation, 1998, pp. 79-105.
15. G. Akdogan and R. H. Eric: *Metall. Trans.*, Vol. 30B, 1999, pp 231-239.

16. Manabu Iguchi, Ryoji Tsujino, Kei-ichi Nkamura and Mitsuhiro Sano: *Metallurgical and Materials Transactions*, vol. 30B, 1999, pp 631.
17. M. Iguchi, S. Hosohara, T. Kondoh, Y. Itoh and Z. Morita: *Iron and Steel Inst. Japan Int.*, vol. 34, 1994, pp 330-337.
18. N. Nakanishi, T. Fuji, and J. Szekely: *Iron and steelmaking*, No. 3, 1975, pp. 193-197.
19. T. Lehner, G. Carlsson and T. Hsiao: *Scaninject II*, International conference on injection Metallurgy, vol. 1, 1980, pp. 22:1-22:34.
20. A.H. Castillejos and J.K. Brimacombe: *Metallurgical Transactions*, 1989, vol. 20B, pp. 595-601.
21. A.H. Castillejos and J.K. Brimacombe: *Metallurgical and Materials Transactions*, vol. 18B, 1987, pp. 659-671.
22. Y. Sahai and R.I.L. Guthrie: *Metallurgical and Materials Transactions*, vol. 13B, 1982, pp.193-202.
23. S. Asai, M.Kawachi and I. Muchi: *Scaninject III*, Lulea, Sweden, no. 12, 1983, pp. 1-29.
24. S.H. Kim and R.J. Fruehan: *Metallurgical Transactions*, vol. 18B, 1987, pp. 381-390.
25. N.J. Themelis and P. Goyal: *Can. Met. Q.*, vol. 22, 1983, pp. 310-320.
26. *Encyclopaedia of Industrial Chemistry*, Ullmann, 5th Ed., Vol.A3, pp. 56.
27. D. Mazumdar, S. K. Kajani and A. Ghosh: *Steel Res.*, 61, 8, 1991, pp. 339.
28. R.J. Matway, R.J. Fruehan and H. Henein: *Iron Steel Steelmaker*, 16, 1989, pp 51-58.
29. G.G. Krishna Murthy, S.P. Mehrotra and A. Ghosh: *Metallurgical Transactions*, vol. 19B, 1988, pp. 839-850
30. D. Mazumdar, H.B. Kim and R.I.L. Guthrie: *Ironmaking and Steelmaking*, vol. 27, No.4, 2000, pp. 302-309
31. D.C. Harris: *Quantitative Chemical Analysis*, W.H Freeman and Company, New York, USA, 1991, pp. 47-65.
32. K. Mori and T. Sakuraya: *Trans. Iron and Steel Institute Japan*, vol. 22, no. 12, 1982, pp. 984-990.

APPENDIX 1**WATER PROPERTIES**

Table 1A: Chart used to perform temperature compensation calculations on the measured pH values.

pH vs. Temperature Error Chart

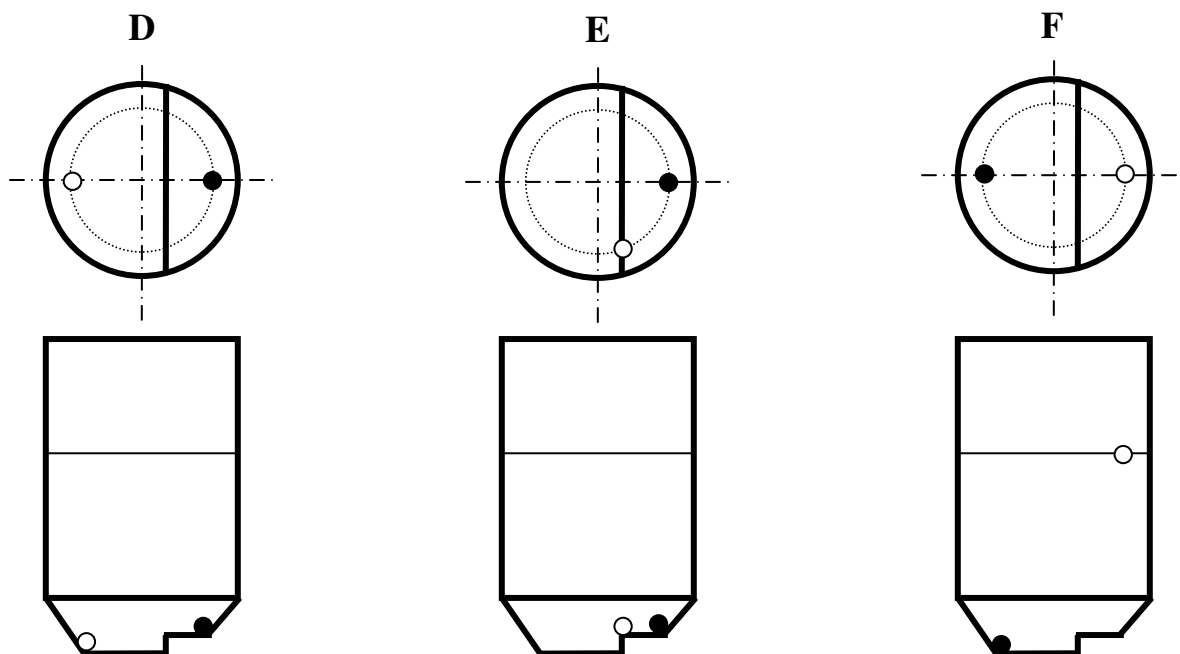
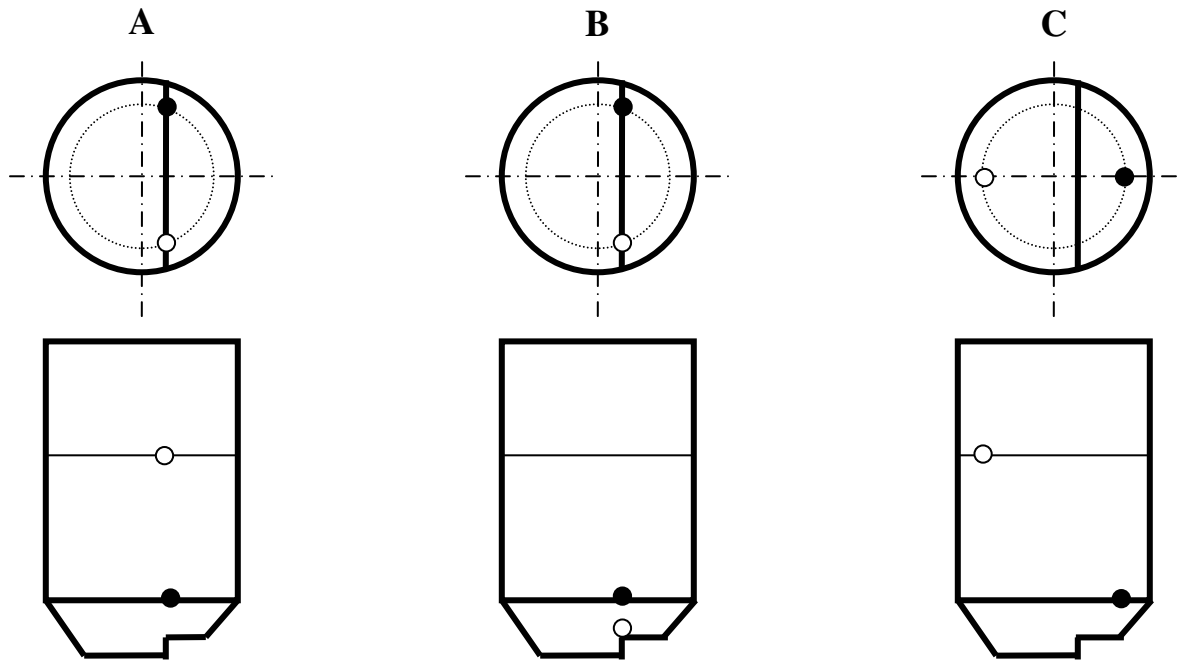
	pH 2	pH 3	pH 4	pH 5	pH 6	pH 7	pH 8	pH 9	pH 10	pH 11	pH 12
5°	.30	.24	.18	.12	.06	0	.06	.12	.18	.24	.30
15°	.15	.12	.09	.06	.03	0	.03	.06	.09	.12	.15
25°	0	0	0	0	0	0	0	0	0	0	0
35°	.15	.12	.09	.06	.03	0	.03	.06	.09	.12	.15
45°	.30	.24	.18	.12	.06	0	.06	.12	.18	.24	.30
55°	.45	.36	.27	.18	.09	0	.09	.18	.27	.36	.45
65°	.60	.48	.36	.24	.12	0	.12	.24	.36	.48	.60
75°	.75	.60	.45	.30	.15	0	.15	.30	.45	.60	.75
85°	.90	.72	.54	.36	.18	0	.18	.36	.54	.72	.90

Table 1B: Values adopted for important physical data of reagents used.

QUANTITY	VALUE USED
ρ_b	$1.186 \times 10^3 \text{ Kg/m}^3$
$v_w (20^\circ\text{C})$	$1.004 \times 10^{-6} \text{ m}^3/\text{s}$
$v_k (20^\circ\text{C})$	$2.710 \times 10^{-6} \text{ m}^3/\text{s}$
$D_{b,w} (25^\circ\text{C})$	$7.970 \times 10^{-10} \text{ m}^2/\text{s}$

APPENDIX 2

ARRANGEMENTS OF TRACER ADDITION POINT AND PROBE LOCATION



Tracer ○ Probe ●

APPENDIX 3

The pictorial views of the equipment used for the experimental work

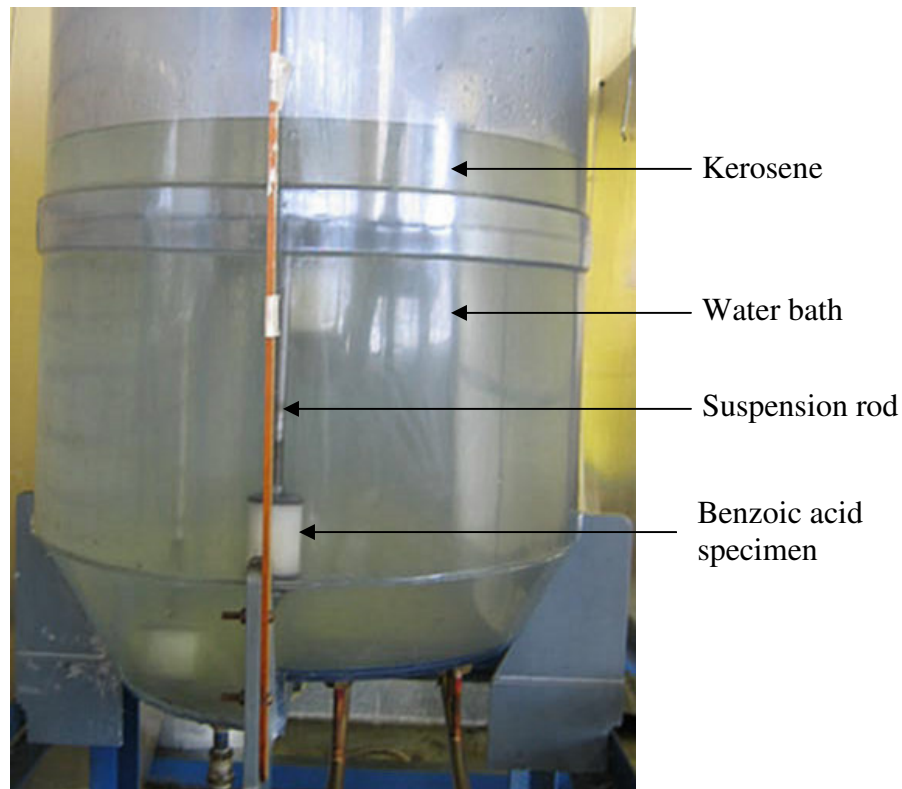


Figure 3A: The CLU-model vessel in which all the reactions were taking place.



Figure 3B: The equipment used to control gas flow rate to the water-kerosene bath.

APPENDIX 4

⁽³¹⁾STATISTICAL METHODS USED

The Q -test

This was used when dealing with bad data. The Q -test is used to help make the decision of whether to retain or discard an experimental value that is thought to be questionable. To apply the Q -test, first arrange the data in order of increasing value and calculate Q defined as,

$$Q = \frac{\text{gap}}{\text{range}}$$

The gap is the difference between the questionable point and the nearest value. The range or spread is the difference between the highest and the lowest values in the given data set.

If Q (observed) $>$ Q (tabulated), the questionable point should be discarded.

Table II: Critical values of Q at the 90% confidence limit.

Q (90%confidence)	0.94	0.76	0.64	0.56	0.51	0.47	0.44	0.41
No. of observations	3	4	5	6	7	8	9	10

Mean Value and standard deviation

The mean value is the sum of the measured values divided by n , the total number of values. The standard deviation, s , measures how closely the data are clustered about the mean. The significance of s is that the smaller the standard deviation, the more closely the data are clustered about the mean. An experimental technique that produces a small standard deviation is more reliable (precise) than one that produces a large standard deviation provided that they are equally accurate.

APPENDIX 5

SAMPLES POSITIONAL ARRANGEMENTS

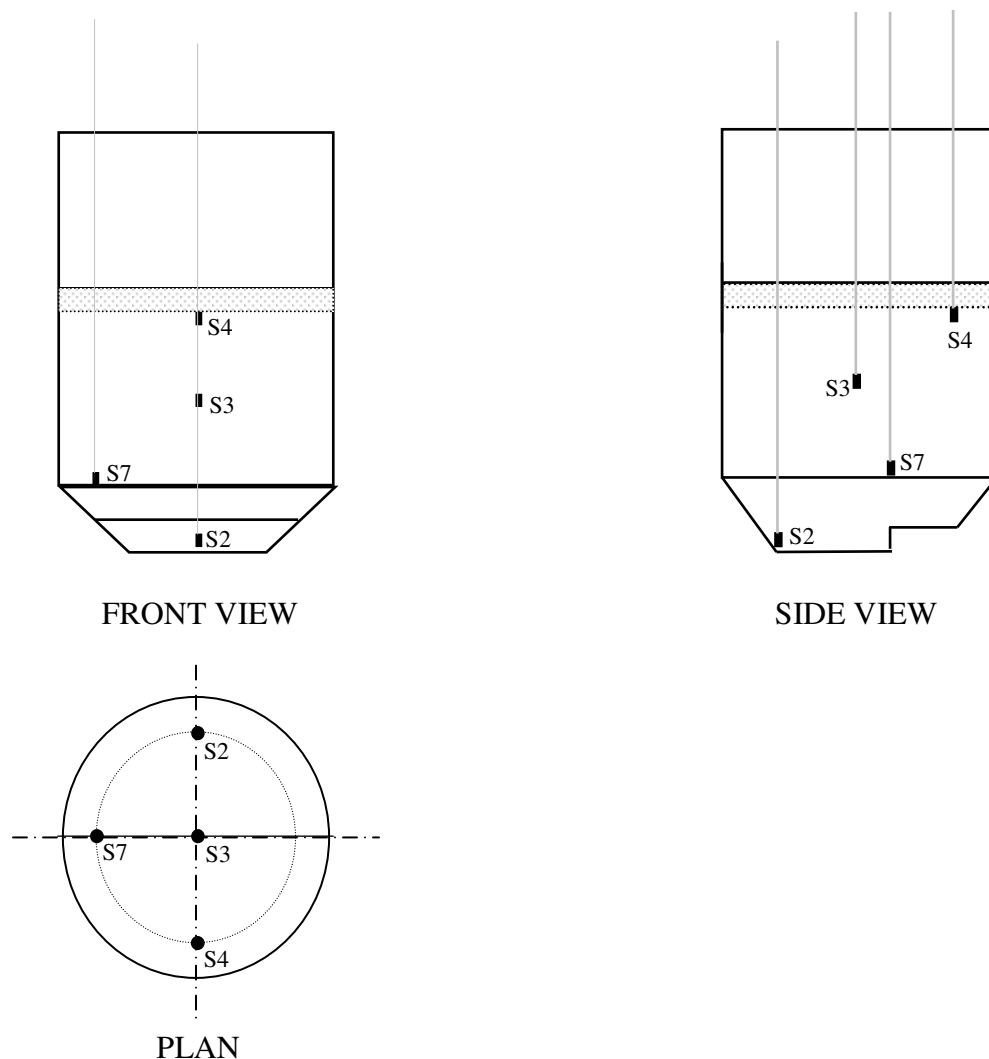
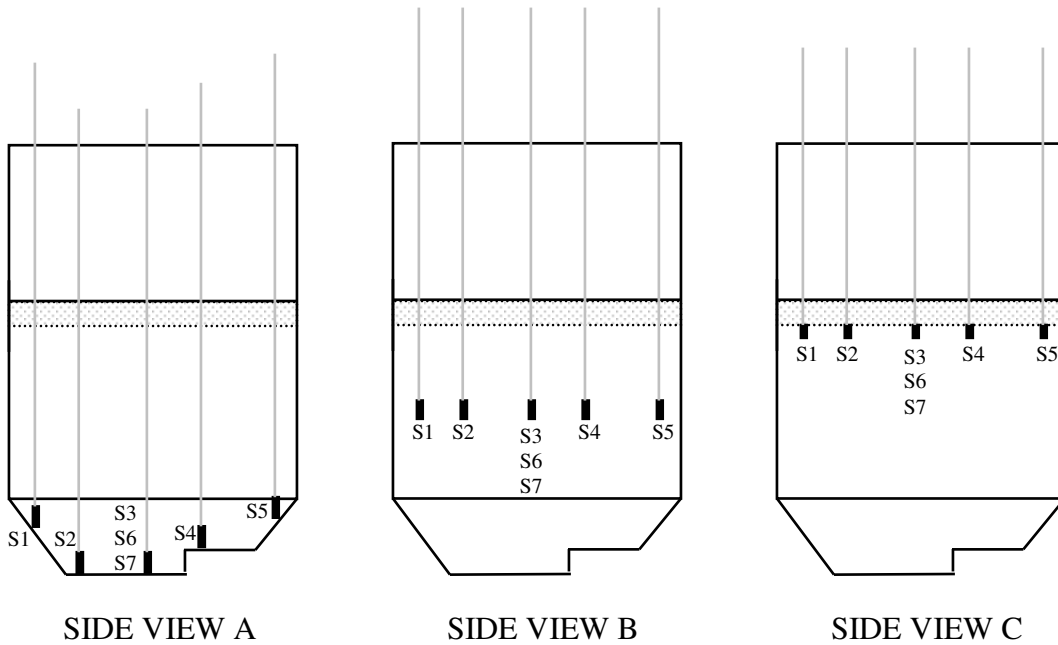


Table 5A: The depths of the specimens into the bath, taking the bath surface as the reference point.

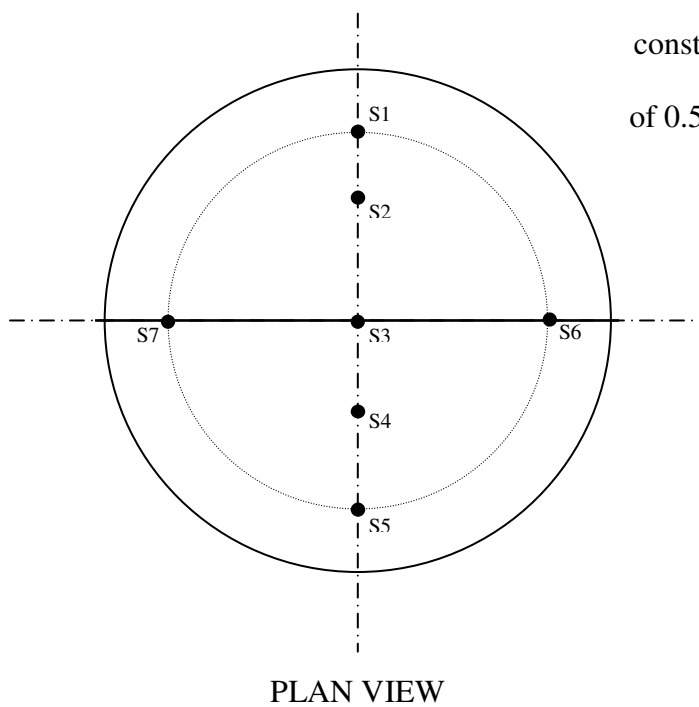
Specimen	Water Bath Height of 0.40m (cm)	Water Bath Height of 0.50m (cm)	Water Bath Height of 0.65m (cm)
S2	40	50	65
S3	12	17	25
S4	0	0	0
S7	24	34	49

APPENDIX 6

SAMPLES POSITIONAL ARRANGEMENTS



NOTE: The bath height was kept at a constant value. The water bath height of 0.5m was used for the experiments.



APPENDIX 7

Table 7A: Weight losses recorded at location S2 at a water bath height of 0.40m and a varying gas flow rate.

At 0.010m³/s gas flow rate

Time (s)	Test 1 (g)	Radius (mm)	Test 2 (g)	Radius (mm)	Test 3 (g)	Radius (mm)	Test 4 (g)	Radius (mm)	Av. Radius (mm)
0	-	22.00	-	22.00	-	22	-	22	22.00
900	0.37	21.97	0.23	21.98	0.31	21.97	0.10	21.99	21.98
1800	0.28	21.94	0.28	21.95	0.39	21.94	0.23	21.97	21.95
2700	0.18	21.92	0.28	21.93	0.46	21.89	0.13	21.95	21.92
3600	0.35	21.89	0.24	21.90	0.29	21.87	0.05	21.95	21.90
4500	0.64	21.83	0.15	21.89	0.20	21.85	0.12	21.93	21.88
5400	0.22	21.81	0.23	21.87	0.33	21.82	0.02	21.93	21.86
6300	0.55	21.76	0.17	21.85	0.29	21.79	0.12	21.92	21.83
7200	0.30	21.73	0.28	21.83	0.31	21.76			21.77
Length (mm)	66.00		65.00		67.00		58.50		

At 0.015m³/s gas flow rate

Time (s)	Test 1 (g)	Radius (mm)	Test 2 (g)	Radius (mm)	Test 3 (g)	Radius (mm)	Test 4 (g)	Radius (mm)	Av. Radius (mm)
0	-	22.00	-	22.00	-	22.00	-	22	22.00
900	0.48	21.96	0.39	21.96	0.31	21.97	0.13	21.99	21.97
1800	0.41	21.92	0.36	21.93	0.29	21.94	0.13	21.97	21.94
2700	0.62	21.86	0.33	21.90	0.27	21.92	0.17	21.96	21.91
3600	0.46	21.82	0.35	21.86	0.27	21.89	0.11	21.95	21.88
4500	0.47	21.78	0.32	21.83	0.25	21.87	0.17	21.93	21.85
5400	0.45	21.74	0.64	21.77	0.36	21.84	0.13	21.92	21.81
6300	0.49	21.69	0.30	21.74	0.29	21.81	0.14	21.90	21.79
7200	0.41	21.65	0.40	21.70	0.40	21.77			21.71
Length (mm)	67.00		64.00		66.00		60.50		

At 0.023m³/s gas flow rate

Time (s)	Test 1 (g)	Radius (mm)	Test 2 (g)	Radius (mm)	Test 3 (g)	Radius (mm)	Test 4 (g)	Radius (mm)	Av. Radius (mm)
0	-	22.00	-	22.00	-	22.00	-	22	22.00
900	0.50	21.95	0.37	21.97	0.48	21.96	0.18	21.98	21.96
1800	0.43	21.91	0.34	21.93	0.47	21.91	0.31	21.95	21.93
2700	0.36	21.88	0.30	21.91	0.46	21.87	0.33	21.92	21.89
3600	0.54	21.83	0.39	21.87	0.51	21.82	0.29	21.89	21.85
4500	0.55	21.78	0.35	21.84	0.51	21.77	0.31	21.85	21.81
5400	0.46	21.74	0.43	21.80	0.46	21.73	0.35	21.82	21.77
6300	0.61	21.68	0.40	21.76	0.48	21.69	0.31	21.79	21.73
Length (mm)	66.00		66.00		66.00		59.20		

Table 7B: Weight losses recorded at location S3 at a water bath height of 0.40m and a varying gas flow rate.

At 0.010m³/s gas flow rate

Time (s)	Test 1* (g)	Radius (mm)	Test 2 (g)	Radius (mm)	Test 3 (g)	Radius (mm)	Test 4 (g)	Radius (mm)	Av. Radius (mm)
0	-	22.00	-	22.00	-	22.00	-	22	22.00
900	0.11	21.99	0.25	21.98	0.11	21.99	0.21	21.98	21.98
1800	0.27	21.97	0.24	21.95	0.19	21.97	0.24	21.95	21.96
2700	0.37	21.93	0.09	21.95	0.34	21.94	0.19	21.93	21.94
3600	0.51	21.89	0.23	21.92	0.37	21.90	0.16	21.92	21.91
4500	0.51	21.84	0.32	21.89	0.39	21.86	0.17	21.90	21.89
5400	0.44	21.80	0.24	21.87	0.42	21.82	0.03	21.90	21.86
6300	0.56	21.75	0.37	21.84	0.43	21.78	0.22	21.88	21.83
7200	0.44	21.71	0.43	21.80	0.43	21.74			21.77
Length (mm)	67.00		65.00		63.00		60.00		

At 0.015m³/s gas flow rate

Time (s)	Test 1 (g)	Radius (mm)	Test 2 (g)	Radius (mm)	Test 3 (g)	Radius (mm)	Test 4 (g)	Radius (mm)	Av. Radius (mm)
0	-	22.00	-	22.00	-	22.00	-	22	22.00
900	0.32	21.97	0.38	21.96	0.08	21.99	0.15	21.98	21.98
1800	0.33	21.94	0.21	21.95	0.24	21.97	0.21	21.96	21.95
2700	0.34	21.91	0.15	21.93	0.17	21.95	0.21	21.94	21.93
3600	0.48	21.86	0.23	21.91	0.20	21.94	0.19	21.92	21.91
4500	0.46	21.82	0.30	21.88	0.26	21.91	0.19	21.90	21.88
5400	0.41	21.78	0.34	21.85	0.33	21.88	0.21	21.88	21.85
6300	0.51	21.74	0.32	21.82	0.28	21.86	0.20	21.86	21.82
7200	0.41	21.70	0.29	21.79	0.38	21.82			21.77
Length (mm)	66.00		66.00		66.00		61.00		

At 0.023m³/s gas flow rate

Time (s)	Test 1 (g)	Radius (mm)	Test 2 (g)	Radius (mm)	Test 3 (g)	Radius (mm)	Test 4 (g)	Radius (mm)	Av. Radius (mm)
0	-	22.00	-	22.00	-	22.00	-	22	22.00
900	0.49	21.95	0.36	21.97	0.36	21.97	0.19	21.98	21.97
1800	0.53	21.90	0.33	21.94	0.35	21.94	0.34	21.95	21.93
2700	0.56	21.85	0.29	21.91	0.33	21.91	0.22	21.93	21.90
3600	0.50	21.80	0.34	21.88	0.28	21.88	0.25	21.90	21.87
4500	0.49	21.76	0.33	21.85	0.40	21.84	0.26	21.88	21.83
5400	0.43	21.72	0.44	21.81	0.37	21.81	0.32	21.85	21.79
6300	0.49	21.67	0.40	21.77	0.40	21.77	0.36	21.81	21.76
7200	0.46	21.63	0.45	21.73	0.50	21.73			21.69
Length (mm)	65.00		66.00		67.00		60.50		

Table 7C: Weight losses recorded at location S4 at a water bath height of 0.40m and a varying gas flow rate.

At 0.010m³/s gas flow rate

Time (s)	Test 1* (g)	Radius (mm)	Test 2 (g)	Radius (mm)	Test 3 (g)	Radius (mm)	Test 4 (g)	Radius (mm)	Av. Radius (mm)
0	-	22.00	-	22.00	-	22.00	-	22	22.00
900	1.03	21.90	0.58	21.95	0.63	21.94	0.46	21.95	21.95
1800	1.00	21.81	0.43	21.91	0.56	21.89	0.71	21.88	21.89
2700	0.96	21.72	0.28	21.88	0.49	21.84	0.58	21.82	21.85
3600	1.11	21.62	0.37	21.85	0.50	21.80	0.58	21.76	21.80
4500	0.84	21.54	0.66	21.79	0.63	21.74	0.62	21.69	21.74
5400	0.86	21.46	0.82	21.71	0.52	21.69	0.50	21.64	21.68
6300	1.38	21.33	0.76	21.64	0.99	21.60	0.57	21.58	21.61
Length /mm	66.00		67.00		66.00		58.50		

At 0.015m³/s gas flow rate

Time (s)	Test 1 (g)	Radius (mm)	Test 2 (g)	Radius (mm)	Test 3 (g)	Radius (mm)	Test 4 (g)	Radius (mm)	Av. Radius (mm)
0	-	22.00	-	22.00	-	22.00	-	22	22.00
900	0.70	21.94	0.52	21.95	0.28	21.97	0.50	21.95	21.95
1800	0.65	21.87	0.48	21.91	0.57	21.92	0.62	21.88	21.90
2700	1.17	21.77	0.69	21.84	0.44	21.88	0.55	21.83	21.83
3600	1.09	21.66	0.66	21.78	0.61	21.82	0.51	21.78	21.76
4500	0.66	21.60	0.82	21.70	0.69	21.76	0.54	21.72	21.69
5400	0.86	21.52	0.76	21.63	1.00	21.66	0.39	21.68	21.62
6300	1.08	21.42	0.90	21.54	0.75	21.59	0.55	21.62	21.54
Length (mm)	66.00		65.00		65.00		59.50		

At 0.023m³/s gas flow rate

Time (s)	Test 1 (g)	Radius (mm)	Test 2 (g)	Radius (mm)	Test 3* (g)	Radius (mm)	Test 4 (g)	Radius (mm)	Av. Radius (mm)
0	-	22.00	-	22.00	-	22.00	-	22	22.00
900	1.03	21.90	0.98	21.91	0.62	21.94	0.63	21.93	21.92
1800	0.89	21.82	0.86	21.83	0.52	21.89	0.84	21.85	21.83
2700	0.75	21.75	0.74	21.76	0.42	21.86	0.96	21.75	21.75
3600	1.05	21.65	0.75	21.70	0.45	21.81	0.63	21.68	21.68
4500	1.09	21.55	0.97	21.61	0.73	21.75	0.81	21.60	21.58
5400	1.01	21.46	1.21	21.49	0.73	21.68	0.67	21.53	21.49
6300	1.24	21.34	1.21	21.38	0.75	21.61	0.92	21.43	21.38
Length (mm)	66.00		67.00		66.00		59.00		

Table 7D: Weight losses recorded at location S7 at a water bath height of 0.40m and a varying gas flow rate.

At 0.010m³/s gas flow rate

Time (s)	Test 1 (g)	Radius (mm)	Test 2 (g)	Radius (mm)	Test 3 (g)	Radius (mm)	Test 4 (g)	Radius (mm)	Av. Radius (mm)
0	-	22.00	-	22.00	-	22.00	-	22	22.00
900	0.11	21.99	0.29	21.97	0.03	22.00	0.13	21.99	21.99
1800	0.30	21.96	0.14	21.96	0.13	21.98	0.17	21.97	21.97
2700	0.26	21.94	0.13	21.95	0.24	21.96	0.15	21.95	21.95
3600	0.40	21.90	0.24	21.92	0.23	21.94	0.09	21.95	21.93
4500	0.26	21.88	0.27	21.90	0.26	21.92	0.12	21.93	21.91
5400	0.26	21.85	0.24	21.88	0.35	21.88	0.04	21.93	21.89
6300	0.53	21.80	0.37	21.84	0.26	21.86	0.09	21.92	21.86
Length (mm)	66.00		65.00		65.00		60.00		

At 0.015m³/s gas flow rate

Time (s)	Test 1 (g)	Radius (mm)	Test 2 (g)	Radius (mm)	Test 3 (g)	Radius (mm)	Test 4 (g)	Radius (mm)	Av. Radius (mm)
0	-	22.00	-	22.00	-	22.00	-	22	22.00
900	0.28	21.97	0.20	21.98	0.11	21.99	0.21	21.98	21.98
1800	0.65	21.92	0.17	21.97	0.18	21.97	0.15	21.96	21.95
2700	0.41	21.88	0.14	21.95	0.12	21.96	0.14	21.95	21.94
3600	0.47	21.84	0.16	21.94	0.20	21.95	0.11	21.94	21.91
4500	0.44	21.80	0.19	21.92	0.18	21.93	0.17	21.92	21.89
5400	0.45	21.76	0.24	21.90	0.24	21.91	0.09	21.91	21.87
6300	0.50	21.71	0.26	21.87	0.26	21.88	0.15	21.90	21.84
Length (mm)	68.00		65.00		68.00		61.00		

At 0.023m³/s gas flow rate

Time (s)	Test 1 (g)	Radius (mm)	Test 2 (g)	Radius (mm)	Test 3 (g)	Radius (mm)	Test 4 (g)	Radius (mm)	Av. Radius (mm)
0	-	22.00	-	22.00	-	22.00	-	22	22.00
900	0.17	21.98	0.20	21.98	0.11	21.99	0.18	21.98	21.98
1800	0.31	21.96	0.29	21.96	0.11	21.98	0.32	21.95	21.96
2700	0.50	21.91	0.32	21.93	0.33	21.95	0.26	21.93	21.93
3600	0.53	21.87	0.36	21.89	0.49	21.90	0.30	21.90	21.89
4500	0.56	21.82	0.44	21.85	0.41	21.86	0.30	21.87	21.85
5400	0.45	21.78	0.51	21.81	0.42	21.82	0.29	21.84	21.81
6300	0.57	21.73	0.41	21.77	0.42	21.78	0.33	21.81	21.77
Length (mm)	69.00		67.00		65.00		58.00		

Table 7E: Weight losses recorded at location S2 at a water bath height of 0.50m and a varying gas flow rate.

At 0.010m³/s gas flow rate

Time (s)	Test 1 (g)	Radius (mm)	Test 2 (g)	Radius (mm)	Test 3 (g)	Radius (mm)	Test 4 (g)	Radius (mm)	Av. Radius (mm)
0	-	22.00	-	22.00	-	22	-	22	22.00
900	0.28	21.97	0.33	21.97	0.26	21.98	0.21	21.98	21.97
1800	0.19	21.96	0.29	21.94	0.19	21.96	0.18	21.96	21.95
2700	0.10	21.95	0.24	21.92	0.14	21.94	0.12	21.95	21.94
3600	0.35	21.92	0.39	21.88	0.30	21.92	0.17	21.93	21.91
4500	0.29	21.89	0.32	21.85	0.16	21.90	0.12	21.92	21.89
5400	0.31	21.86	0.36	21.81	0.34	21.87	0.17	21.90	21.86
6300	0.35	21.83	0.33	21.78	0.38	21.83	0.07	21.89	21.83
Length (mm)	66.50		63.50		64.50		60.00		

At 0.015m³/s gas flow rate

Time (s)	Test 1 (g)	Radius (mm)	Test 2 (g)	Radius (mm)	Test 3 (g)	Radius (mm)	Test 4 (g)	Radius (mm)	Av. Radius (mm)
0	-	22.00	-	22.00	-	22.00	-	22	22.00
900	0.25	21.98	0.36	21.97	0.30	21.97	0.30	21.97	21.97
1800	0.17	21.96	0.33	21.94	0.24	21.95	0.21	21.95	21.95
2700	0.06	21.95	0.29	21.91	0.18	21.93	0.13	21.94	21.93
3600	0.35	21.92	0.38	21.87	0.34	21.90	0.19	21.92	21.90
4500	0.25	21.90	0.39	21.84	0.33	21.87	0.20	21.90	21.88
5400	0.28	21.87	0.27	21.81	0.35	21.84	0.17	21.88	21.85
6300	0.31	21.84	0.48	21.77	0.32	21.81	0.16	21.86	21.82
Length (mm)	65.00		66.50		67.00		61.00		

At 0.023m³/s gas flow rate

Time (s)	Test 1 (g)	Radius (mm)	Test 2 (g)	Radius (mm)	Test 3 (g)	Radius (mm)	Test 4 (g)	Radius (mm)	Av. Radius (mm)
0	-	22.00	-	22.00	-	22.00	-	22	22.00
900	0.29	21.97	0.43	21.96	0.35	21.97	0.38	21.96	21.97
1800	0.10	21.96	0.35	21.93	0.19	21.95	0.30	21.93	21.94
2700	0.15	21.95	0.22	21.91	0.13	21.94	0.26	21.90	21.92
3600	0.29	21.92	0.37	21.87	0.41	21.90	0.33	21.87	21.89
4500	0.31	21.89	0.30	21.84	0.29	21.88	0.40	21.83	21.86
5400	0.37	21.85	0.38	21.81	0.29	21.85	0.31	21.79	21.83
6300	0.32	21.82	0.31	21.78	0.58	21.80	0.38	21.75	21.79
Length (mm)	63.00		65.50		68.00		59.00		

Table 7E: Weight losses recorded at location S3 at a water bath height of 0.50m and a varying gas flow rate.

At 0.010m³/s gas flow rate

Time (s)	Test 1 (g)	Radius (mm)	Test 2 (g)	Radius (mm)	Test 3 (g)	Radius (mm)	Test 4 (g)	Radius (mm)	Av. Radius (mm)
0	-	22.00	-	22.00	-	22.00	-	22	22.00
900	0.21	21.98	0.24	21.98	0.28	21.97	0.21	21.98	21.98
1800	0.15	21.97	0.20	21.96	0.22	21.95	0.20	21.96	21.96
2700	0.08	21.96	0.16	21.94	0.19	21.93	0.17	21.94	21.94
3600	0.28	21.93	0.26	21.92	0.32	21.90	0.21	21.92	21.92
4500	0.24	21.91	0.23	21.90	0.19	21.88	0.13	21.91	21.90
5400	0.20	21.89	0.29	21.87	0.30	21.85	0.18	21.89	21.88
6300	0.24	21.86	0.25	21.85	0.39	21.81	0.17	21.88	21.85
Length (mm)	62.50		65.00		61.50		63.00		

At 0.015m³/s gas flow rate

Time (s)	Test 1 (g)	Radius (mm)	Test 2 (g)	Radius (mm)	Test 3 (g)	Radius (mm)	Test 4 (g)	Radius (mm)	Av. Radius (mm)
0	-	22.00	-	22.00	-	22.00	-	22	22.00
900	0.34	21.97	0.26	21.98	0.38	21.96	0.21	21.98	21.97
1800	0.23	21.95	0.09	21.97	0.27	21.94	0.27	21.95	21.95
2700	0.17	21.93	0.12	21.96	0.20	21.92	0.18	21.94	21.93
3600	0.37	21.89	0.21	21.94	0.33	21.89	0.24	21.91	21.91
4500	0.32	21.86	0.24	21.91	0.35	21.85	0.20	21.89	21.88
5400	0.28	21.84	0.15	21.90	0.31	21.83	0.22	21.87	21.86
6300	0.38	21.80	0.31	21.87	0.33	21.79	0.18	21.85	21.83
Length (mm)	64.00		64.00		64.50		62.50		

At 0.023m³/s gas flow rate

Time (s)	Test 1 (g)	Radius (mm)	Test 2* (g)	Radius (mm)	Test 3 (g)	Radius (mm)	Test 4 (g)	Radius (mm)	Av. Radius (mm)
0	-	22.00	-	22.00	-	22.00	-	22	22.00
900	0.32	21.97	0.54	21.95	0.44	21.96	0.40	21.96	21.96
1800	0.26	21.95	0.50	21.90	0.35	21.93	0.29	21.93	21.93
2700	0.19	21.93	0.38	21.86	0.25	21.90	0.32	21.90	21.91
3600	0.32	21.90	0.55	21.81	0.48	21.86	0.37	21.86	21.87
4500	0.29	21.87	0.46	21.76	0.40	21.82	0.41	21.82	21.84
5400	0.46	21.83	0.44	21.72	0.38	21.78	0.30	21.79	21.80
6300	0.32	21.80	0.38	21.68	0.72	21.71	0.40	21.75	21.75
Length (mm)	65.00		63.00		65.00		60.00		

Table 7G: Weight losses recorded at location S4 at a water bath height of 0.50m and a varying gas flow rate.

At 0.010m³/s gas flow rate

Time (s)	Test 1* (g)	Radius (mm)	Test 2 (g)	Radius (mm)	Test 3 (g)	Radius (mm)	Test 4 (g)	Radius (mm)	Av. Radius (mm)
0	-	22.00	-	22.00	-	22.00	-	22	22.00
900	0.78	21.93	0.48	21.96	0.48	21.95	0.47	21.95	21.95
1800	0.65	21.87	0.36	21.92	0.34	21.92	0.55	21.89	21.90
2700	0.54	21.82	0.23	21.90	0.26	21.90	0.67	21.82	21.86
3600	0.89	21.74	0.45	21.86	0.59	21.84	0.71	21.74	21.80
4500	0.79	21.67	0.46	21.82	0.53	21.79	0.57	21.68	21.74
5400	0.84	21.59	0.61	21.76	0.30	21.76	0.68	21.60	21.68
6300	0.85	21.51	0.65	21.70	0.74	21.69	0.59	21.54	21.61
Length (mm)	67.50		67.00		64.00		56.50		

At 0.015m³/s gas flow rate

Time (s)	Test 1' (g)	Radius (mm)	Test 2 (g)	Radius (mm)	Test 3 (g)	Radius (mm)	Test 4 (g)	Radius (mm)	Av. Radius (mm)
0	-	22.00	-	22.00	-	22.00	-	22	22.00
900	0.89	21.91	0.11	21.99	0.12	21.99	0.60	21.94	21.96
1800	0.88	21.83	0.32	21.96	0.29	21.96	0.42	21.90	21.91
2700	0.85	21.74	0.29	21.93	0.15	21.95	0.78	21.82	21.86
3600	0.86	21.66	0.45	21.89	0.39	21.91	0.84	21.73	21.80
4500	0.86	21.58	0.60	21.84	0.45	21.87	0.84	21.65	21.73
5400	0.89	21.49	0.62	21.78	0.48	21.83	0.85	21.56	21.66
6300	0.97	21.39	0.76	21.71	0.60	21.77	0.79	21.48	21.59
Length (mm)	63.00		66.50		64.50		60.50		

At 0.023m³/s gas flow rate

Time (s)	Test 1 (g)	Radius (mm)	Test 2* (g)	Radius (mm)	Test 3 (g)	Radius (mm)	Test 4 (g)	Radius (mm)	Av. Radius (mm)
0	-	22.00	-	22.00	-	22.00	-	22	22.00
900	0.54	21.95	1.08	21.90	0.75	21.93	0.64	21.94	21.93
1800	0.39	21.91	1.10	21.80	0.52	21.88	0.88	21.85	21.86
2700	0.24	21.89	1.12	21.69	0.43	21.84	0.87	21.76	21.80
3600	0.47	21.85	1.13	21.59	0.60	21.78	1.03	21.66	21.72
4500	0.52	21.80	1.15	21.48	0.70	21.71	1.00	21.56	21.64
5400	0.81	21.73	0.90	21.40	0.71	21.64	0.88	21.47	21.56
6300	0.68	21.66	1.12	21.29	1.33	21.51	0.91	21.38	21.46
Length (mm)	67.00		66.50		63.50		62.00		

Table 7H: Weight losses recorded at location S7 at a water bath height of 0.50m and a varying gas flow rate.

At 0.010m³/s gas flow rate

Time (s)	Test 1 (g)	Radius (mm)	Test 2 (g)	Radius (mm)	Test 3 (g)	Radius (mm)	Test 4 (g)	Radius (mm)	Av. Radius (mm)
0	-	22.00	-	22.00	-	22.00	-	22	22.00
900	0.12	21.99	0.19	21.98	0.24	21.98	0.17	21.98	21.98
1800	0.14	21.98	0.14	21.97	0.17	21.96	0.08	21.97	21.97
2700	0.04	21.97	0.08	21.96	0.11	21.95	0.01	21.97	21.97
3600	0.14	21.96	0.28	21.94	0.33	21.92	0.06	21.97	21.95
4500	0.13	21.95	0.20	21.92	0.10	21.91	0.02	21.97	21.94
5400	0.17	21.93	0.18	21.90	0.33	21.88	0.05	21.96	21.92
6300	0.13	21.92	0.20	21.88	0.33	21.85	0.00	21.96	21.90
Length (mm)	66.50		65.50		66.50		60.00		

At 0.015m³/s gas flow rate

Time (s)	Test 1 (g)	Radius (mm)	Test 2 (g)	Radius (mm)	Test 3 (g)	Radius (mm)	Test 4 (g)	Radius (mm)	Av. Radius (mm)
0	-	22.00	-	22.00	-	22.00	-	22	22.00
900	0.26	21.98	0.14	21.99	0.13	21.99	0.14	21.99	21.98
1800	0.21	21.96	0.08	21.98	0.08	21.98	0.08	21.98	21.97
2700	0.16	21.94	0.02	21.98	0.02	21.98	0.14	21.96	21.97
3600	0.36	21.91	0.15	21.96	0.21	21.96	0.05	21.96	21.95
4500	0.25	21.88	0.18	21.95	0.08	21.95	0.13	21.95	21.93
5400	0.26	21.86	0.09	21.94	0.19	21.93	0.12	21.93	21.92
6300	0.26	21.83	0.24	21.92	0.13	21.92	0.12	21.92	21.90
Length (mm)	65.00		66.00		66.00		61.50		

At 0.023m³/s gas flow rate

Time (s)	Test 1 (g)	Radius (mm)	Test 2 (g)	Radius (mm)	Test 3 (g)	Radius (mm)	Test 4 (g)	Radius (mm)	Av. Radius (mm)
0	-	22.00	-	22.00	-	22.00	-	22	22.00
900	0.21	21.98	0.25	21.98	0.22	21.98	0.24	21.98	21.98
1800	0.08	21.97	0.12	21.97	0.07	21.97	0.04	21.97	21.97
2700	0.12	21.96	0.19	21.95	0.05	21.97	0.04	21.97	21.96
3600	0.23	21.94	0.13	21.94	0.24	21.94	0.15	21.95	21.94
4500	0.25	21.92	0.14	21.93	0.16	21.93	0.16	21.94	21.93
5400	0.32	21.88	0.13	21.92	0.14	21.92	0.12	21.92	21.91
6300	0.26	21.86	0.13	21.91	0.45	21.87	0.19	21.90	21.89
Length (mm)	64.00		64.50		64.00		59.50		

Table 7I: Weight losses recorded at location S2 at a water bath height of 0.65m and a varying gas flow rate.

At 0.010m³/s gas flow rate

Time (s)	Test 1 (g)	Radius (mm)	Test 2 (g)	Radius (mm)	Test 3 (g)	Radius (mm)	Test 4 (g)	Radius (mm)	Av. Radius (mm)
0	-	22.00	-	22.00	-	22	-	22	22.00
900	0.28	21.97	0.33	21.97	0.26	21.98	0.21	21.98	21.97
1800	0.19	21.96	0.29	21.94	0.19	21.96	0.18	21.96	21.95
2700	0.10	21.95	0.24	21.92	0.14	21.94	0.12	21.95	21.94
3600	0.35	21.92	0.39	21.88	0.30	21.92	0.17	21.93	21.91
4500	0.29	21.89	0.32	21.85	0.16	21.90	0.12	21.92	21.89
5400	0.31	21.86	0.36	21.81	0.34	21.87	0.17	21.90	21.86
6300	0.35	21.83	0.33	21.78	0.38	21.83	0.07	21.89	21.83
Length (mm)	66.50		63.50		64.50		61.00		

At 0.015m³/s gas flow rate

Time (s)	Test 1 (g)	Radius (mm)	Test 2 (g)	Radius (mm)	Test 3 (g)	Radius (mm)	Test 4 (g)	Radius (mm)	Av. Radius (mm)
0	-	22.00	-	22.00	-	22.00	-	22	22.00
900	0.25	21.98	0.36	21.97	0.30	21.97	0.30	21.97	21.97
1800	0.17	21.96	0.33	21.94	0.24	21.95	0.21	21.95	21.95
2700	0.06	21.95	0.29	21.91	0.18	21.93	0.13	21.94	21.93
3600	0.35	21.92	0.38	21.87	0.34	21.90	0.19	21.92	21.90
4500	0.25	21.90	0.39	21.84	0.33	21.87	0.20	21.90	21.88
5400	0.28	21.87	0.27	21.81	0.35	21.84	0.17	21.88	21.85
6300	0.31	21.84	0.48	21.77	0.32	21.81	0.16	21.86	21.82
Length (mm)	65.00		66.50		67.00		61.50		

At 0.023m³/s gas flow rate

Time (s)	Test 1 (g)	Radius (mm)	Test 2 (g)	Radius (mm)	Test 3 (g)	Radius (mm)	Test 4 (g)	Radius (mm)	Av. Radius (mm)
0	-	22.00	-	22.00	-	22.00	-	22	22.00
900	0.29	21.97	0.43	21.96	0.35	21.97	0.38	21.96	21.97
1800	0.10	21.96	0.35	21.93	0.19	21.95	0.30	21.93	21.94
2700	0.15	21.95	0.22	21.91	0.13	21.94	0.26	21.90	21.92
3600	0.29	21.92	0.37	21.87	0.41	21.90	0.33	21.87	21.89
4500	0.31	21.89	0.30	21.84	0.29	21.88	0.40	21.83	21.86
5400	0.37	21.85	0.38	21.81	0.29	21.85	0.31	21.79	21.83
6300	0.32	21.82	0.31	21.78	0.58	21.80	0.38	21.75	21.79
Length (mm)	63.00		65.50		68.00		61.00		

Table 7J: Weight losses recorded at location S3 at a water bath height of 0.65m and a varying gas flow rate.

At 0.010m³/s gas flow rate

Time (s)	Test 1 (g)	Radius (mm)	Test 2 (g)	Radius (mm)	Test 3 (g)	Radius (mm)	Test 4 (g)	Radius (mm)	Av. Radius (mm)
0	-	22.00	-	22.00	-	22.00	-	22	22.00
900	0.21	21.98	0.24	21.98	0.28	21.97	0.21	21.98	21.98
1800	0.15	21.97	0.20	21.96	0.22	21.95	0.20	21.96	21.96
2700	0.08	21.96	0.16	21.94	0.19	21.93	0.17	21.94	21.94
3600	0.28	21.93	0.26	21.92	0.32	21.90	0.21	21.92	21.92
4500	0.24	21.91	0.23	21.90	0.19	21.88	0.13	21.91	21.90
5400	0.20	21.89	0.29	21.87	0.30	21.85	0.18	21.89	21.88
6300	0.24	21.86	0.25	21.85	0.39	21.81	0.17	21.88	21.85
Length (mm)	62.50		65.00		61.50		60.00		

At 0.015m³/s gas flow rate

Time (s)	Test 1 (g)	Radius (mm)	Test 2 (g)	Radius (mm)	Test 3 (g)	Radius (mm)	Test 4 (g)	Radius (mm)	Av. Radius (mm)
0	-	22.00	-	22.00	-	22.00	-	22	22.00
900	0.34	21.97	0.26	21.98	0.38	21.96	0.21	21.98	21.97
1800	0.23	21.95	0.09	21.97	0.27	21.94	0.27	21.95	21.95
2700	0.17	21.93	0.12	21.96	0.20	21.92	0.18	21.94	21.93
3600	0.37	21.89	0.21	21.94	0.33	21.89	0.24	21.91	21.91
4500	0.32	21.86	0.24	21.91	0.35	21.85	0.20	21.89	21.88
5400	0.28	21.84	0.15	21.90	0.31	21.83	0.22	21.87	21.86
6300	0.38	21.80	0.31	21.87	0.33	21.79	0.18	21.85	21.83
Length (mm)	64.00		64.00		64.50		59.00		

At 0.023m³/s gas flow rate

Time (s)	Test 1 (g)	Radius (mm)	Test 2* (g)	Radius (mm)	Test 3 (g)	Radius (mm)	Test 4 (g)	Radius (mm)	Av. Radius (mm)
0	-	22.00	-	22.00	-	22.00	-	22	22.00
900	0.32	21.97	0.54	21.95	0.44	21.96	0.40	21.96	21.96
1800	0.26	21.95	0.50	21.90	0.35	21.93	0.29	21.93	21.93
2700	0.19	21.93	0.38	21.86	0.25	21.90	0.32	21.90	21.91
3600	0.32	21.90	0.55	21.81	0.48	21.86	0.37	21.86	21.87
4500	0.29	21.87	0.46	21.76	0.40	21.82	0.41	21.82	21.84
5400	0.46	21.83	0.44	21.72	0.38	21.78	0.30	21.79	21.80
6300	0.32	21.80	0.38	21.68	0.72	21.71	0.40	21.75	21.75
Length (mm)	65.00		63.00		65.00		55.50		

Table 7K: Weight losses recorded at location S4 at a water bath height of 0.65m and a varying gas flow rate.

At 0.010m³/s gas flow rate

Time (s)	Test 1* (g)	Radius (mm)	Test 2 (g)	Radius (mm)	Test 3 (g)	Radius (mm)	Test 4 (g)	Radius (mm)	Av. Radius (mm)
0	-	22.00	-	22.00	-	22.00	-	22	22.00
900	0.78	21.93	0.48	21.96	0.48	21.95	0.47	21.95	21.95
1800	0.65	21.87	0.36	21.92	0.34	21.92	0.55	21.89	21.90
2700	0.54	21.82	0.23	21.90	0.26	21.90	0.67	21.82	21.86
3600	0.89	21.74	0.45	21.86	0.59	21.84	0.71	21.74	21.80
4500	0.79	21.67	0.46	21.82	0.53	21.79	0.57	21.68	21.74
5400	0.84	21.59	0.61	21.76	0.30	21.76	0.68	21.60	21.68
6300	0.85	21.51	0.65	21.70	0.74	21.69	0.59	21.54	21.61
Length (mm)	67.50		67.00		64.00		57.50		

At 0.015m³/s gas flow rate

Time (s)	Test 1' (g)	Radius (mm)	Test 2 (g)	Radius (mm)	Test 3 (g)	Radius (mm)	Test 4 (g)	Radius (mm)	Av. Radius (mm)
0	-	22.00	-	22.00	-	22.00	-	22	22.00
900	0.89	21.91	0.11	21.99	0.12	21.99	0.60	21.94	21.96
1800	0.88	21.83	0.32	21.96	0.29	21.96	0.42	21.90	21.91
2700	0.85	21.74	0.29	21.93	0.15	21.95	0.78	21.82	21.86
3600	0.86	21.66	0.45	21.89	0.39	21.91	0.84	21.73	21.80
4500	0.86	21.58	0.60	21.84	0.45	21.87	0.84	21.65	21.73
5400	0.89	21.49	0.62	21.78	0.48	21.83	0.85	21.56	21.66
6300	0.97	21.39	0.76	21.71	0.60	21.77	0.79	21.48	21.59
Length (mm)	63.00		66.50		64.50		58.50		

At 0.023m³/s gas flow rate

Time (s)	Test 1 (g)	Radius (mm)	Test 2* (g)	Radius (mm)	Test 3 (g)	Radius (mm)	Test 4 (g)	Radius (mm)	Av. Radius (mm)
0	-	22.00	-	22.00	-	22.00	-	22	22.00
900	0.54	21.95	1.08	21.90	0.75	21.93	0.64	21.94	21.93
1800	0.39	21.91	1.10	21.80	0.52	21.88	0.88	21.85	21.86
2700	0.24	21.89	1.12	21.69	0.43	21.84	0.87	21.76	21.80
3600	0.47	21.85	1.13	21.59	0.60	21.78	1.03	21.66	21.72
4500	0.52	21.80	1.15	21.48	0.70	21.71	1.00	21.56	21.64
5400	0.81	21.73	0.90	21.40	0.71	21.64	0.88	21.47	21.56
6300	0.68	21.66	1.12	21.29	1.33	21.51	0.91	21.38	21.46
Length (mm)	67.00		66.50		63.50		61.50		

Table 7L: Weight losses recorded at location S7 at a water bath height of 0.65m and a varying gas flow rate.

At 0.010m³/s gas flow rate

Time (s)	Test 1 (g)	Radius (mm)	Test 2 (g)	Radius (mm)	Test 3 (g)	Radius (mm)	Test 4 (g)	Radius (mm)	Av. Radius (mm)
0	-	22.00	-	22.00	-	22.00	-	22	22.00
900	0.12	21.99	0.19	21.98	0.24	21.98	0.17	21.98	21.98
1800	0.14	21.98	0.14	21.97	0.17	21.96	0.08	21.97	21.97
2700	0.04	21.97	0.08	21.96	0.11	21.95	0.01	21.97	21.97
3600	0.14	21.96	0.28	21.94	0.33	21.92	0.06	21.97	21.95
4500	0.13	21.95	0.20	21.92	0.10	21.91	0.02	21.97	21.94
5400	0.17	21.93	0.18	21.90	0.33	21.88	0.05	21.96	21.92
6300	0.13	21.92	0.20	21.88	0.33	21.85	0.00	21.96	21.90
Length (mm)	66.50		65.50		66.50		60.00		

At 0.015m³/s gas flow rate

Time (s)	Test 1 (g)	Radius (mm)	Test 2 (g)	Radius (mm)	Test 3 (g)	Radius (mm)	Test 4 (g)	Radius (mm)	Av. Radius (mm)
0	-	22.00	-	22.00	-	22.00	-	22	22.00
900	0.26	21.98	0.14	21.99	0.13	21.99	0.14	21.99	21.98
1800	0.21	21.96	0.08	21.98	0.08	21.98	0.08	21.98	21.97
2700	0.16	21.94	0.02	21.98	0.02	21.98	0.14	21.96	21.97
3600	0.36	21.91	0.15	21.96	0.21	21.96	0.05	21.96	21.95
4500	0.25	21.88	0.18	21.95	0.08	21.95	0.13	21.95	21.93
5400	0.26	21.86	0.09	21.94	0.19	21.93	0.12	21.93	21.92
6300	0.26	21.83	0.24	21.92	0.13	21.92	0.12	21.92	21.90
Length (mm)	65.00		66.00		66.00		60.00		

At 0.023m³/s gas flow rate

Time (s)	Test 1 (g)	Radius (mm)	Test 2 (g)	Radius (mm)	Test 3 (g)	Radius (mm)	Test 4 (g)	Radius (mm)	Av. Radius (mm)
0	-	22.00	-	22.00	-	22.00	-	22	22.00
900	0.21	21.98	0.25	21.98	0.22	21.98	0.24	21.98	21.98
1800	0.08	21.97	0.12	21.97	0.07	21.97	0.04	21.97	21.97
2700	0.12	21.96	0.19	21.95	0.05	21.97	0.04	21.97	21.96
3600	0.23	21.94	0.13	21.94	0.24	21.94	0.15	21.95	21.94
4500	0.25	21.92	0.14	21.93	0.16	21.93	0.16	21.94	21.93
5400	0.32	21.88	0.13	21.92	0.14	21.92	0.12	21.92	21.91
6300	0.26	21.86	0.13	21.91	0.45	21.87	0.19	21.90	21.89
Length (mm)	64.00		64.50		64.00		60.50		

APPENDIX 8**Table 8A:** Specimen's mass/radius change in the bottom region at gas flow rate, 0.01m³/s.

	Time (s)	0	900	1800	2700	3600	4500	5400	6300	Length (mm)
Pos. S1	Test 1 (g)	-	0.48	0.36	0.44	0.38	0.45	0.43	0.39	63.50
	Radius (mm)	22.00	21.95	21.92	21.88	21.84	21.80	21.76	21.72	
	Test 2 (g)	-	0.38	0.38	0.41	0.30	0.43	0.39	0.36	68.00
	Radius (mm)	22.00	21.97	21.93	21.89	21.87	21.83	21.79	21.76	
	Ave. rad (mm)	22.00	21.96	21.93	21.89	21.85	21.81	21.77	21.74	
S2	Test 1 (g)	-	0.47	0.35	0.45	0.30	0.45	0.47	0.38	65.50
	Radius (mm)	22.00	21.96	21.92	21.88	21.85	21.81	21.77	21.73	
	Test 2 (g)	-	0.45	0.45	0.44	0.34	0.64	0.43	0.40	63.50
	Radius (mm)	22.00	21.96	21.91	21.87	21.84	21.78	21.73	21.70	
	Ave. rad (mm)	22.00	21.96	21.92	21.88	21.85	21.79	21.75	21.71	
S3	Test 1 (g)	-	0.67	0.51	0.60	0.46	0.61	0.68	0.60	65.00
	Radius (mm)	22.00	21.94	21.89	21.83	21.79	21.73	21.67	21.61	
	Test 2 (g)	-	0.62	0.57	0.66	0.56	0.45	0.68	0.63	64.00
	Radius (mm)	22.00	21.94	21.89	21.82	21.77	21.73	21.66	21.60	
	Ave. rad (mm)	22.00	21.94	21.89	21.83	21.78	21.73	21.66	21.60	
S4	Test 1 (g)	-	0.57	0.47	0.58	0.40	0.55	0.59	0.47	68.00
	Radius (mm)	22.00	21.95	21.91	21.85	21.82	21.77	21.72	21.67	
	Test 2 (g)	-	0.51	0.50	0.54	0.43	0.56	0.52	0.47	63.00
	Radius (mm)	22.00	21.95	21.90	21.85	21.81	21.75	21.70	21.66	
	Ave. rad (mm)	22.00	21.95	21.90	21.85	21.81	21.76	21.71	21.66	
S5	Test 1 (g)	-	0.43	0.42	0.42	0.40	0.44	0.45	0.41	68.00
	Radius (mm)	22.00	21.96	21.92	21.89	21.85	21.81	21.77	21.73	
	Test 2 (g)	-	0.40	0.40	0.41	0.35	0.47	0.43	0.35	62.50
	Radius (mm)	22.00	21.96	21.92	21.88	21.85	21.80	21.76	21.72	
	Ave. rad (mm)	22.00	21.96	21.92	21.88	21.85	21.81	21.76	21.73	
S6	Test 1 (g)	-	0.66	0.41	0.55	0.44	0.57	0.59	0.52	63.50
	Radius (mm)	22.00	21.94	21.90	21.84	21.80	21.75	21.69	21.64	
	Test 2 (g)	-	0.65	0.33	0.53	0.34	0.55	0.51	0.52	61.50
	Radius (mm)	22.00	21.94	21.90	21.85	21.82	21.76	21.71	21.66	
	Ave. rad (mm)	22.00	21.94	21.90	21.85	21.81	21.75	21.70	21.65	
S7	Test 1 (g)	-	0.38	0.31	0.37	0.26	0.32	0.46	0.31	65.00
	Radius (mm)	22.00	21.96	21.94	21.90	21.88	21.85	21.80	21.77	
	Test 2 (g)	-	0.44	0.43	0.57	0.38	0.43	0.44	0.35	64.50
	Radius (mm)	22.00	21.96	21.92	21.86	21.83	21.79	21.74	21.71	
	Ave. rad (mm)	22.00	21.96	21.93	21.88	21.85	21.82	21.77	21.74	

Table 8B: Change in specimen's mass and radius in the bottom region at a gas flow rate of $0.015\text{m}^3/\text{s}$.

	Time (s)	0	900	1800	2700	3600	4500	5400	6300	Length (mm)
Pos. S1	Test 1 (g)	-	0.52	0.51	0.69	0.43	0.52	0.53	0.40	61.00
	Radius (mm)	22.00	21.95	21.90	21.83	21.78	21.73	21.68	21.64	62.50
	Test 2 (g)	-	0.56	0.30	0.44	0.36	0.42	0.48	0.45	
	Radius (mm)	22.00	21.95	21.92	21.87	21.84	21.80	21.75	21.70	
	Ave. rad (mm)	22.00	21.95	21.91	21.85	21.81	21.76	21.71	21.67	
S2	Test 1 (g)	-	0.49	0.48	0.62	0.38	0.51	0.49	0.42	63.50
	Radius (mm)	22.00	21.95	21.91	21.85	21.81	21.76	21.71	21.67	64.50
	Test 2 (g)	-	0.50	0.50	0.55	0.47	0.48	0.51	0.49	
	Radius (mm)	22.00	21.95	21.91	21.85	21.81	21.76	21.71	21.67	
	Ave. rad (mm)	22.00	21.95	21.91	21.85	21.81	21.76	21.71	21.67	
S3	Test 1 (g)	-	0.74	0.73	0.77	0.66	0.76	0.79	0.69	62.00
	Radius (mm)	22.00	21.93	21.85	21.78	21.71	21.64	21.56	21.49	63.50
	Test 2 (g)	-	0.69	0.68	0.75	0.63	0.66	0.68	0.70	
	Radius (mm)	22.00	21.93	21.87	21.80	21.73	21.67	21.60	21.54	
	Ave. rad (mm)	22.00	21.93	21.86	21.79	21.72	21.65	21.58	21.51	
S4	Test 1 (g)	-	0.60	0.59	0.64	0.54	0.62	0.64	0.54	62.50
	Radius (mm)	22.00	21.94	21.88	21.82	21.77	21.71	21.64	21.59	66.50
	Test 2 (g)	-	0.65	0.49	0.61	0.48	0.57	0.59	0.60	
	Radius (mm)	22.00	21.94	21.90	21.84	21.79	21.74	21.69	21.63	
	Ave. rad (mm)	22.00	21.94	21.89	21.83	21.78	21.72	21.66	21.61	
S5	Test 1 (g)	-	0.55	0.33	0.42	0.38	0.47	0.50	0.42	62.00
	Radius (mm)	22.00	21.95	21.91	21.87	21.83	21.79	21.74	21.70	61.00
	Test 2 (g)	-	0.43	0.42	0.47	0.36	0.42	0.45	0.42	
	Radius (mm)	22.00	21.96	21.91	21.87	21.83	21.79	21.74	21.70	
	Ave. rad (mm)	22.00	21.95	21.91	21.87	21.83	21.79	21.74	21.70	
S6	Test 1 (g)	-	0.58	0.57	0.74	0.46	0.55	0.55	0.57	62.50
	Radius (mm)	22.00	21.94	21.89	21.81	21.77	21.72	21.66	21.60	60.50
	Test 2 (g)	-	0.61	0.39	0.50	0.47	0.50	0.56	0.48	
	Radius (mm)	22.00	21.94	21.90	21.85	21.80	21.75	21.69	21.64	
	Ave. rad (mm)	22.00	21.94	21.89	21.83	21.78	21.73	21.68	21.62	
S7	Test 1 (g)	-	0.58	0.36	0.56	0.38	0.45	0.52	0.45	63.00
	Radius (mm)	22.00	21.94	21.91	21.85	21.82	21.77	21.72	21.68	63.00
	Test 2 (g)	-	0.48	0.36	0.48	0.37	0.41	0.41	0.43	
	Radius (mm)	22.00	21.95	21.92	21.87	21.84	21.80	21.76	21.71	
	Ave. rad (mm)	22.00	21.95	21.91	21.86	21.83	21.78	21.74	21.70	

Table 8C: Change in specimen's mass and radius in the bottom region at a gas flow rate of $0.023\text{m}^3/\text{s}$.

	Time (s)	0	900	1800	2700	3600	4500	5400	6300	Length (mm)
Pos. S1	Test 1 (g)	-	0.65	0.50	0.64	0.42	0.63	0.60	0.58	62.00
	Radius (mm)	22.00	21.94	21.89	21.82	21.78	21.72	21.66	21.60	
	Test 2 (g)	-	0.60	0.47	0.58	0.41	0.54	0.66	0.48	64.00
	Radius (mm)	22.00	21.94	21.90	21.84	21.80	21.75	21.69	21.64	
	Ave. rad (mm)	22.00	21.94	21.89	21.83	21.79	21.74	21.67	21.62	
S2	Test 1 (g)	-	0.67	0.46	0.67	0.40	0.59	0.67	0.49	63.50
	Radius (mm)	22.00	21.94	21.89	21.83	21.79	21.73	21.67	21.62	
	Test 2 (g)	-	0.71	0.53	0.66	0.47	0.63	0.70	0.63	65.00
	Radius (mm)	22.00	21.93	21.88	21.82	21.78	21.72	21.65	21.59	
	Ave. rad (mm)	22.00	21.93	21.89	21.82	21.78	21.72	21.66	21.60	
S3	Test 1 (g)	-	0.96	0.79	0.94	0.78	0.90	0.92	0.83	65.00
	Radius (mm)	22.00	21.91	21.84	21.75	21.67	21.59	21.50	21.42	
	Test 2 (g)	-	1.00	0.79	0.93	0.72	0.88	1.04	0.90	64.00
	Radius (mm)	22.00	21.90	21.83	21.74	21.67	21.58	21.48	21.40	
	Ave. rad (mm)	22.00	21.91	21.83	21.74	21.67	21.59	21.49	21.41	
S4	Test 1 (g)	-	0.87	0.57	0.72	0.60	0.73	0.81	0.74	62.00
	Radius (mm)	22.00	21.91	21.86	21.79	21.73	21.65	21.57	21.50	
	Test 2 (g)	-	0.79	0.75	0.80	0.67	0.77	0.88	0.73	60.50
	Radius (mm)	22.00	21.92	21.84	21.76	21.69	21.62	21.53	21.45	
	Ave. rad (mm)	22.00	21.92	21.85	21.77	21.71	21.63	21.55	21.47	
S5	Test 1 (g)	-	0.58	0.57	0.64	0.44	0.57	0.62	0.61	62.50
	Radius (mm)	22.00	21.94	21.89	21.82	21.78	21.73	21.66	21.60	
	Test 2 (g)	-	0.60	0.46	0.51	0.36	0.63	0.56	0.58	62.50
	Radius (mm)	22.00	21.94	21.90	21.85	21.81	21.75	21.69	21.64	
	Ave. rad (mm)	22.00	21.94	21.89	21.84	21.80	21.74	21.68	21.62	
S6	Test 1 (g)	-	0.47	0.47	0.52	0.37	0.46	0.55	0.45	62.50
	Radius (mm)	22.00	21.95	21.91	21.86	21.82	21.78	21.72	21.68	
	Test 2 (g)	-	0.56	0.51	0.59	0.39	0.59	0.59	0.52	60.50
	Radius (mm)	22.00	21.94	21.89	21.83	21.79	21.73	21.67	21.62	
	Ave. rad (mm)	22.00	21.95	21.90	21.84	21.81	21.75	21.70	21.65	
S7	Test 1 (g)	-	0.40	0.39	0.54	0.29	0.37	0.39	0.39	60.00
	Radius (mm)	22.00	21.96	21.92	21.86	21.83	21.80	21.76	21.72	
	Test 2 (g)	-	0.43	0.39	0.52	0.30	0.37	0.47	0.38	61.50
	Radius (mm)	22.00	21.96	21.92	21.87	21.84	21.80	21.75	21.72	
	Ave. rad (mm)	22.00	21.96	21.92	21.87	21.84	21.80	21.75	21.72	

Table 8D: Change in specimen's mass and radius in the near cone region at a gas flow rate of $0.010\text{m}^3/\text{s}$.

	Time (s)	0	900	1800	2700	3600	4500	5400	6300	Length (mm)
Pos. S1	Test 1 (g)	-	0.35	0.34	0.30	0.36	0.33	0.38	0.35	65.50
	Radius (mm)	22.00	21.97	21.94	21.91	21.87	21.84	21.81	21.77	
	Test 2 (g)	-	0.34	0.34	0.37	0.35	0.29	0.36	0.33	61.50
	Radius (mm)	22.00	21.97	21.93	21.90	21.86	21.83	21.80	21.76	
	Ave. rad (mm)	22.00	21.97	21.93	21.90	21.87	21.84	21.80	21.77	
S2	Test 1 (g)	-	0.36	0.36	0.35	0.42	0.33	0.35	0.34	66.50
	Radius (mm)	22.00	21.97	21.93	21.90	21.86	21.83	21.80	21.77	
	Test 2 (g)	-	0.34	0.34	0.33	0.36	0.32	0.31	0.38	62.00
	Radius (mm)	22.00	21.97	21.93	21.90	21.86	21.83	21.80	21.76	
	Ave. rad (mm)	22.00	21.97	21.93	21.90	21.86	21.83	21.80	21.77	
S3	Test 1 (g)	-	0.46	0.46	0.46	0.48	0.45	0.47	0.43	62.00
	Radius (mm)	22.00	21.95	21.91	21.86	21.82	21.77	21.72	21.68	
	Test 2 (g)	-	0.41	0.41	0.39	0.41	0.39	0.40	0.47	62.50
	Radius (mm)	22.00	21.96	21.92	21.88	21.84	21.80	21.76	21.72	
	Ave. rad (mm)	22.00	21.96	21.91	21.87	21.83	21.79	21.74	21.70	
S4	Test 1 (g)	-	0.90	0.90	0.87	0.91	0.83	1.00	0.88	64.50
	Radius (mm)	22.00	21.91	21.83	21.75	21.66	21.58	21.48	21.40	
	Test 2 (g)	-	0.90	0.90	0.91	0.94	0.86	0.91	0.87	62.00
	Radius (mm)	22.00	21.91	21.82	21.73	21.64	21.55	21.46	21.37	
	Ave. rad (mm)	22.00	21.91	21.83	21.74	21.65	21.57	21.47	21.38	
S5	Test 1 (g)	-	0.60	0.60	0.51	0.62	0.65	0.57	0.65	63.00
	Radius (mm)	22.00	21.94	21.88	21.83	21.77	21.71	21.65	21.59	
	Test 2 (g)	-	0.61	0.60	0.57	0.58	0.60	0.64	0.64	63.00
	Radius (mm)	22.00	21.94	21.88	21.83	21.77	21.71	21.65	21.59	
	Ave. rad (mm)	22.00	21.94	21.88	21.83	21.77	21.71	21.65	21.59	
S6	Test 1 (g)	-	0.25	0.24	0.20	0.30	0.25	0.29	0.19	67.50
	Radius (mm)	22.00	21.98	21.96	21.94	21.91	21.89	21.86	21.84	
	Test 2 (g)	-	0.35	0.20	0.24	0.31	0.25	0.31	0.26	61.00
	Radius (mm)	22.00	21.97	21.95	21.92	21.89	21.86	21.83	21.81	
	Ave. rad (mm)	22.00	21.97	21.95	21.93	21.90	21.88	21.85	21.83	
S7	Test 1 (g)	-	0.27	0.27	0.30	0.27	0.25	0.29	0.24	63.50
	Radius (mm)	22.00	21.97	21.95	21.92	21.89	21.87	21.84	21.82	
	Test 2 (g)	-	0.36	0.26	0.34	0.33	0.22	0.32	0.34	64.00
	Radius (mm)	22.00	21.97	21.94	21.91	21.88	21.86	21.82	21.79	
	Ave. rad (mm)	22.00	21.97	21.94	21.91	21.88	21.86	21.83	21.81	

Table 8E: Change in specimen's mass and radius in the near cone region at a gas flow rate of $0.015\text{m}^3/\text{s}$.

	Time (s)	0	900	1800	2700	3600	4500	5400	6300	Length (mm)
Pos. S1	Test 1 (g)	-	0.41	0.41	0.38	0.46	0.36	0.40	0.46	64.00
	Radius (mm)	22.00	21.96	21.92	21.89	21.84	21.81	21.77	21.72	65.00
	Test 2 (g)	-	0.42	0.42	0.39	0.46	0.41	0.41	0.43	
	Radius (mm)	22.00	21.96	21.92	21.88	21.84	21.80	21.76	21.72	
	Ave. rad (mm)	22.00	21.96	21.92	21.88	21.84	21.80	21.77	21.72	
S2	Test 1 (g)	-	0.45	0.44	0.49	0.47	0.38	0.43	0.46	61.50
	Radius (mm)	22.00	21.96	21.91	21.86	21.82	21.78	21.73	21.69	65.50
	Test 2 (g)	-	0.35	0.34	0.34	0.31	0.37	0.34	0.37	
	Radius (mm)	22.00	21.97	21.94	21.90	21.87	21.84	21.81	21.77	
	Ave. rad (mm)	22.00	21.96	21.92	21.88	21.85	21.81	21.77	21.73	
S3	Test 1 (g)	-	0.54	0.53	0.55	0.54	0.52	0.53	0.54	63.50
	Radius (mm)	22.00	21.95	21.90	21.84	21.79	21.74	21.69	21.64	63.00
	Test 2 (g)	-	0.49	0.49	0.48	0.52	0.47	0.47	0.50	
	Radius (mm)	22.00	21.95	21.90	21.86	21.81	21.76	21.72	21.67	
	Ave. rad (mm)	22.00	21.95	21.90	21.85	21.80	21.75	21.70	21.65	
S4	Test 1 (g)	-	0.98	0.98	1.00	0.99	0.95	0.97	0.98	63.00
	Radius (mm)	22.00	21.90	21.81	21.71	21.61	21.52	21.42	21.33	67.50
	Test 2 (g)	-	0.89	0.88	0.85	0.86	0.86	0.89	0.97	
	Radius (mm)	22.00	21.92	21.84	21.76	21.68	21.60	21.52	21.43	
	Ave. rad (mm)	22.00	21.91	21.82	21.74	21.65	21.56	21.47	21.38	
S5	Test 1 (g)	-	0.78	0.77	0.69	0.77	0.77	0.75	0.89	66.50
	Radius (mm)	22.00	21.93	21.86	21.79	21.72	21.65	21.58	21.50	64.00
	Test 2 (g)	-	0.74	0.73	0.64	0.69	0.81	0.71	0.83	
	Radius (mm)	22.00	21.93	21.86	21.80	21.73	21.65	21.58	21.50	
	Ave. rad (mm)	22.00	21.93	21.86	21.80	21.73	21.65	21.58	21.50	
S6	Test 1 (g)	-	0.37	0.37	0.39	0.39	0.36	0.35	0.35	62.50
	Radius (mm)	22.00	21.96	21.93	21.89	21.85	21.82	21.78	21.75	64.50
	Test 2 (g)	-	0.22	0.22	0.19	0.21	0.24	0.17	0.29	
	Radius (mm)	22.00	21.98	21.96	21.94	21.92	21.90	21.88	21.85	
	Ave. rad (mm)	22.00	21.97	21.94	21.91	21.89	21.86	21.83	21.80	
S7	Test 1 (g)	-	0.36	0.36	0.39	0.39	0.36	0.38	0.29	61.50
	Radius (mm)	22.00	21.96	21.93	21.89	21.85	21.81	21.78	21.75	62.50
	Test 2 (g)	-	0.33	0.33	0.32	0.30	0.28	0.37	0.39	
	Radius (mm)	22.00	21.97	21.94	21.90	21.87	21.85	21.81	21.77	
	Ave. rad (mm)	22.00	21.97	21.93	21.90	21.86	21.83	21.79	21.76	

Table 8F: Change in specimen's mass and radius in the near cone region at a gas flow rate of $0.023\text{m}^3/\text{s}$.

	Time (s)	0	900	1800	2700	3600	4500	5400	6300	Length (mm)
Pos. S1	Test 1 (g)	-	0.49	0.49	0.42	0.51	0.47	0.47	0.58	61.50
	Radius (mm)	22.00	21.95	21.90	21.86	21.81	21.76	21.72	21.66	
	Test 2 (g)	-	0.53	0.52	0.54	0.58	0.49	0.49	0.52	64.00
	Radius (mm)	22.00	21.95	21.90	21.85	21.79	21.75	21.70	21.65	
	Ave. rad (mm)	22.00	21.95	21.90	21.85	21.80	21.75	21.71	21.65	
S2	Test 1 (g)	-	0.47	0.47	0.40	0.50	0.44	0.48	0.53	60.00
	Radius (mm)	22.00	21.95	21.90	21.86	21.81	21.77	21.72	21.66	
	Test 2 (g)	-	0.60	0.46	0.52	0.55	0.47	0.52	0.59	63.00
	Radius (mm)	22.00	21.94	21.90	21.85	21.79	21.75	21.70	21.64	
	Ave. rad (mm)	22.00	21.95	21.90	21.86	21.80	21.76	21.71	21.65	
S3	Test 1 (g)	-	0.63	0.47	0.54	0.58	0.50	0.53	0.60	62.00
	Radius (mm)	22.00	21.94	21.89	21.84	21.78	21.73	21.68	21.62	
	Test 2 (g)	-	0.69	0.53	0.62	0.65	0.54	0.62	0.61	62.00
	Radius (mm)	22.00	21.93	21.88	21.82	21.75	21.70	21.64	21.58	
	Ave. rad (mm)	22.00	21.94	21.89	21.83	21.77	21.72	21.66	21.60	
S4	Test 1 (g)	-	1.32	1.00	1.25	1.15	1.01	1.17	1.22	62.50
	Radius (mm)	22.00	21.87	21.77	21.65	21.53	21.43	21.32	21.19	
	Test 2 (g)	-	1.14	1.13	1.16	1.18	1.07	1.10	1.17	62.00
	Radius (mm)	22.00	21.89	21.78	21.66	21.54	21.43	21.32	21.20	
	Ave. rad (mm)	22.00	21.88	21.77	21.65	21.54	21.43	21.32	21.20	
S5	Test 1 (g)	-	1.10	0.64	0.76	0.83	0.84	0.92	1.01	61.00
	Radius (mm)	22.00	21.89	21.82	21.75	21.66	21.58	21.48	21.38	
	Test 2 (g)	-	0.90	0.89	0.86	0.83	0.84	0.92	1.02	61.50
	Radius (mm)	22.00	21.91	21.82	21.74	21.65	21.57	21.47	21.37	
	Ave. rad (mm)	22.00	21.90	21.82	21.74	21.66	21.57	21.48	21.38	
S6	Test 1 (g)	-	0.40	0.30	0.13	0.44	0.34	0.36	0.47	62.50
	Radius (mm)	22.00	21.96	21.93	21.92	21.88	21.84	21.81	21.76	
	Test 2 (g)	-	0.42	0.41	0.37	0.47	0.37	0.43	0.44	63.50
	Radius (mm)	22.00	21.96	21.92	21.88	21.84	21.80	21.76	21.72	
	Ave. rad (mm)	22.00	21.96	21.93	21.90	21.86	21.82	21.78	21.74	
S7	Test 1 (g)	-	0.46	0.31	0.33	0.43	0.37	0.38	0.41	64.00
	Radius (mm)	22.00	21.96	21.93	21.90	21.85	21.82	21.78	21.74	
	Test 2 (g)	-	0.48	0.39	0.43	0.43	0.44	0.44	0.43	62.50
	Radius (mm)	22.00	21.95	21.92	21.87	21.83	21.79	21.74	21.70	
	Ave. rad (mm)	22.00	21.95	21.92	21.88	21.84	21.80	21.76	21.72	

Table 8H: Change in specimen's mass and radius near the water bath surface region at a gas flow rate of 0.010m³/s.

	Time (s)	0	900	1800	2700	3600	4500	5400	6300	Length (mm)
Pos. S1	Test 1 (g)	-	0.52	0.44	0.46	0.53	0.42	0.52	0.47	66.50
	Radius (mm)	22.00	21.95	21.91	21.87	21.82	21.78	21.73	21.69	
	Test 2 (g)	-	0.44	0.44	0.42	0.47	0.42	0.47	0.42	64.50
	Radius (mm)	22.00	21.96	21.92	21.88	21.83	21.79	21.75	21.71	
	Ave. rad (mm)	22.00	21.96	21.91	21.87	21.83	21.79	21.74	21.70	
S2	Test 1 (g)	-	0.78	0.52	0.63	0.70	0.56	0.71	0.65	66.00
	Radius (mm)	22.00	21.93	21.88	21.82	21.76	21.70	21.64	21.58	
	Test 2 (g)	-	0.58	0.58	0.60	0.45	0.58	0.62	0.65	66.00
	Radius (mm)	22.00	21.95	21.89	21.84	21.79	21.74	21.68	21.62	
	Ave. rad (mm)	22.00	21.94	21.89	21.83	21.78	21.72	21.66	21.60	
S3	Test 1 (g)	-	0.68	0.67	0.65	0.68	0.66	0.72	0.67	60.50
	Radius (mm)	22.00	21.93	21.86	21.80	21.73	21.66	21.59	21.52	
	Test 2 (g)	-	0.67	0.68	0.69	0.60	0.65	0.69	0.74	64.50
	Radius (mm)	22.00	21.94	21.87	21.81	21.75	21.69	21.62	21.55	
	Ave. rad (mm)	22.00	21.93	21.87	21.80	21.74	21.67	21.60	21.53	
S4	Test 1 (g)	-	1.08	1.03	1.02	1.23	1.08	0.99	1.07	66.50
	Radius (mm)	22.00	21.90	21.81	21.71	21.60	21.50	21.40	21.30	
	Test 2 (g)	-	1.02	1.01	1.06	1.02	0.93	1.07	1.00	65.50
	Radius (mm)	22.00	21.90	21.81	21.71	21.61	21.53	21.42	21.33	
	Ave. rad (mm)	22.00	21.90	21.81	21.71	21.61	21.51	21.41	21.31	
S5	Test 1 (g)	-	0.99	0.71	0.83	0.93	0.79	0.85	0.85	68.50
	Radius (mm)	22.00	21.91	21.85	21.77	21.69	21.62	21.54	21.46	
	Test 2 (g)	-	0.83	0.83	0.79	0.76	0.77	0.90	0.93	63.50
	Radius (mm)	22.00	21.92	21.84	21.76	21.69	21.61	21.53	21.43	
	Ave. rad (mm)	22.00	21.92	21.84	21.77	21.69	21.62	21.53	21.45	
S6	Test 1 (g)	-	0.85	0.84	0.83	0.92	0.79	0.89	0.80	65.00
	Radius (mm)	22.00	21.92	21.84	21.76	21.67	21.60	21.51	21.44	
	Test 2 (g)	-	0.82	0.82	0.85	0.77	0.76	0.87	0.85	64.00
	Radius (mm)	22.00	21.92	21.84	21.76	21.69	21.61	21.53	21.45	
	Ave. rad (mm)	22.00	21.92	21.84	21.76	21.68	21.61	21.52	21.44	
S7	Test 1 (g)	-	0.71	0.71	0.71	0.74	0.61	0.76	0.72	64.00
	Radius (mm)	22.00	21.93	21.86	21.80	21.72	21.67	21.59	21.52	
	Test 2 (g)	-	0.67	0.67	0.67	0.67	0.63	0.71	0.68	64.50
	Radius (mm)	22.00	21.94	21.87	21.81	21.75	21.68	21.62	21.55	
	Ave. rad (mm)	22.00	21.93	21.87	21.80	21.74	21.68	21.60	21.54	

Table 8I: Change in specimen's mass and radius near the water bath surface region at a gas flow rate of 0.015m³/s.

	Time (s)	0	900	1800	2700	3600	4500	5400	6300	Length (mm)
Pos. S1	Test 1 (g)	-	0.36	0.35	0.31	0.34	0.38	0.36	0.39	66.50
	Radius (mm)	22.00	21.97	21.93	21.91	21.87	21.84	21.81	21.77	
	Test 2 (g)	-	0.36	0.36	0.34	0.35	0.32	0.40	0.39	66.50
	Radius (mm)	22.00	21.97	21.93	21.90	21.87	21.84	21.80	21.77	
	Ave. rad (mm)	22.00	21.97	21.93	21.90	21.87	21.84	21.81	21.77	
S2	Test 1 (g)	-	0.65	0.65	0.64	0.63	0.62	0.69	0.68	62.00
	Radius (mm)	22.00	21.94	21.87	21.81	21.75	21.68	21.62	21.55	
	Test 2 (g)	-	0.70	0.53	0.56	0.56	0.61	0.71	0.64	67.50
	Radius (mm)	22.00	21.94	21.89	21.84	21.79	21.73	21.67	21.61	
	Ave. rad (mm)	22.00	21.94	21.88	21.82	21.77	21.71	21.64	21.58	
S3	Test 1 (g)	-	0.68	0.68	0.60	0.70	0.62	0.69	0.80	68.00
	Radius (mm)	22.00	21.94	21.88	21.82	21.76	21.70	21.64	21.57	
	Test 2 (g)	-	0.75	0.74	0.75	0.72	0.69	0.70	0.86	66.50
	Radius (mm)	22.00	21.93	21.86	21.79	21.73	21.66	21.60	21.52	
	Ave. rad (mm)	22.00	21.94	21.87	21.81	21.74	21.68	21.62	21.54	
S4	Test 1 (g)	-	1.24	1.08	1.21	1.15	1.13	1.17	1.14	65.00
	Radius (mm)	22.00	21.88	21.78	21.67	21.56	21.45	21.34	21.22	
	Test 2 (g)	-	0.93	0.93	0.83	0.91	0.84	0.99	1.09	65.50
	Radius (mm)	22.00	21.91	21.83	21.75	21.66	21.58	21.49	21.38	
	Ave. rad (mm)	22.00	21.90	21.80	21.71	21.61	21.52	21.41	21.30	
S5	Test 1 (g)	-	0.89	0.89	0.90	0.86	0.82	0.93	0.95	62.50
	Radius (mm)	22.00	21.91	21.83	21.74	21.65	21.57	21.48	21.38	
	Test 2 (g)	-	0.89	0.89	0.88	0.82	0.84	0.90	1.02	66.50
	Radius (mm)	22.00	21.92	21.84	21.75	21.68	21.60	21.52	21.42	
	Ave. rad (mm)	22.00	21.92	21.83	21.75	21.67	21.59	21.50	21.40	
S6	Test 1 (g)	-	0.72	0.72	0.64	0.66	0.68	0.78	0.84	66.50
	Radius (mm)	22.00	21.93	21.87	21.81	21.75	21.68	21.61	21.53	
	Test 2 (g)	-	0.76	0.76	0.72	0.74	0.67	0.79	0.88	64.00
	Radius (mm)	22.00	21.93	21.85	21.79	21.71	21.65	21.57	21.49	
	Ave. rad (mm)	22.00	21.93	21.86	21.80	21.73	21.67	21.59	21.51	
S7	Test 1 (g)	-	0.77	0.77	0.72	0.79	0.69	0.84	0.82	66.50
	Radius (mm)	22.00	21.93	21.86	21.79	21.72	21.65	21.58	21.50	
	Test 2 (g)	-	0.85	0.62	0.73	0.66	0.69	0.78	0.81	67.00
	Radius (mm)	22.00	21.92	21.87	21.80	21.74	21.67	21.60	21.53	
	Ave. rad (mm)	22.00	21.93	21.86	21.80	21.73	21.66	21.59	21.51	

Table 8J: Change in specimen's mass and radius near the water bath surface region at a gas flow rate of 0.023m³/s.

	Time (s)	0	900	1800	2700	3600	4500	5400	6300	Length (mm)
Pos. S1	Test 1 (g)	-	0.35	0.35	0.33	0.38	0.33	0.39	0.33	62.50
	Radius (mm)	22.00	21.97	21.93	21.90	21.86	21.83	21.79	21.76	
	Test 2 (g)	-	0.56	0.55	0.48	0.50	0.47	0.74	0.50	66.00
	Radius (mm)	22.00	21.95	21.90	21.85	21.81	21.76	21.69	21.65	
	Ave. rad (mm)	22.00	21.96	21.91	21.88	21.83	21.80	21.74	21.70	
S2	Test 1 (g)	-	0.54	0.53	0.49	0.59	0.55	0.59	0.46	65.50
	Radius (mm)	22.00	21.95	21.90	21.85	21.80	21.75	21.69	21.65	
	Test 2 (g)	-	0.59	0.58	0.52	0.59	0.56	0.72	0.53	64.50
	Radius (mm)	22.00	21.94	21.89	21.84	21.78	21.73	21.66	21.61	
	Ave. rad (mm)	22.00	21.95	21.89	21.85	21.79	21.74	21.68	21.63	
S3	Test 1 (g)	-	0.59	0.58	0.57	0.59	0.55	0.65	0.56	64.50
	Radius (mm)	22.00	21.94	21.89	21.83	21.78	21.73	21.66	21.61	
	Test 2 (g)	-	0.66	0.65	0.49	0.51	0.52	1.13	0.62	67.00
	Radius (mm)	22.00	21.94	21.88	21.84	21.79	21.74	21.64	21.58	
	Ave. rad (mm)	22.00	21.94	21.88	21.84	21.78	21.73	21.65	21.59	
S4	Test 1 (g)	-	1.14	1.13	1.13	1.10	1.10	1.23	1.11	62.50
	Radius (mm)	22.00	21.89	21.78	21.67	21.56	21.45	21.32	21.21	
	Test 2 (g)	-	1.27	1.27	1.45	1.22	1.25	1.19	1.23	63.00
	Radius (mm)	22.00	21.88	21.75	21.61	21.49	21.37	21.25	21.12	
	Ave. rad (mm)	22.00	21.88	21.77	21.64	21.52	21.41	21.28	21.17	
S5	Test 1 (g)	-	1.01	1.01	0.96	1.00	1.00	1.07	1.03	64.00
	Radius (mm)	22.00	21.90	21.81	21.71	21.62	21.52	21.42	21.31	
	Test 2 (g)	-	0.99	0.98	1.04	1.08	0.93	0.82	1.05	66.00
	Radius (mm)	22.00	21.91	21.82	21.72	21.62	21.53	21.45	21.35	
	Ave. rad (mm)	22.00	21.91	21.81	21.72	21.62	21.53	21.43	21.33	
S6	Test 1 (g)	-	0.82	0.82	0.75	0.83	0.77	0.89	0.85	65.00
	Radius (mm)	22.00	21.92	21.85	21.77	21.70	21.62	21.54	21.46	
	Test 2 (g)	-	0.79	0.78	0.66	0.86	0.80	0.77	0.84	64.00
	Radius (mm)	22.00	21.92	21.85	21.79	21.70	21.63	21.55	21.47	
	Ave. rad (mm)	22.00	21.92	21.85	21.78	21.70	21.62	21.54	21.46	
S7	Test 1 (g)	-	0.84	0.84	0.85	0.81	0.79	0.89	0.85	62.50
	Radius (mm)	22.00	21.92	21.84	21.75	21.67	21.59	21.50	21.42	
	Test 2 (g)	-	0.78	0.77	0.82	0.81	0.75	0.68	0.82	64.50
	Radius (mm)	22.00	21.93	21.85	21.77	21.70	21.63	21.56	21.48	
	Ave. rad (mm)	22.00	21.92	21.84	21.76	21.68	21.61	21.53	21.45	

APPENDIX 9

Table 9A: Mass transfer parameters in the bottom region at 0.5m water bath height

Flow rate (m ³ /s)	Sample location	dR/dt (*10 ⁻⁵ m/s)	Mass transfer coefficient, <i>K</i> (*10 ⁻⁵ m/s)	Sherwood number <i>Sh</i>	Turbulence Parameters (Re _{loc,r}) ^{0.25} (Re _t) ^{0.32}
0.010	S1	3.08	1.26	8850	71762
	S2	3.37	1.38	9684	78519
	S3	4.61	1.89	13247	107410
	S4	3.96	1.62	11379	92265
	S5	3.20	1.31	9195	74558
	S6	4.12	1.68	11839	95993
	S7	3.07	1.26	8822	71529
0.015	S1	3.92	1.60	11264	91333
	S2	3.93	1.61	11293	91566
	S3	5.74	2.35	16494	133738
	S4	4.58	1.87	13161	106711
	S5	3.53	1.44	10144	82247
	S6	4.45	1.82	12787	103682
	S7	3.60	1.47	10345	83878
0.023	S1	4.44	1.82	12758	103449
	S2	4.65	1.90	13362	108342
	S3	6.94	2.84	19942	161697
	S4	6.13	2.51	17615	142825
	S5	4.44	1.82	12758	103449
	S6	4.12	1.68	11839	95993
	S7	3.37	1.38	9684	78519

Table 9B: Mass transfer parameters in the near cone region at 0.5m water bath height

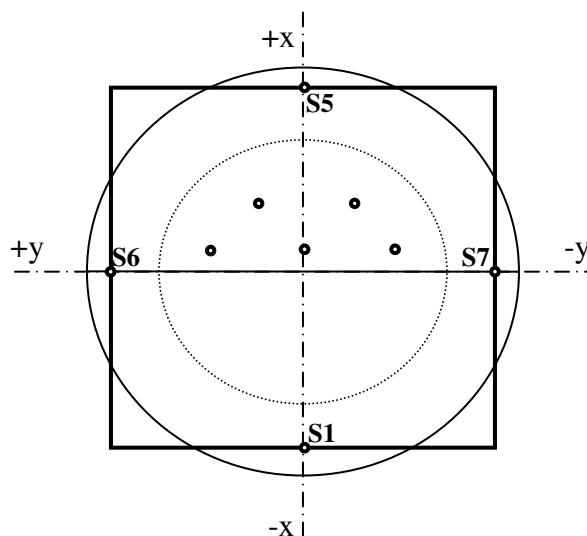
Flow rate (m ³ /s)	Sample location	dR/dt (*10 ⁻⁵ m/s)	Mass transfer coefficient, <i>K</i> (*10 ⁻⁵ m/s)	Sherwood number <i>Sh</i>	Turbulence Parameters (Re _{loc,r}) ^{0.25} (Re _t) ^{0.32}
0.010	S1	2.71	1.11	7787	63141
	S2	2.75	1.12	7902	64073
	S3	3.52	1.44	10115	82014
	S4	7.22	2.95	20747	168221
	S5	4.79	1.96	13764	111604
	S6	2.05	0.84	5891	47764
	S7	2.30	0.94	6609	53588
0.015	S1	3.23	1.32	9282	75257
	S2	3.16	1.29	9080	73626
	S3	4.10	1.68	11781	95527
	S4	7.25	2.97	20833	168920
	S5	5.76	2.36	16552	134204
	S6	2.34	0.96	6724	54520
	S7	2.82	1.15	8103	65704
0.023	S1	4.06	1.66	11667	94595
	S2	4.04	1.65	11609	94129
	S3	4.72	1.93	13563	109973
	S4	9.40	4.84	27011	219014
	S5	7.19	2.94	20661	167522
	S6	2.97	1.21	8534	69199
	S7	3.26	1.33	9368	75956

Table 9C: Mass transfer parameters near the water bath surface region at 0.5m water bath height.

Flow rate (m ³ /s)	Sample location	dR/dt (*10 ⁻⁵ m/s)	Mass transfer coefficient, <i>K</i> (*10 ⁻⁵ m/s)	Sherwood number <i>Sh</i>	Turbulence Parameters (Re _{loc,r}) ^{0.25} (Re _t) ^{0.32}
0.010	S1	3.55	1.45	10201	82713
	S2	4.67	1.91	13419	108808
	S3	5.44	2.22	15632	126748
	S4	8.05	4.29	23132	187560
	S5	6.41	2.62	18419	149349
	S6	6.55	2.68	18822	152611
	S7	5.42	2.22	15575	126282
0.015	S1	3.23	1.32	9282	75257
	S2	4.91	2.01	14109	114400
	S3	5.29	2.16	15201	123253
	S4	8.09	4.31	23247	188492
	S5	6.94	2.84	19942	161697
	S6	5.63	2.30	16178	131175
	S7	5.65	2.31	16235	131641
0.023	S1	3.47	1.42	9971	80849
	S2	4.35	1.78	12500	101352
	S3	4.65	1.90	13362	108342
	S4	9.80	4.01	28161	228333
	S5	7.80	4.19	22414	181735
	S6	6.24	2.55	17931	145388
	S7	6.45	2.64	18534	150281

APPENDIX 10

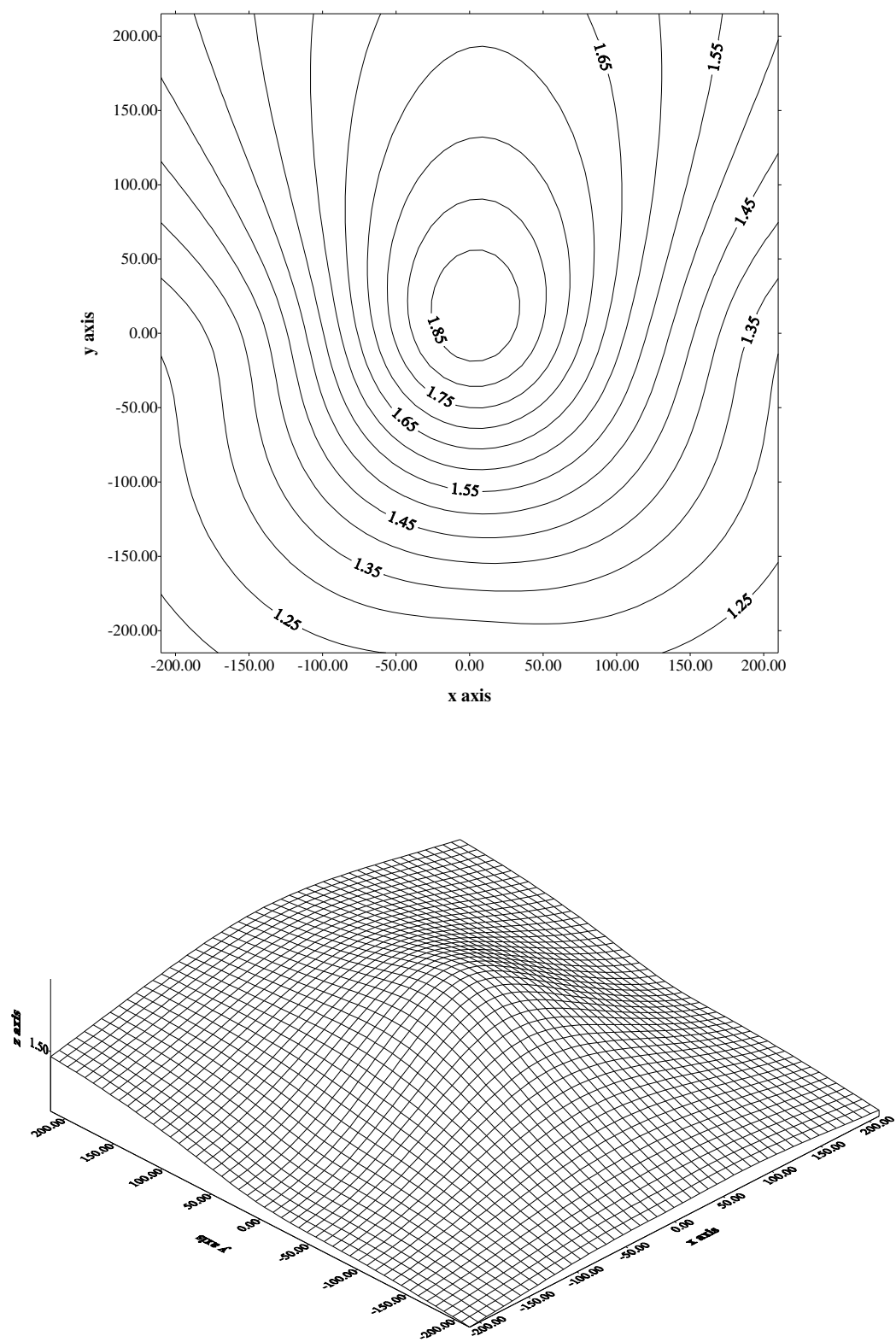
MAPPING: The square super imposed on the cross sectional area of the model vessel represents the area that was represented by contour maps below.



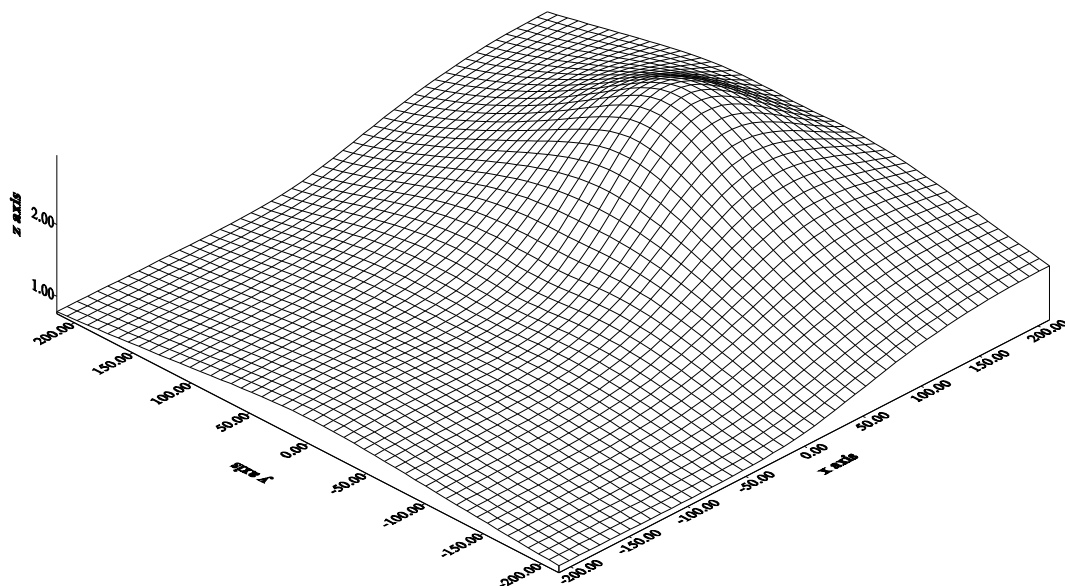
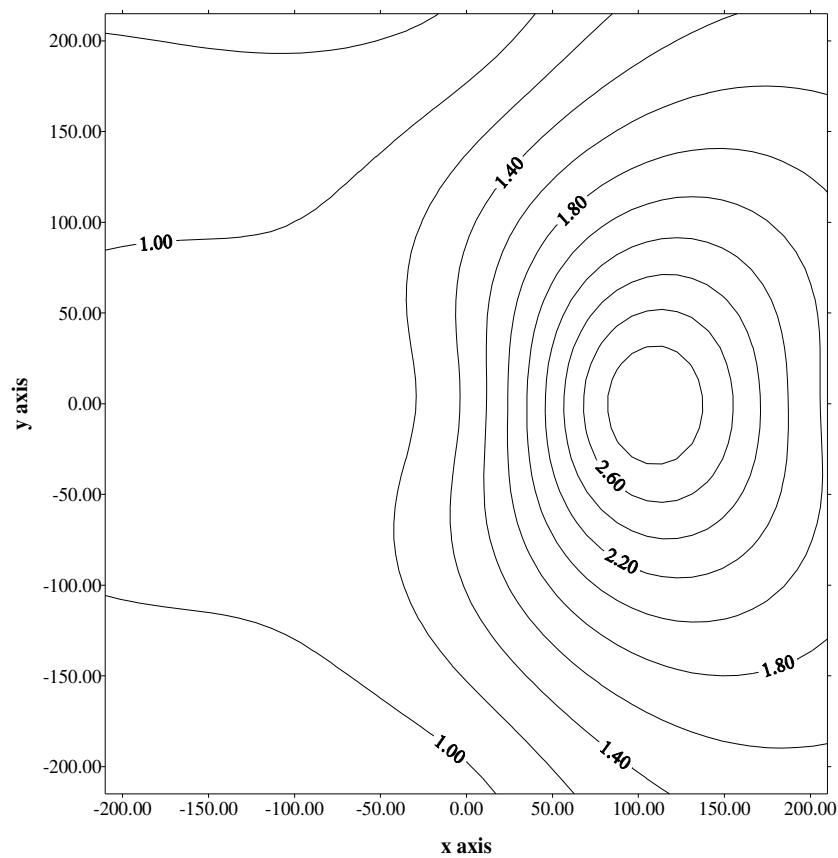
	At 0.01m ³ /s gas flow rate			At 0.015m ³ /s gas flow rate			At 0.023 m ³ /s gas flow rate		
	X	Y	Z	X	Y	Z	X	Y	Z
Bottom of Bath region	-210	0	1.11	-210	0	1.32	-210	0	1.66
	-145	0	1.12	-145	0	1.29	-145	0	1.65
	0	0	1.44	0	0	1.68	0	0	1.93
	100	0	2.95	100	0	2.97	100	0	4.84
	210	0	1.96	210	0	2.36	210	0	2.94
	0	215	0.84	0	215	0.96	0	215	1.21
	0	-215	0.94	0	-215	1.15	0	-215	1.33
Near cone region	-210	0	1.26	-210	0	1.60	-210	0	1.82
	-145	0	1.38	-145	0	1.61	-145	0	1.90
	0	0	1.89	0	0	2.35	0	0	2.84
	100	0	1.62	100	0	1.87	100	0	2.51
	210	0	1.31	210	0	1.44	210	0	1.82
	0	215	1.68	0	215	1.82	0	215	1.68
Water Bath Surface region	0	-215	1.26	0	-215	1.47	0	-215	1.38
	-210	0	1.45	-210	0	1.32	-210	0	1.42
	-145	0	1.91	-145	0	2.01	-145	0	1.78
	0	0	2.22	0	0	2.16	0	0	1.90
	100	0	4.29	100	0	4.31	100	0	4.01
	210	0	2.62	210	0	2.84	210	0	4.19
	0	215	2.68	0	215	2.30	0	215	2.55
	0	-215	2.22	0	-215	2.31	0	-215	2.64

The **z**-axis represents the mass transfer coefficients (**K**) that were established in the experiments. Where, $K = Z * 10^{-5} \text{ m/s}$.

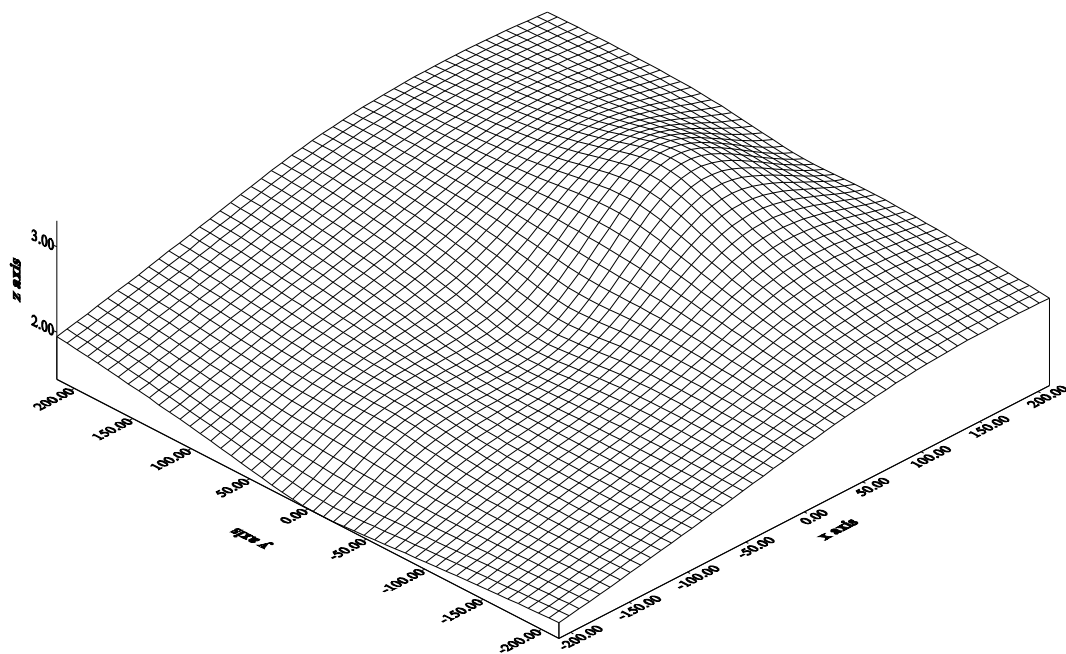
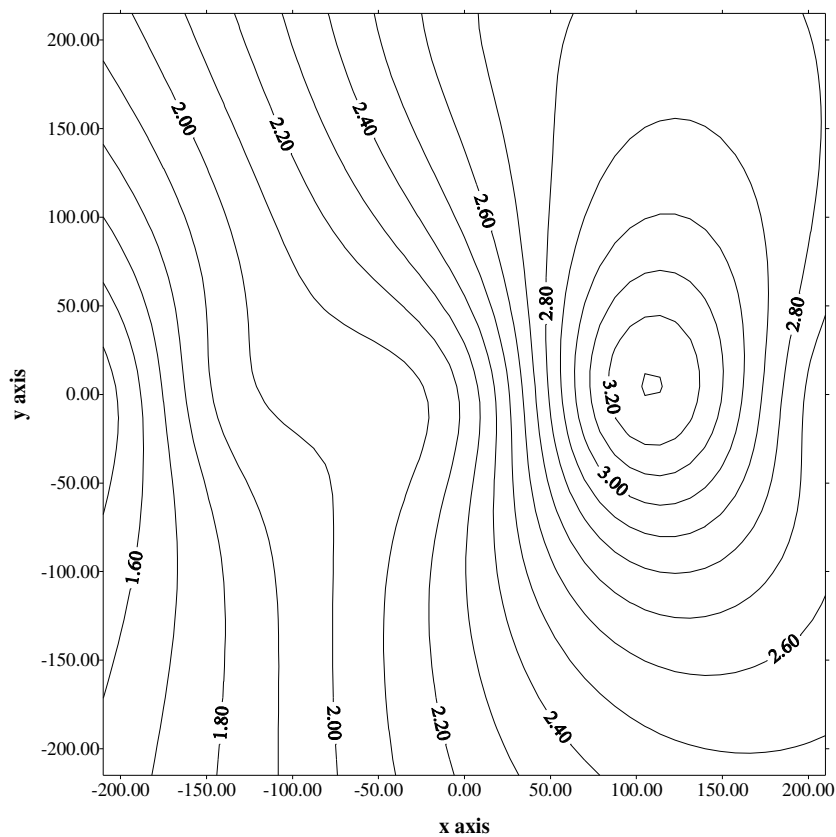
Map 10A: Contour and surface plots of mass transfer coefficients in the bottom region of the bath at $0.01\text{m}^3/\text{s}$ gas flow rate.



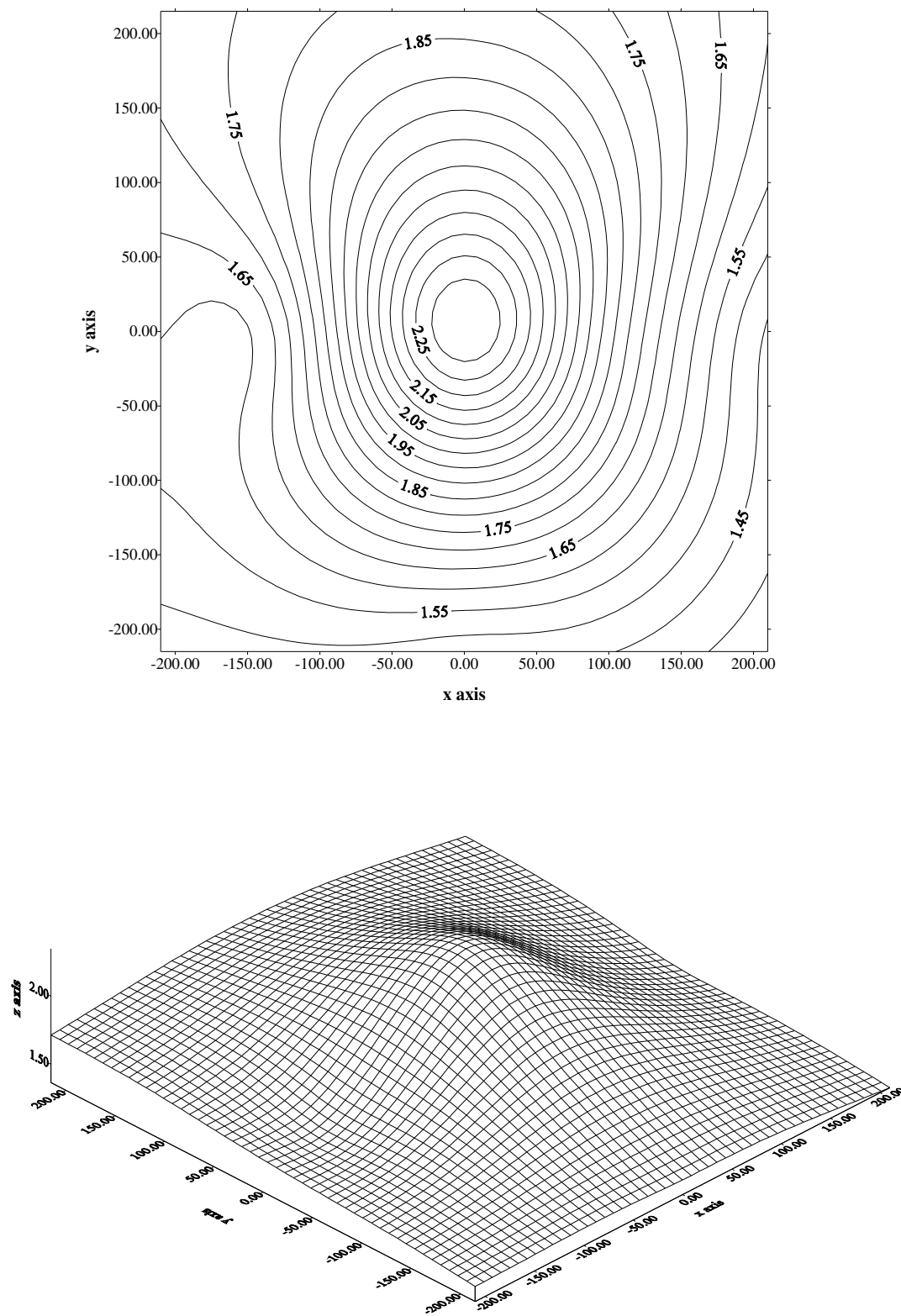
Map 10B: Contour and surface plots of mass transfer coefficients near the cone region of the bath at $0.01\text{m}^3/\text{s}$ gas flow rate.



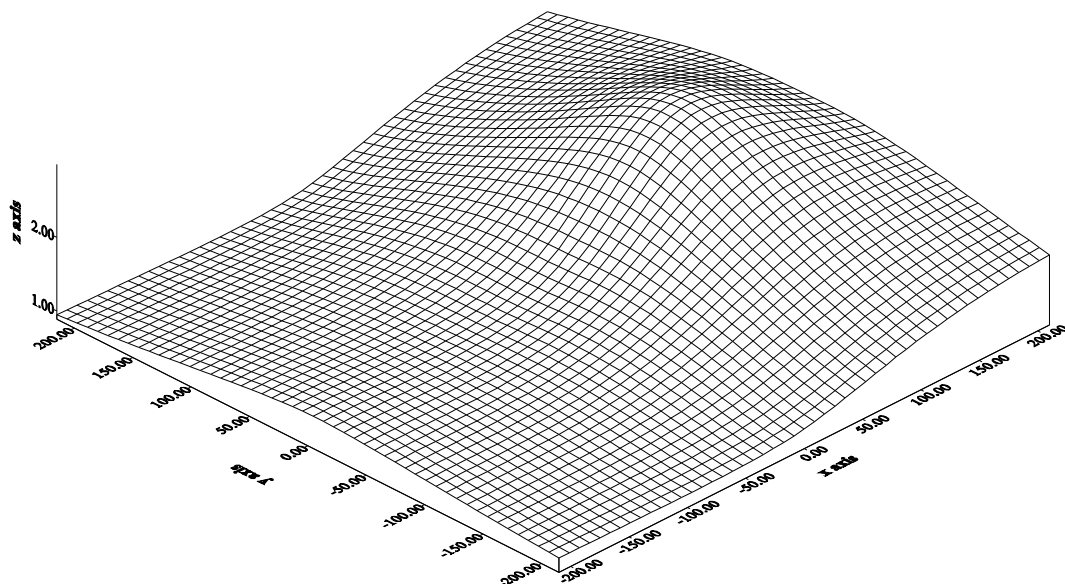
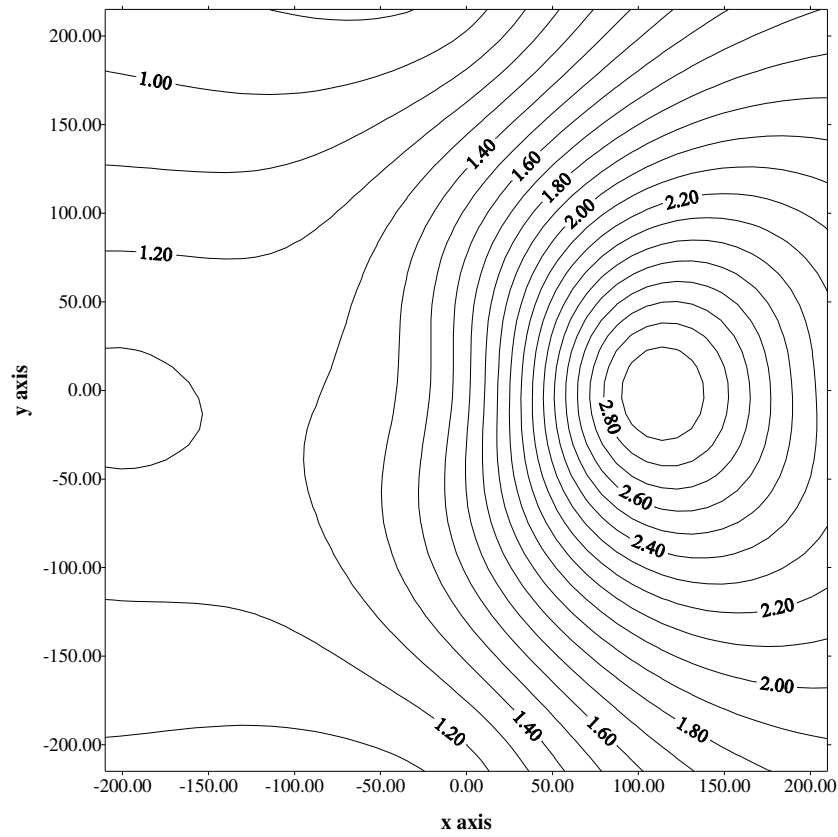
Map 10C: Contour and surface plots of mass transfer coefficients at the water bath surface at $0.01\text{m}^3/\text{s}$ gas flow rate.



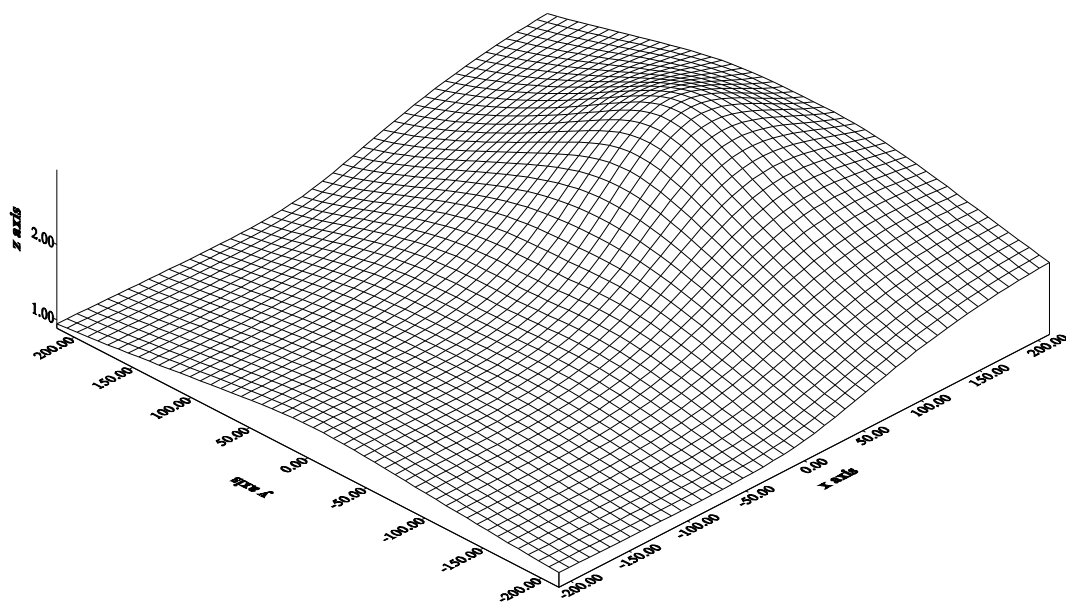
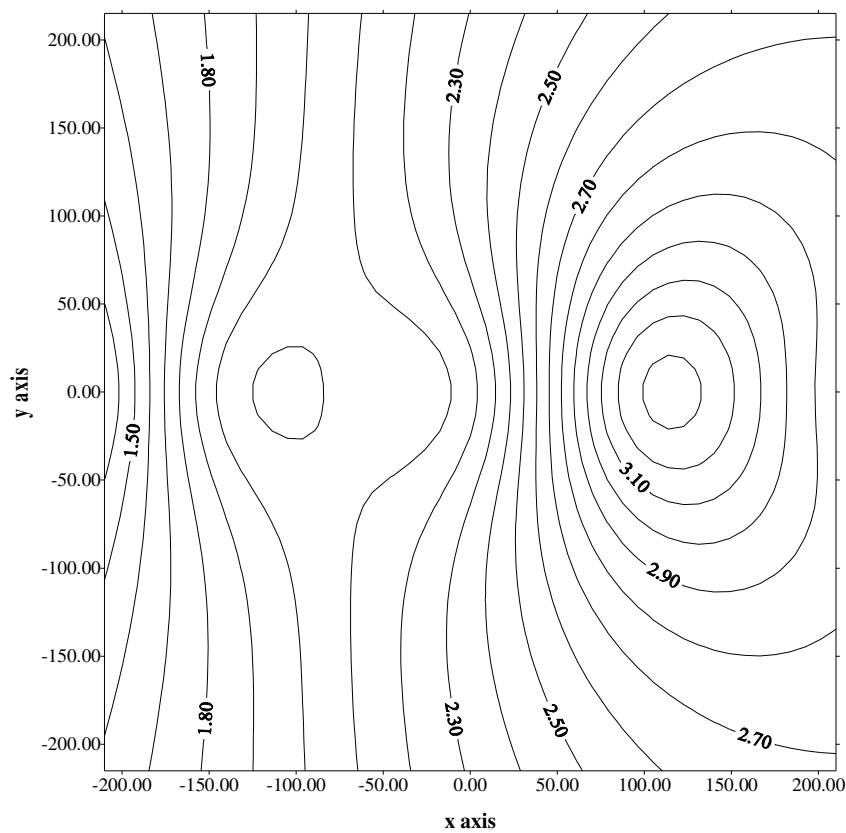
Map 10D: Contour and surface plots of mass transfer coefficients in the bottom region of the bath at $0.015\text{m}^3/\text{s}$ gas flow rate.



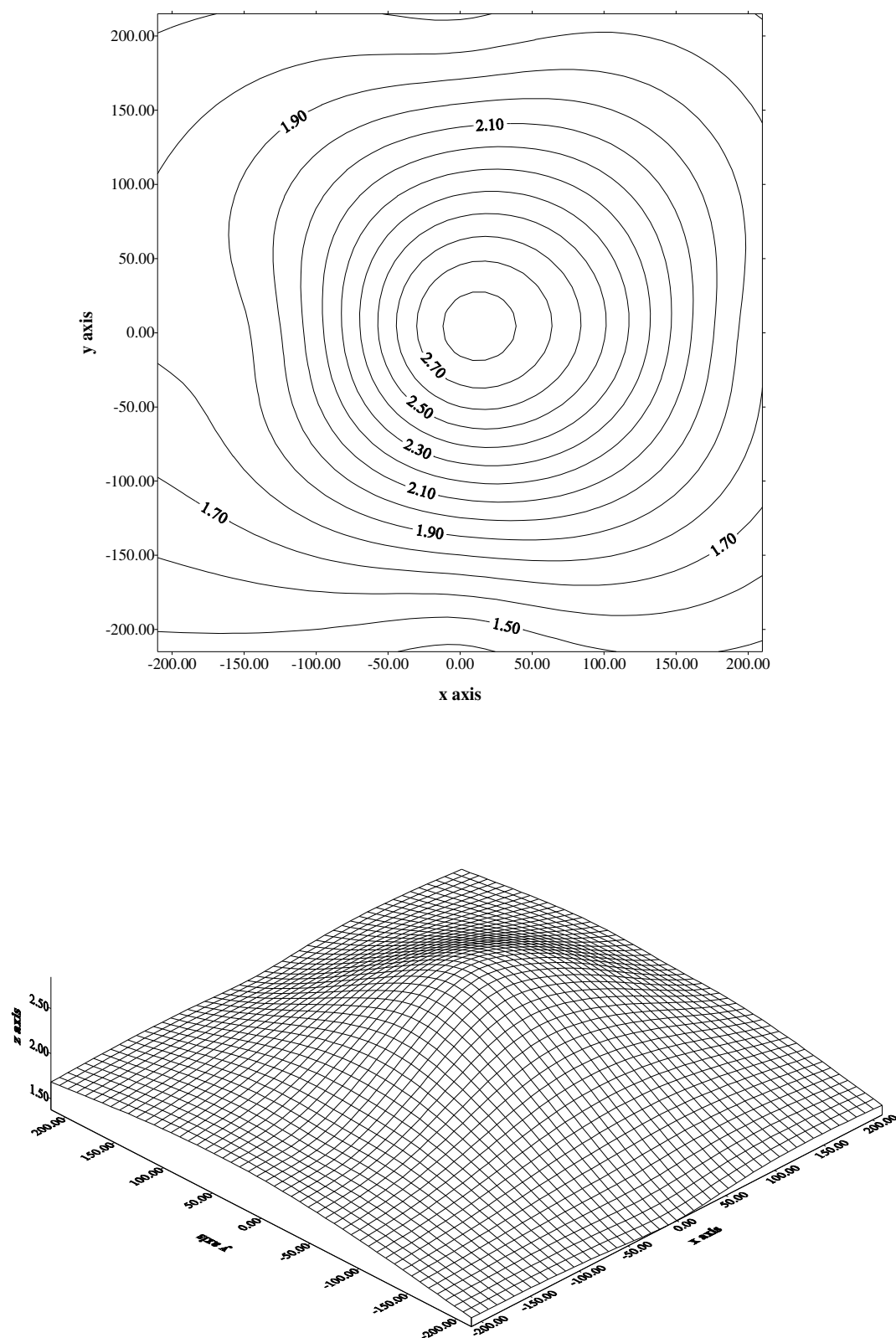
Map 10E: Contour and surface plots of mass transfer coefficients near the cone region of the bath at $0.015\text{m}^3/\text{s}$ gas flow rate.



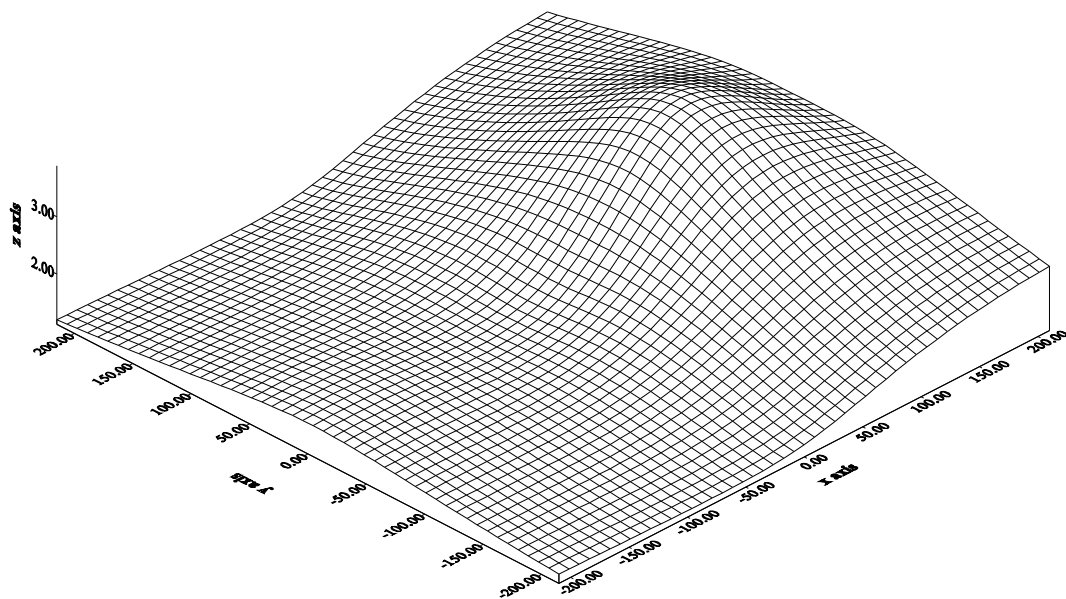
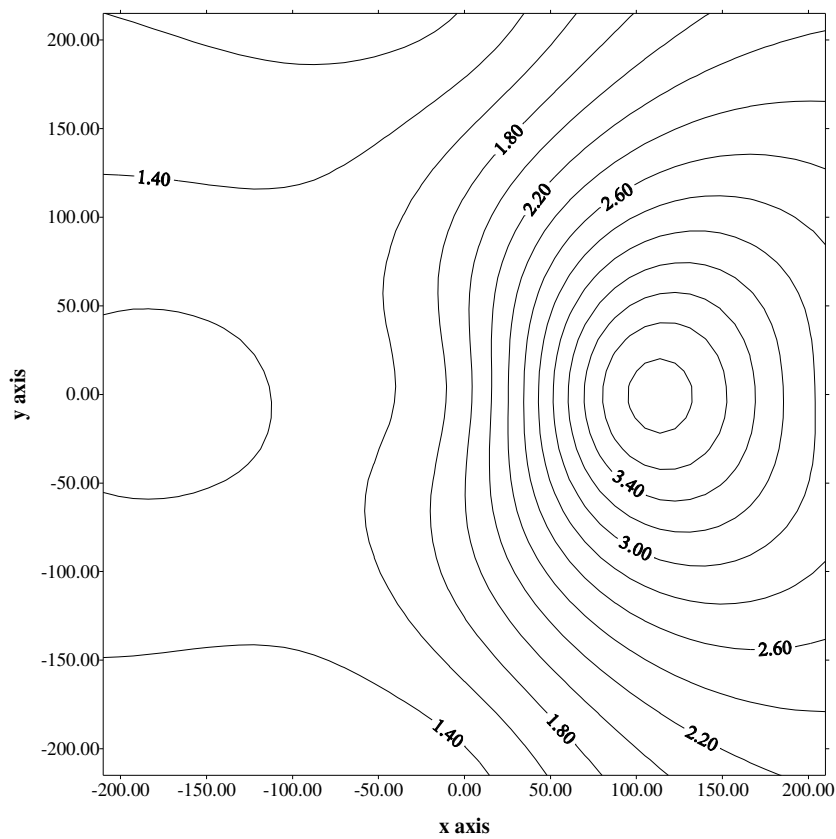
Map 10F: Contour and surface plots of mass transfer coefficients at the water bath surface at $0.015\text{m}^3/\text{s}$ gas flow rate.



Map 10G: Contour and surface plots of mass transfer coefficients in the bottom region of the bath at $0.023\text{m}^3/\text{s}$ gas flow rate.



Map 10H: Contour and surface plots of mass transfer coefficients near the cone region of the bath at $0.023\text{m}^3/\text{s}$ gas flow rate.



Appendix 10I: Contour and surface plots of mass transfer coefficients at the water bath surface at $0.023\text{m}^3/\text{s}$ gas flow rate.

